Accurate Discontinuous Galerkin Finite Element Methods for Computing Light Propagation in Photonic Crystals

Master Thesis

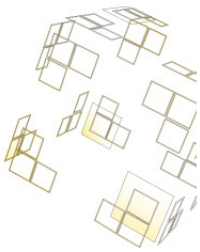

by
Magdalena Metzger

May 14, 2015

Faculty of Electrical Engineering, Mathematics and Computer Science (EEMCS)
Chair of Mathematics of Computational Science (MaCS)

UNIVERSITEIT TWENTE.

Magdalena Metzger
s1493930

Graduation Committee:
Prof. Dr. ir. J. W. W. van der Vegt (Chairman)
Dr. M. A. Botchev
Dr. C. Brune

Contents

1. Introduction

Throughout the ages, mankind developed skills in controlling the properties of materials. While people first only tried to work with different natural materials, they soon started to create artificial ones with a large range of mechanical features. Further technological developments were possible as men were able to even control electrical properties of materials. In the last few decades, research has spread to the field of optical characteristics. Controlling these would enable us to engineer materials that could e. g. reflect light perfectly over a desired range of frequencies or allow the light waves to propagate in predefined directions. One possibility to do so are manipulations of photonic crystals at the nano-scale [10].

The arrangement of atoms or molecules in a repetitive lattice is called a *crystal*, through which electrons propagate as waves. When organising macroscopic media with different dielectric constants in the same way, we obtain *photonic crystals*. Instead of the periodic potential we consider now the dielectric function within these metamaterials, which varies periodically with the position at length scales smaller than the wavelength of light. Photons in these structures behave similarly to electrons in traditional crystals [10].

Due to the periodicity of the structure, photonic crystals have a discrete translation symmetry, which means that they are invariant under translations of lengths that are multiples of a fixed step-size. This size, the *lattice constant* a, depends on the lattice structure and thus on the employed materials. The vector describing such a basic step is called the *primitive lattice vector* $\mathbf{a}$. Then, for the dielectric function, it holds that

$$\varepsilon(\mathbf{r}) = \varepsilon(\mathbf{r} + l \cdot \mathbf{a}) = \varepsilon(\mathbf{r} + \mathbf{R}),$$

where $\mathbf{r}$ denotes the position, $\mathbf{R}$ is any *lattice vector* and l an integer. If the symmetry occurs in one direction only, we speak of a one-dimensional photonic crystal. For symmetry in two or three directions, we obtain two- or three-dimensional crystals, respectively. In a three-dimensional grid, a lattice vector is given by

$$\mathbf{R} = l_1 \cdot a_1 + l_2 \cdot a_2 + l_3 \cdot a_3,$$

where a_1, a_2 and a_3 are the components of the lattice vectors for the corresponding dimensions and l_1, l_2, l_3 are integers. Based on these considerations, we can regard the crystal to be built by the repetition of a smallest possible dielectric unit, the so-called *unit cell* [10].

When analysing periodic functions, the Fourier transform is a common tool. As the dielectric function is repetitive within the lattice, the values of its Fourier transform

equal zero unless $e^{i\mathbf{G}\cdot\mathbf{R}} = 1$ for some lattice vector $\mathbf{R}$. Therefore, only those terms with a *reciprocal lattice vector* $\mathbf{G}$ have to be considered, where $\mathbf{G}$ is determined by

$$\mathbf{R} \cdot \mathbf{G} = 2\pi\mathbb{N}.$$

The vectors $\mathbf{G}$ also form a lattice.

A translation symmetry offers the possibility to classify the transverse *electromagnetic modes*. Modes are patterns of the electromagnetic field considered in a plane orthogonal to the propagation direction of the initial beam. They behave differently under the translation operator $\mathrm{T}_{\mathbf{d}}$ for a displacement $\mathbf{d}$. It can be shown that a mode of the functional form e^{ikz} is an eigenfunction of the translation operating in the z-direction with corresponding eigenvalue e^{-ikd}. Therefore, we can choose the modes of an electromagnetic system to be the eigenfunctions of T_d and distinguish them by the values of the *wave vector* $\mathbf{k}$. If the photonic crystal possesses a continuous translation symmetry in all directions, it is said to be an *homogeneous medium*. It is noticeable that we do not necessarily obtain distinct modes for different values of $\mathbf{k}$. In particular, a mode with the wave vector $\mathbf{k}$ is the same as one with a wave vector of $\mathbf{k} + \mathbf{G}$. It is thus advantageous to restrict the investigations to a domain in the reciprocal space in which we cannot move from one part of the volume to another by adding $\mathbf{G}$. These domains are so-called *Brillouin zones* and the one closest to $\mathbf{k} = \mathbf{0}$ is the *first Brillouin zone* (BZ1). General considerations are often restricted to this domain [10].

To classify the modes, first consider the wave vector. Sort all modes with the same $\mathbf{k}$ by their frequency ω in increasing order. A number n can then be assigned to the modes corresponding to their place in this list. The discrete or continuous values of n are called the *band number* or *band index*. A diagram demonstrating the dependence of the mode frequency on the wave vector shows uniformly rising lines, the so-called *bands*. Such a plot is called a *dispersion relation* or *band structure* [10].

If light enters a photonic crystal, it is scattered and reflected. The resulting beams interfere with each other. The path of the light depends on the structure of the crystal. Thus, examining the medium itself leads to new ways of manipulating the behaviour of photons. Mirrors, cavities (producing a pattern of standing waves) and waveguides (leading waves in one dimension, while preventing a loss of power) have interesting and useful properties. Photonic crystals can be constructed to not only exploit these properties, but also generalise them. For that purpose, we can use the fact that the lattice of a photonic crystal can prohibit the propagation of light with a certain frequency range. This produces gaps in the band structure of the system. If the propagation of electromagnetic waves of a particular frequency range with any polarisation and traveling in any direction is totally prevented, we speak of a *photonic band gap*. This is only possible in three-dimensional photonic crystals [10]. Another tool for changing the photonic properties of structures are *crystallographic defects*. They are disturbances in the lattice of a (photonic) crystal. Intentionally placing such defects at particular positions alters the behaviour of light inside the structure.

Nowadays, there exists a large range of applications for photonic crystals. For example, the effectiveness of solar panels can be improved by reflecting the incident light-beam,

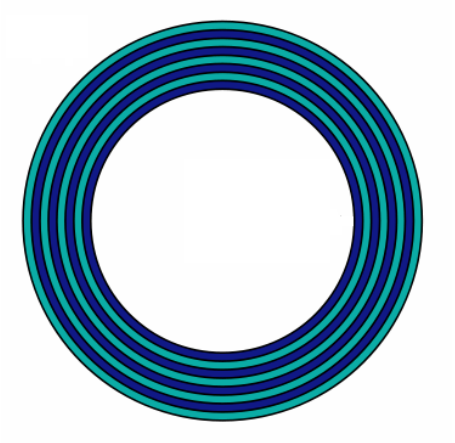

(a) Fibers that are coated by photonic crystals trap the light inside cables. This possible arrangement is described in [10].

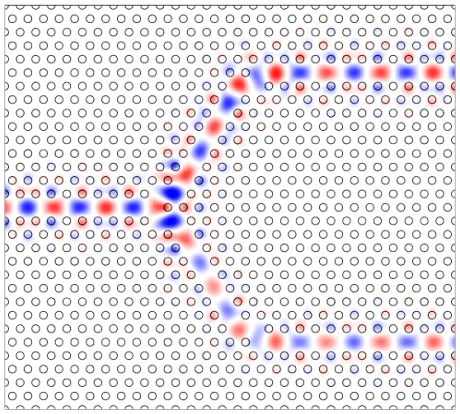

(b) Picture of the path of light through a waveguide using defects of a photonic crystal. Here, the y-shape as explained in [13] is seen.

Figure 1.1.: Visualisation of some of the applications of photonic crystals.

optic fibers are coated with band gap materials to trap the light inside the cable (see Figure 1.1a) or the focus of light can be improved by passing it through photonic material and steering the light by interference. Furthermore, defects in a crystal do not only enable us to guide electromagnetic waves straight into one direction, but also along angles of up to 90° without losing any power (see Figure 1.1b). It is moreover possible to build antennas and photonic integrated circuits or to construct sources with a broad spectrum or high-power fiber lasers [19].

Band gap materials could lead to a localisation of light and strong alterations in the rate of spontaneous emission. In order to improve applications it is important to be able to control changes in the light emission inside a photonic crystal. Therefore, we consider the *local density of states* (LDOS), which is proportional to the emission rate in a material. The LDOS gives a value for the number of the electromagnetic states present at a certain frequency and for a given orientation of the dipolar emitters. To be able to evaluate experiments regarding the spontaneous emission in constructed photonic crystals we need to be able to perform LDOS calculations [16]. It is, however, problematic to compute the LDOS accurately, as it is directly related to a Green's function.

Three-dimensional photonic crystals can have different basic structures, like the simple assembly of colloidal nanoparticles, opal, inverse opal, woodpile and inverse woodpile. Some of these can be seen in Figure 1.2. When fabricating photonic crystals we require them to have a high photonic strength. This means that we expect a high contrast between the refractive indices of the used materials and the high index-material should only take up a small part of the volume. Additionally, a low absorption and the interconnection of the various materials are desirable [24]. The inverse woodpile structure has the benefits to be robust to imperfections and to provide the possibility for broad band gaps and an excellent ordering. With the etching fabrication method we are able to produce high-quality photonic crystals [23].

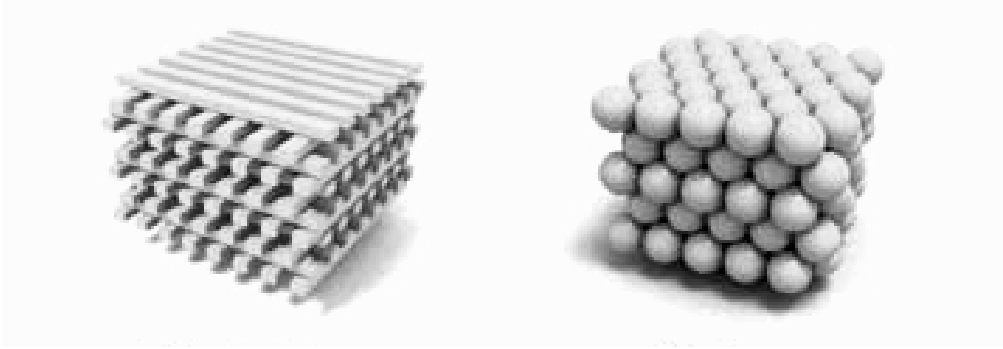

(a) The structures *woodpile* and *opal*.
Source: `http://www.photonic-lattice.com/en/technology/photoniccrystal/`, May 14, 2015.

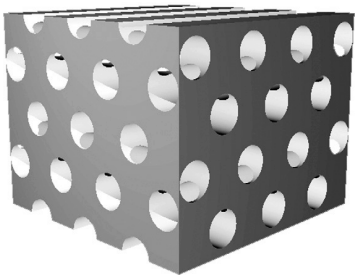

(b) The *inverse woodpile* structure, [23].

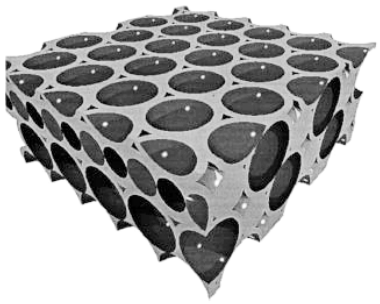

(c) The *inverse opal* structure, [4].

Figure 1.2.: Different geometries or basic structures of photonic crystals.

Both the geometry of the crystal and the different materials influence the propagation properties of light. A photonic crystal is subject to the physics of solid-states (crystal structures) and electromagnetics (electromagnetic waves represent electrons). As the production of three-dimensional photonic crystals is complex, it is advantageous to determine and optimise its influence on the propagation of light before it is manufactured. In order to study the optical behaviour, we consider the propagation of light as electromagnetic waves.

In the Chapter 2 the mathematical model for light propagation in photonic crystals is explained. To that end, Maxwell's equations are presented and simplified. They are four partial differential equations (PDEs), which, together with Lorentz' force law, express the complete theory of electromagnetics [6]. Within this framework, we will only consider the time-harmonic case. Furthermore, we can assume that we have an inhomogeneous, macroscopic, isotropic and linear material. With these restrictions we obtain a PDE that describes our problem mathematically. Finally, boundary conditions are discussed shortly.

In Chapter 3 the numerical method used in this study, the discontinuous Galerkin finite element method (DG FEM) on tetrahedral meshes, is described and examined. Definitions and properties of the needed function space $\mathrm{H}(\mathrm{curl};\Omega)$, of the finite element space of

consideration (such as curl-conformity and unisolvency) and of the finite elements are presented. We also introduce the concept of a reference element. Computations are first carried out on this element before an affine map transforms the results to the physical element. In the end, the advantages of Nédélec's basis functions of the first family are discussed and a technique is established that provides the basis functions of any order and in any dimension. Computations for order $p = 1$ are performed as example.

Following the general description of the DG FEM, we apply it to the problem equation discussed in Chapter 2. The discretisation of the PDE is shown in Chapter 4. Step by step, we transform the second order PDE into a system of first-order equations and determine their weak formulation. Introducing numerical fluxes with penalty terms and applying the Galerkin method, we can then solve a linear system for the discontinuous Galerkin coefficients in the separate elements. The overall solution is finally obtained by the assembly of the elementwise solutions.

Chapter 5 shortly introduces the C++ software package `hpGEM` and its application `DG-Max`. This implementation helps to numerically solve Maxwell's equations as described in this framework. However, the toolkit uses the basis function set by Ainsworth and Coyle [1], which might produce non-physical results. Therefore, the described set of Nédélec's basis functions will be included into the code. Then tests have to be run to prove the functionality of the modified implementation.

As mentioned before, the calculations of the LDOS are of great interest. Hence, in Chapter 6, we concentrate on determining it more accurately. Different formulas for the computation of the LDOS are explained. Then, we present a numerical technique for the calculation, which was introduced in [26] and looks promising for the implementation in `DG-Max`.

The results will be summarised and an outlook on future work will be given in Chapter 7.

2. The mathematical model of electromagnetism – Maxwell's equations

In this chapter the problem setting, given by Maxwell's equations, is described. The full problem is then reduced to a simpler one, the time-harmonic Maxwell system for linear media, which is relevant to nanophotonic crystals. After deriving the differential equations describing the problem, boundary conditions have to be chosen to complete the model.

2.1. Problem modeling

Maxwell's equations are a set of four partial differential equations in position and time that summarise (together with the Lorentz force law) the entire theory of classical electrodynamics. Actually, Maxwell only resolved a theoretical inconsistency in Ampère's law and joined the equations to the compact system that was later named after him [6]. The physical content was, however, already known in his time.

Let us consider the domain $\Omega \subseteq \mathbb{R}^3$, where $\mathcal{E}$ and $\mathcal{H}$ are the electric and magnetic field intensities, respectively, $\mathcal{D}$ is the electric displacement and $\mathcal{B}$ the magnetic induction. The distribution of the charges is given by the charge density function ρ and the currents by a corresponding density function $\mathcal{J}$. All of these variables depend on the position $\mathbf{r}$ and the time t. Then we can introduce the notion of the normalised equations, where the fields are on the left hand side and the source terms on the right hand side:

$$\begin{cases} \dfrac{\partial \mathcal{B}}{\partial t} + \nabla \times \mathcal{E} = 0 & \text{Faraday's law} \\ \nabla \cdot \mathcal{D} = \rho & \text{Gauß' law} \\ \dfrac{\partial \mathcal{D}}{\partial t} - \nabla \times \mathcal{H} = -\mathcal{J} & \text{Ampère's circuital law} \\ \nabla \cdot \mathcal{B} = 0 & \text{magnetic induction is solenoidal.} \end{cases} \tag{2.1}$$

This form clearly demonstrates that electromagnetic fields are imputable to charges and currents [6].

With the help of constitutive relations, which depend on the properties of the materials, $\mathcal{D}$ and $\mathcal{H}$ can be expressed in terms of $\mathcal{E}$ and $\mathcal{B}$, respectively. To specify such a law, we have to establish assumptions for the matter, which is inside the electromagnetic field. As in practice we often have several different materials inside a domain, we therefore presume inhomogeneity. The materials should also be macroscopic and isotropic, where the latter

means that its properties do not depend on the direction of the field. Additionally, we assume linearity. This restriction is justifiable, as it results already in a large number of interesting observations [10]. Thus, we obtain

$$\begin{aligned} \mathcal{D} &= \varepsilon \mathcal{E} \\ \mathcal{H} &= \frac{1}{\mu} \mathcal{B} \end{aligned} \tag{2.2}$$

as constitutive relations. Here, ε is the dielectric constant and μ the permeability of the material. We can assume that both are only depending on the position x.

As we study linear Maxwell equations, we can separate the time dependence from the spatial dependence. This can be done by considering time-harmonic modes of the fields. Combining these, all solutions of the equations can be obtained. The described harmonic modes of the fields are given by

$$\begin{aligned} \mathcal{E}(\mathbf{r},t) &= \mathrm{Re}\left(e^{-i\omega t}\hat{\mathbf{E}}(\mathbf{r})\right), & \mathcal{D}(\mathbf{r},t) &= \mathrm{Re}\left(e^{-i\omega t}\hat{\mathbf{D}}(\mathbf{r})\right), \\ \mathcal{H}(\mathbf{r},t) &= \mathrm{Re}\left(e^{-i\omega t}\hat{\mathbf{H}}(\mathbf{r})\right), & \mathcal{B}(\mathbf{r},t) &= \mathrm{Re}\left(e^{-i\omega t}\hat{\mathbf{B}}(\mathbf{r})\right), \end{aligned} \tag{2.3}$$

where $\hat{\mathbf{E}}$, $\hat{\mathbf{D}}$, $\hat{\mathbf{H}}$ and $\hat{\mathbf{B}}$ are complex-valued vector functions that represent the space-dependent component of Maxwell's equations. Taking the real part results in the physical functions. We can find corresponding expressions for $\mathcal{J}$ and ρ:

$$\mathcal{J}(\mathbf{r},t) = \mathrm{Re}\left(e^{-i\omega t}\hat{\mathbf{J}}(\mathbf{r})\right), \qquad \rho(\mathbf{r},t) = \mathrm{Re}\left(e^{-i\omega t}\hat{\boldsymbol{\rho}}(\mathbf{r})\right).$$

Since $i\omega\hat{\boldsymbol{\rho}} = \nabla\cdot\hat{\mathbf{J}}$, where $\hat{\mathbf{J}} = \sigma\hat{\mathbf{E}} + \hat{\mathbf{J}}_a$ by Ohm's law with the conductivity σ and a given current density $\hat{\mathbf{J}}_a$, and by using the constitutive relations (2.2) and the variables (2.3), we can find the time-harmonic version of Maxwell's equations in differential form to be

$$\begin{cases} -i\omega\mu\hat{\mathbf{H}} + \nabla\times\hat{\mathbf{E}} = 0 \\ \nabla\cdot\left(\varepsilon\hat{\mathbf{E}}\right) = \dfrac{1}{i\omega}\nabla\cdot\hat{\mathbf{J}} \\ -i\omega\varepsilon\hat{\mathbf{E}} - \nabla\times\hat{\mathbf{H}} = -\hat{\mathbf{J}} \\ \nabla\cdot\left(\mu\hat{\mathbf{H}}\right) = 0. \end{cases} \tag{2.4}$$

Note that we write $\hat{\mathbf{H}}$, $\hat{\mathbf{E}}$ and $\hat{\mathbf{J}}$ for the position-dependent terms.

Following [14], we can express the fields $\mathbf{E}$ and $\mathbf{H}$ by

$$\mathbf{E} = \sqrt{\varepsilon_0}\hat{\mathbf{E}} \qquad \text{and} \qquad \mathbf{H} = \sqrt{\mu_0}\hat{\mathbf{H}} \tag{2.5}$$

and define the relative permittivity and permeability as

$$\varepsilon_r = \frac{1}{\varepsilon_0}\left(\varepsilon + \frac{i\sigma}{\omega}\right) \qquad \text{and} \qquad \mu_r = \frac{\mu}{\mu_0}. \tag{2.6}$$

We suppose that both functions are piecewise smooth, positive and do not depend on time.

When plugging (2.5) and (2.6) into the harmonic system (2.4), a new system is obtained:

$$\begin{cases} -ik\mu_r\mathbf{H} + \nabla \times \mathbf{E} = & 0 \\ \nabla \cdot (\varepsilon_r \mathbf{E}) = & -\dfrac{1}{k^2}\nabla \cdot \mathbf{E} \\ -ik\varepsilon_r\mathbf{E} - \nabla \times \mathbf{H} = & -\dfrac{1}{ik}\underbrace{(ik\sqrt{\mu_0}\mathbf{J}_a)}_{\mathbf{F}} \\ \nabla \cdot (\mu_r \mathbf{H}) = & 0, \end{cases} \tag{2.7}$$

where $k = \omega\sqrt{\varepsilon_0\mu_0} = \frac{\omega}{c}$ is the wavenumber, which is the magnitude of the wave vector, and ω^2 should not be a Maxwell eigenvalue.

Now, we can eliminate either the magnetic field $\mathbf{H}$ or the electric field $\mathbf{E}$ by solving the first or the third equation of system (2.7), respectively, and substitute the result into the other one. Here, we express the system as a second order Maxwell equation depending only on $\mathbf{E}$ and obtain the final PDE:

$$\nabla \times (\mu_r^{-1}\nabla \times \mathbf{E}) - k^2\varepsilon_r\mathbf{E} = \mathbf{F}. \tag{2.8}$$

Note that, in the considered case of conserved charges, ρ and $\mathcal{J}$ are connected by $\nabla \cdot \mathcal{J} + \frac{\partial \rho}{\partial t} = 0$. Thus, equations two and four of the system of Maxwell's equations (2.4) and also of the transformed version (2.7) hold for all time.

When setting the source term $\mathbf{F}$ to zero we can compute the n-th Maxwell eigenvalue ω_n and corresponding eigenfunction $\mathbf{E}_n$ by solving the following problem:
Find $(\omega_n, \mathbf{E}_n) \neq (0, \mathbf{0})$ such that

$$\nabla \times \left(\mu_r^{-1}\nabla \times \mathbf{E}_n\right) - k_n^2\varepsilon_r\mathbf{E}_n = \nabla \times \left(\mu_r^{-1}\nabla \times \mathbf{E}_n\right) - \frac{\omega_n^2}{c^2}\varepsilon_r\mathbf{E}_n = 0 \qquad \text{in } \Omega. \tag{2.9}$$

2.2. Periodicity and boundary conditions

If we consider a perfectly periodic medium that is extended infinitely into all directions, the domain Ω equals $\mathbb{R}^3$ and no boundary conditions are needed. However, for the computation of a numerical solution, we have to restrict the problem to a finite domain.

As the photonic crystal is built by the repetition of unit cells, we can choose boundaries of a finite crystals to coincide with those of some unit cells. Fundamental computations for the Maxwell system (2.8) can then be performed on a unit cell with periodic boundary conditions in the interior of the finite crystal and e. g. Dirichlet conditions at outer faces:

$$\mathbf{n} \times \mathbf{E} = \mathbf{g} \qquad \text{on } \partial\Omega.$$

For $\mathbf{g} = \mathbf{0}$ we call these boundary conditions homogeneous.

3. Nédélec's basis functions for discontinuous Galerkin finite element methods

In this chapter, the basic idea of finite element methods and in particular of the discontinuous Galerkin version is presented. Moreover, it is described why this method is beneficial when solving Maxwell's equations numerically. After the introduction to this approach, some features regarding the mesh construction as well as the function spaces and elements, which are used in this study, are discussed. We will then consider the curl-conforming Nédélec basis functions on edge elements. This includes not only their properties, but also why they are applied in the considered case. At the end of this chapter, we establish a technique for the determination of these basis functions.

3.1. Discontinuous Galerkin finite element methods

Finite element methods (FEM) are a class of numerical methods for the solution of partial differential equations where the domain of computation is divided into subdomains (elements). The solution is then approximated elementwise by previously chosen basis functions which are not related to the specific problem. This is done using only local information and without considering neighbouring elements (see [11]). The advantage of these methods, as explained in [7, 8, 11], is that they can handle complex geometries with high-order accuracy. The strictly local character allows the usage of unstructured grids and a straightforward implementation.

Galerkin finite element methods can be applied to all kinds of PDEs. The procedure consists of three major steps. First, a weak formulation of the problem has to be derived. To do so, we take the inner product of each of the equations with a test function. Subsequent integration by parts (to get rid of higher-order derivatives) and the given boundary conditions can be used to further simplify the result. Next, Galerkin's method is applied, meaning that the solution function is expressed in terms of a linear combination of a finite set of basis functions. Finally, the domain is divided into elements by a mesh. The linear system resulting from the previous step can then be solved numerically for each sub-domain, leading to a global approximate solution of the problem [11].

For the *discontinuous Galerkin* (DG) FEM the normal and tangential components do not have to be continuous across element faces[8]. As a main drawback, the continuous case is difficult to combine with a local mesh refinement, which is beneficial for capturing singularities at corners, edges and material interfaces. Furthermore, Maxwell's equations

problematic due to complex geometries and material discontinuities [20]. Discontinuous methods are well suited to the problems of electromagnetism as they offer a great flexibility in the mesh design and a larger choice of basis functions [3, 7]. Thus, they are a good choice for time-harmonic Maxwell equations in periodic media.

In the following, we will have a closer look on some of the features of DG FEM. As this section should only give a short insight to the theory, we will present selected issues that are adopted from [14]. This book is a good reference for a more detailed discussion of the topic and for proofs, which will not be shown here.

3.1.1. The mesh

As mentioned before, the domain of consideration, Ω, has to be divided into a finite number of subdomains that form the set $\mathcal{T}_h = \{K\}$. Such a mesh has to fulfill the following geometric constraints for FEM:

1. $\bar{\Omega} = \bigcup_{K \in \mathcal{T}_h} \bar{K}$, where $\bar{\cdot}$ denotes the closure.
2. For each $K \in \mathcal{T}_h$, K is an open set with a positive volume.
3. If K_1 and K_2 are distinct elements in $\mathcal{T}_h$, then they are disjoint ($K_1 \cap K_2 = \emptyset$).
4. Each $K \in \mathcal{T}_h$ is a Lipschitz domain (i. e. boundaries are sufficiently regular).

For elements we can define the following parameters and properties:

Definition 3.1. We call h_K, the diameter of the smallest sphere that contains $\bar{K}$, the *diameter of the element*. Then, $h = \max_{K \in \mathcal{T}_h} h_K$ denotes the *maximal diameter of all elements* $K \in \mathcal{T}_h$. Let further ρ_K be the diameter of the largest sphere contained in $\bar{K}$.

The relationship between h_K and ρ_K can be expressed through $\sigma_K = \frac{h_K}{\rho_K}$. Similarly, define $\sigma_h = \max_{K \in \mathcal{T}_h} \sigma_K$ as a parameter of the mesh.

Suppose we have a family of meshes $\{\mathcal{T}_h \mid h > 0\}$. We speak of the *standard h-version*, when analysing the error of a numerical method on these meshes with decreasing parameter h.

Such a family of meshes is called *regular* as $h \to 0$ if we can find constants $\sigma_{min} > 0$ and $h_0 > 0$ such that

$$\sigma_h \geq \sigma_{min} \qquad \forall h \text{ with } 0 < h \leq h_0.$$

For good approximations of the solution, regular meshes are desirable. Irregular ones with $\sigma_{min} \approx 0$ lead to ill-conditioned linear systems.

Generating a grid requires a geometric model of the domain Ω and a fixed value for h. For the process of the finite element discretisation, it is necessary that, during the creation of the mesh, a list of all vertices, edges and faces is provided. It is also important to indicate which vertices belong to the various elements and to label boundary nodes.

Before the grid is used, it has to be checked whether it is non-degenerate and satisfies the geometric constraints.

The simplest three-dimensional mesh that can be built is a tetrahedral mesh of a polyhedral domain. Therefore, we will restrict ourselves to a regular-shaped grid of tetrahedra. To obtain a well-defined finite element mesh, next to the general constraints of FEM, we can find that elements $K \in \mathcal{T}_h$ have to satisfy one of the following geometric restrictions:

- Two elements meet at a single point that is vertex of both elements.
- Two elements meet along a common edge and the endpoints of this edge are vertices of both of the elements.
- Two elements meet at a common face and the vertices of the face are vertices of both elements.

Families of grids of this kind are regular if the tetrahedra do not flatten out when decreasing h.

Tetrahedral meshes are in general *unstructured*. That means that the arrangement of the elements does not follow a fixed pattern. This setting is suitable for more complex domains. However, due to a simpler implementation and a better performance, structured grids are often preferred.

3.1.2. The reference element and affine mappings

Often it is easier to consider a *reference element* $\hat{K}$ of simple shape and given size. All operations are first defined on this element and general results are then obtained by mapping from the reference element to the physical one.

In the case of tetrahedra, the reference element is defined by the vertices $\hat{v}_1 = (0,0,0)^T$, $\hat{v}_2 = (1,0,0)^T$, $\hat{v}_3 = (0,1,0)^T$ and $\hat{v}_4 = (0,0,1)^T$. Directed edges $\hat{e}_j$ point from a node v_{i_1} to another one v_{i_2}, where $i_1 < i_2$. Here, $\boldsymbol{\tau}_j$ denotes the corresponding unit tangential vector. For the faces $\hat{f}_1, \ldots, \hat{f}_4$ have outward pointing normal vectors $\mathbf{n}_1, \ldots, \mathbf{n}_4$, respectively. The tetrahedron can be seen in Figure 3.1.

Definition 3.2. For any $K \in \mathcal{T}_h$ there is an *affine mapping* $F_K : \hat{K} \mapsto K$, such that

$$F_K\left(\hat{K}\right) = K \qquad \text{and} \qquad F_K\hat{\mathbf{x}} = B_K\hat{\mathbf{x}} + \mathbf{b}_K,$$

where $\mathbf{b}_K$ is a vector, B_K a non-singular (3×3)-matrix and $\hat{\mathbf{x}}$ a point in the reference element. K has a non-empty interior and its volume is given by $\frac{|\det(B_K)|}{6}$, as the volume of the reference element is $\frac{1}{6}$. The properties of B_K define the effects of the mapping F_K.

Both $\mathbf{b}_K$ and B_K are easy to compute. Let the vertices of K be $v_1, \ldots, v_4$. Choose the affine mapping F_K such that $F_K(\hat{v}_i) = v_i$, where $1 \leq i \leq 4$. Then

$$\mathbf{b}_k = v_1 \qquad \text{and} \qquad B_K \text{ is the matrix with } j\text{-th column given by } v_{j+1} - v_1.$$

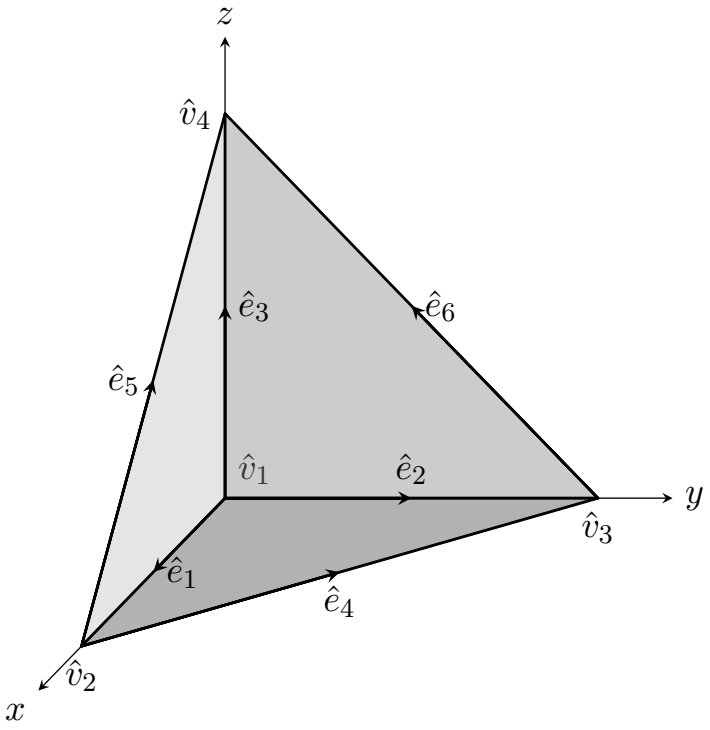

Figure 3.1.: The reference tetrahedron that is used in the finite element discretisation is shown here. The vertices and directed edges are labeled. For clarity, the outward pointing normals of the faces are not pictured.

The affine mapping between the reference element and the element in the physical space also induces functions defined on the corresponding vertices.

Lemma 3.3. *Scalar functions experience a change of variables. When $\hat{q}$ is a scalar function on $\hat{K}$, we can determine the function q on the physical element by*

$$q\left(F_K\left(\hat{\mathbf{x}}\right)\right) = \hat{q}\left(\hat{\mathbf{x}}\right), \quad (\textit{or } q \circ F_K = \hat{q}).$$

The transformation of gradients is given by

$$\left(\nabla q\right) \circ F_K = B_K^{-T} \hat{\nabla} \hat{q},$$

where $\hat{\nabla}$ is the gradient with respect to $\hat{\mathbf{x}}$.

3.1.3. The considered function spaces

We need a finite element space that is suitable for discretising Maxwell's equations. That means that the space has to provide elements that can deal with geometric complexities and their consequences as well as discontinuous electromagnetic properties. $\mathrm{H}\left(\mathrm{curl}; \Omega\right)$, corresponding to the space of finite-energy solutions, is of great importance

for problem (2.8). As mentioned before, only some relations (without proof) will be presented here. However, a wide range of mathematical properties of $\mathrm{H}(\mathrm{curl};\Omega)$ and their consequences are discussed in detail in [14].

Let us first recall some definitions of simple functional spaces and establish the corresponding notions. We consider $\Omega \subseteq \mathbb{R}^N$ for $N \in \mathbb{N}$ open.

Definition 3.4. $\mathrm{C}^k(\Omega)$ denotes the space of all k times continuously differentiable functions, $\mathrm{C}_0^k(\Omega)$ is the set of functions in $\mathrm{C}^k(\Omega)$ with compact support and $\mathrm{L}^p(\Omega)$, $1 \leq p < \infty$ is the space of functions $\mathbf{u}$ on Ω with $\int\limits_\Omega |\mathbf{u}|^p \,\mathrm{d}\, V < \infty$. For $p = 2$ we obtain the square-integrable functions.

Consider two locally integrable functions $\mathbf{u}, \mathbf{v} \in \mathrm{L}^1_{\mathrm{loc}}(\Omega)$. Let $\boldsymbol{\alpha}$ be a multi-index. Then $\mathbf{v}$ is called the $\boldsymbol{\alpha}$-th *weak partial derivative* of $\mathbf{u}$, written $\mathrm{D}^{\boldsymbol{\alpha}}\mathbf{u} = \mathbf{v}$, if

$$\int\limits_\Omega \mathbf{u}\mathrm{D}^{\boldsymbol{\alpha}}\psi \,\mathrm{d}\, V = (-1)^{|\boldsymbol{\alpha}|} \int\limits_\Omega \mathbf{v}\psi \,\mathrm{d}\, V$$

for all test functions $\psi \in \mathrm{C}_0^\infty(\Omega)$.

Sobolov spaces for s being a non-negative integer, $1 \leq p < \infty$, are defined as

$$\mathrm{W}^{s,p}(\Omega) = \left\{\mathrm{L}^p(\Omega) \mid \mathbf{v} = \mathrm{D}^{\boldsymbol{\alpha}}\mathbf{u} \in \mathrm{L}^p(\Omega), \quad \forall |\boldsymbol{\alpha}| \leq s\right\}.$$

Their norms are given by

$$\|\mathbf{u}\|_{\mathrm{W}^{s,p}(\Omega)} = \left(\sum_{|\boldsymbol{\alpha}| \leq s}\right) \int\limits_\Omega |\mathrm{D}^{\boldsymbol{\alpha}}|^p \,\mathrm{d}\, V^{1/p}.$$

Particularly important is again the case of $p = 2$. Denote $\mathrm{W}^{s,2}(\Omega)$ by $\mathrm{H}^s(\Omega)$. $\mathrm{H}_0^s(\Omega)$ is the closure of $\mathrm{C}_0^\infty(\Omega)$ in the $\mathrm{H}^s(\Omega)$-norm.

With that basis in mind we can specify the space of interest:

Definition 3.5. The energy space for Maxwell's equations is given by

$$\mathrm{H}(\mathrm{curl};\Omega) = \left\{\mathbf{v} \in \left(\mathrm{L}^2(\Omega)\right)^3 \mid \nabla \times \mathbf{v} \in \left(\mathrm{L}^2(\Omega)\right)^3\right\}$$

with norm

$$\|\mathbf{v}\|_{\mathrm{H}(\mathrm{curl};\Omega)} = \left(\|\mathbf{v}\|_{(\mathrm{L}^2(\Omega))^3} + \|\nabla \times \mathbf{v}\|_{(\mathrm{L}^2(\Omega))^3}\right)^{1/2}.$$

We denote with $\mathrm{H}_0(\mathrm{curl};\Omega)$ the closure of $(\mathrm{C}_0^\infty(\Omega))^3$ in $\mathrm{H}(\mathrm{curl};\Omega)$.

In the following, let Ω be a bounded Lipschitz domain in $\mathbb{R}^3$.

Lemma 3.6. *Choose* $\mathbf{u} \in \mathrm{H}(\mathrm{curl};\Omega)$ *such that*

$$\forall \phi \in \left(\mathrm{C}^\infty\left(\bar{\Omega}\right)\right)^3 : \quad (\nabla \times \mathbf{u}, \phi) - (\mathbf{u}, \nabla \times \phi) = 0.$$

Then, $\mathbf{u} \in \mathrm{H}_0(\mathrm{curl};\Omega)$.

The energy space of Maxwell's equations is subject to the physical requirement that well-defined electric fields need a tangential trace. Therefore, trace properties of $\mathrm{H}(\mathrm{curl};\Omega)$ have to be considered.

Definition 3.7. Let $\mathbf{v} \in \left(\mathrm{C}^\infty\left(\bar{\Omega}\right)\right)^3$ be a smooth vector function and $\mathbf{n}$ the unit outward normal to Ω. Then two trace functions can be defined:

$$\gamma_t(\mathbf{v}) = \mathbf{n} \times \mathbf{v}|_{\partial\Omega}$$

$$\gamma_T(\mathbf{v}) = (\mathbf{n} \times \mathbf{v}|_{\partial\Omega}) \times \mathbf{n}$$

The trace space is given by

$$\mathrm{Y}(\partial\Omega) = \left\{\mathbf{f} \in \left(\mathrm{H}^{-1/2}(\partial\Omega)\right)^3 \mid \exists \mathbf{u} \in \mathrm{H}(\mathrm{curl};\Omega) \text{ with } \gamma_t(\mathbf{u}) = \mathbf{f}\right\}$$

and provides the norm

$$\|\mathbf{f}\|_{\mathrm{Y}(\partial\Omega)} = \inf_{\mathbf{u}\in\mathrm{H}(\mathrm{curl};\Omega),\gamma_t(\mathbf{u})=\mathbf{f}} \|\mathbf{u}\|_{\mathrm{H}(\mathrm{curl};\Omega)}.$$

The trace space $\mathrm{Y}(\partial\Omega)$ is a Hilbert space and the mapping $\gamma_t : \mathrm{H}(\mathrm{curl};\Omega) \mapsto \mathrm{Y}(\partial\Omega)$ is surjective.

Lemma 3.8. *Let* $\mathbf{v} \in \mathrm{H}(\mathrm{curl};\Omega)$ *and* $\phi \in \left(\mathrm{H}^1(\Omega)\right)^3$. *Then, the following version of Green's theorem holds:*

$$(\nabla \times \mathbf{v}, \phi) - (\mathbf{v}, \nabla \times \phi) = \langle \gamma_t(\mathbf{v}), \phi \rangle_{\partial\Omega}.$$

Lemma 3.9. *With the former result, an alternative definition for the space* $\mathrm{H}_0(\mathrm{curl};\Omega)$ *can be found:*

$$\begin{aligned}\mathrm{H}_0(\mathrm{curl};\Omega) &= \{\mathbf{v} \in \mathrm{H}(\mathrm{curl};\Omega) \mid \gamma_t(\mathbf{v}) = 0\} \\ &= \left\{\mathbf{v} \in \mathrm{H}(\mathrm{curl};\Omega) \mid (\mathbf{u}, \nabla \times \phi) = (\nabla \times \mathbf{u}, \phi), \quad \forall \phi \in \left(\mathrm{C}^\infty\left(\bar{\Omega}\right)\right)^3\right\}.\end{aligned}$$

This energy space and its properties are of importance when discretising Maxwell's equations.

3.1.4. Finite elements

Following a common approach, we describe finite elements with the triple (K, P_K, Σ_K), where

- K is the geometric domain (in our case a tetrahedron),
- P_K is a space of functions (polynomials) on K and
- Σ_K is a set of linear functionals on P_K, called the *degrees of freedom* of the FE.

We will now examine general finite elements by considering features that influence the FEM.

Definition 3.10. A finite element is called *unisolvent*, if each function in P_K is uniquely determined by the corresponding degrees of freedom.

Then the degrees of freedom can be used to construct a basis for P_K:
Consider a general FE with degrees of freedom $\Sigma_K = \{l_n, 1 \leq n \leq m\}, \quad m \geq 1, \quad m, n \in \mathbb{Z}^+$. Unisolvency requires that the space P_K is of dimension m. We can then find a consistent well-defined basis $\{\varphi_j\}_{j=1}^m$ of P_K and $l_n(\varphi_j) = \delta_{nj}$, $1 \leq n \leq m$. Then all $q \in P_K$ can be expressed by

$$q(x) = \sum_{j=1}^{m} l_j(q)\, \phi_j(x).$$

The interpolant of a FE can be used to estimate the error in the solution of FEM.

Definition 3.11. Let (K, P_K, Σ_K) be a finite element and u a suitably smooth function. Then the *interpolant* $\pi_K u$ on K is a unique function such that

$$l(\pi_K u - u) = 0 \quad \forall l \in \Sigma_K.$$

The operator $\pi_K : \mathrm{C}(K) \mapsto P_K$ is the *interpolation operator*.

As the definition of the interpolant shows, the properties of a finite element depend on its degrees of freedom. Thus, when constructing a space of functions not only on one element K, but on the whole domain Ω with a set of elements $\mathcal{T}_h$, we have to consider the global degrees of freedom. They are obtained by uniting Σ_K for all $K \in \mathcal{T}_h$:

$$\Sigma = \bigcup_{K \in \mathcal{T}_h} \Sigma_K.$$

Reversely, the values for all the degrees of freedom in Σ also specify the ones on each element. Computing the degrees of freedom, we can determine the global FE functions.

A global interpolant $\pi_h u$ in the FE space can be computed for a suitably smooth function u based on $\pi_K u$ on K. Then

$$\pi_h u \in S_h = \{u_h \in \mathrm{C}(\Omega) \mid u_h \mid_K \in P_K \text{ for every element } K \text{ in the mesh}\}.$$

An estimate helps to determine the rate at which the interpolation error decreases (and thus at which the approximation error does) as the mesh is refined.

Definition 3.12. Let $\mathcal{W}$ be a space of functions. The FE (K, P_K, Σ_K) is said to be $\mathcal{W}$*-conforming* if the corresponding global finite element space is a subspace of $\mathcal{W}$.

Lemma 3.13. *Suppose K_1 and K_2 are non-overlapping Lipschitz domains that meet at a common surface, Σ, of non-zero measure. Assume further that $\bar{K_1} \cap \bar{K_2} = \Sigma$.*

1. *Let $q_1 \in \mathrm{H}^1(K_1), q_2 \in \mathrm{H}^1(K_2)$. Define $q \in \mathrm{L}^2(K_1 \cup K_2 \cup \Sigma)$ by*

$$q = \begin{cases} q_1 & \text{on } K_1, \\ q_2 & \text{on } K_2. \end{cases}$$

   If $q_1 = q_2$ on Σ, then $q \in \mathrm{H}^1(K_1 \cup K_2 \cup \Sigma)$.

2. *Let $\mathbf{u}_1 \in \mathrm{H}(\mathrm{curl}; K_1)$, $\mathbf{u}_2 \in \mathrm{H}(\mathrm{curl}; K_2)$. Define $\mathbf{u} \in \left(\mathrm{L}^2(K_1 \cup K_2 \cup \Sigma)\right)^3$ by*

$$\mathbf{u} = \begin{cases} \mathbf{u}_1 & \text{on } K_1, \\ \mathbf{u}_2 & \text{on } K_2. \end{cases}$$

   Then, if $\mathbf{u}_1 \times \mathbf{n} = \mathbf{u}_2 \times \mathbf{n}$ on Σ and for $\mathbf{n}$ being the unit normal to Σ, we have

$$\mathbf{u} \in \mathrm{H}(\mathrm{curl}; K_1 \cup K_2 \cup \Sigma).$$

3.1.5. Curl-conforming edge elements

In this section we will discuss a type of elements that are appropriate for the discretisation of Maxwell's equations, the so-called *curl-conforming edge elements*. *Edge elements* owe their name to the fact that the degrees of freedom at lowest order ($p = 1$) are associated with the edges of the mesh. They are created such that tangential continuity between neighbouring elements is provided. This feature simplifies the handling of boundary and interface conditions as well as the modeling of field singularities. Curl-conformity relates to the fact that these elements are $\mathrm{H}(\mathrm{curl}; \Omega)$-conforming.

As finite element spaces are built using piecewise polynomial functions, we define some sets of polynomials. These will be used for the construction of the curl-conforming elements.

Definition 3.14. Let

$$P_p = \{\text{polynomials of maximum total degree } p \text{ in } x_1, x_2, x_3\}$$

and

$$\tilde{P}_p = \{\text{homogeneous polynomials of total degree exactly } p \text{ in } x_1, x_2, x_3\}.$$

The *subspace of homogeneous vector polynomials of degree p* is given by

$$\mathcal{S}_p = \left\{ \mathbf{q} \in \left(\tilde{P}_p\right)^3 \mid \mathbf{x} \cdot \mathbf{q} = 0 \right\}$$

with dimension

$$\dim \mathcal{S}_p = 3 \cdot \dim\left(\tilde{P}_p\right) - \dim\left(\tilde{P}_{p+1}\right) = \frac{3}{2}(p+2)(p+1) - \frac{1}{2}(p+3)(p+2) = p(p+2).$$

Define the *Nédélec space*, a special space of polynomials, by

$$R_p = (P_{p-1})^3 \oplus \mathcal{S}_p,$$

where $\oplus$ denotes the direct sum, with dimension

$$\dim(R_p) = 3 \cdot \dim(P_{p-1}) + \dim(\mathcal{S}_p) = \frac{1}{2}(p+3)(p+2)p.$$

Then the following algebraic decomposition holds:

$$(P_p)^3 = R_p \oplus \nabla \tilde{P}_{p+1}.$$

Lemma 3.15. *If* $\mathbf{u} \in R_p$ *satisfies* $\nabla \times \mathbf{u} = 0$*, then* $\mathbf{u} = \nabla q$ *for some* $q \in P_k$*.*

The curl-conforming element on the reference tetrahedron can then be defined using the special polynomial space.

Definition 3.16. A *curl-conforming element* is defined by

- $\hat{K}$, the reference tetrahedron
- $P_{\hat{K}} = R_p$, the polynomial space
- degrees of freedom of three types: those associated with the edges $\hat{e}$, those associated with the faces $\hat{f}$ and those associated with the element $\hat{K}$.

For the unit vector $\hat{\boldsymbol{\tau}}$ in the direction of $\hat{e}$ and the outward pointing normal $\hat{\mathbf{n}}$ at the face $\hat{f}$, the degrees of freedom are defined as follows:

1. degrees of freedom associated to edges

$$M_{\hat{e}}(\hat{\mathbf{u}}) = \left\{ \int_{\hat{e}} \hat{\mathbf{u}} \cdot \hat{\boldsymbol{\tau}} \hat{q} \, \mathrm{d}\hat{s}, \quad \forall \hat{q} \in P_{p-1}(\hat{e}) \text{ for each edge } \hat{e} \text{ of } \hat{K} \right\}$$

2. degrees of freedom associated to faces

$$M_{\hat{f}}(\hat{\mathbf{u}}) = \left\{ \frac{1}{\operatorname{area}\left(\hat{f}\right)} \int_{\hat{f}} \hat{\mathbf{u}} \cdot \hat{\mathbf{q}} \, \mathrm{d}\hat{A}, \quad \text{for each face } \hat{f} \text{ of } \hat{K}, \right.$$
$$\left. \hat{\mathbf{q}} \in \left(P_{p-2}\left(\hat{f}\right)\right)^3 \text{ and } \hat{\mathbf{q}} \cdot \hat{\mathbf{n}} = 0 \right\}$$

3. degrees of freedom associated to the element

$$M_{\hat{K}}(\hat{\mathbf{u}}) = \left\{ \int_{\hat{K}} \hat{\mathbf{u}} \cdot \hat{\mathbf{q}} \, \mathrm{d}\hat{V}, \quad \forall \hat{\mathbf{q}} \in \left(P_{p-3}\left(\hat{K}\right)\right)^3 \right\}.$$

Then, the degrees of freedom are given by

$$\Sigma_{\hat{K}} = M_{\hat{e}}\left(\hat{\mathbf{u}}\right) \cup M_{\hat{f}}\left(\hat{\mathbf{u}}\right) \cup M_{\hat{K}}\left(\hat{\mathbf{u}}\right).$$

To obtain the finite elements on a general tetrahedron in $\mathrm{H}\left(\mathrm{curl}; \hat{K}\right)$, we have to apply a special transformation:

- Let $\hat{\mathbf{u}} \in R_p$ be a vector function on $\hat{K}$. Define $\mathbf{u}$ on K in the special case of an affine map F_K by the transformation

$$\mathbf{u} \circ F_K = \left(B_K{}^T\right)^{-1} \hat{\mathbf{u}}.$$

- Curls of $\mathbf{u}$ and $\hat{\mathbf{u}}$ are then related through

$$\nabla \times \mathbf{u} = \frac{1}{\det\left(B_K\right)} B_K \hat{\nabla} \times \hat{\mathbf{u}}.$$

- Also, the tangent vectors have to be transformed under the affine map. Let $\hat{\boldsymbol{\tau}}$ be the tangential to $\hat{e}$ in the reference element. Then

$$\boldsymbol{\tau} = \frac{B_K \hat{\boldsymbol{\tau}}}{|B_K \hat{\boldsymbol{\tau}}|}$$

  is tangent vector to the edge e of element K.

Lemma 3.17. *R_p is invariant under this special transformation.*

Definition 3.18. The *curl conforming element on a general tetrahedron K* are defined by

- K, the tetrahedron
- $P_K = R_p$, the polynomial space
- degrees of freedom associated with edges e of K, the faces f of K and the element K.

Let $\boldsymbol{\tau}$ be the unit vector in the direction of e. The degrees of freedom are given by

1. degrees of freedom associated with edges

$$M_e\left(\mathbf{u}\right) = \left\{ \int_e \mathbf{u} \cdot \boldsymbol{\tau} q \,\mathrm{d}\, s, \quad \forall q \in P_{p-1}\left(e\right) \text{ for each edge } e \text{ of } K \right\}$$

2. degrees of freedom associated with faces

$$M_f\left(\mathbf{u}\right) = \Bigg\{ \frac{1}{\mathrm{area}\left(f\right)} \int_f \mathbf{u} \cdot \mathbf{q} \,\mathrm{d}\, A, \quad \text{for each face } f \text{ of } K$$
$$\text{and for all } \mathbf{q} = B_K \hat{\mathbf{q}}, \quad \hat{\mathbf{q}} \in \left(P_{k-2}\left(\hat{f}\right)\right)^3, \hat{\mathbf{q}} \cdot \hat{\mathbf{n}} = 0 \Bigg\}$$

3. degrees of freedom associated with volume

$$M_K(\mathbf{u}) = \Big\{ \int_K \mathbf{u}\cdot\mathbf{q}\,\mathrm{d}V, \quad \forall \mathbf{q} \text{ obtained by mapping } \hat{\mathbf{q}} \in (P_{k-3})^3 \text{ by } \mathbf{q}\circ F_K = \frac{1}{\det(B_K)} B_K \hat{\mathbf{q}} \Big\}.$$

Then

$$\Sigma_K = M_e(\mathbf{u}) \cup M_f(\mathbf{u}) \cup M_K(\mathbf{u}).$$

We can relate the curl-conforming elements on the reference element to those on a general tetrahedron by considering the degrees of freedom.

Lemma 3.19. *Suppose* $\det(B_K) > 0$. *Let* $\boldsymbol{\tau}$ *be the tangent vectors on the edges of* K *obtained from* $\hat{K}$ *under the affine mapping* F_K. *Then each of the sets of degrees of freedom for* $\mathbf{u}$ *on* K *is identical to degrees of freedom for* $\hat{\mathbf{u}}$ *on* $\hat{K}$.

Lemma 3.20. *The finite elements described in Definitions 3.16 and 3.18 are* $\mathrm{H}(\mathrm{curl};\Omega)$*-conforming and unisolvent (see Definitions 3.10 and 3.12).*

Definition 3.21. The corresponding global *finite element space* on the mesh $\mathcal{T}_h$ for the curl-conforming elements is given by

$$V_h = \{\mathbf{u} \in \mathrm{H}(\mathrm{curl};\Omega) \mid \mathbf{u}|_K \in R_k \text{ for all } K \in \mathcal{T}_h\}.$$

Definition 3.22. For a necessarily smooth function $\mathbf{u}$, the *interpolant* $\mathbf{r}_K\mathbf{u}$ is in R_k for $K \in \mathcal{T}_h$ and characterized by the vanishing of the degrees of freedom on $\mathbf{u} - \mathbf{r}_K\mathbf{u}$,

$$M_e(\mathbf{u} - \mathbf{r}_K\mathbf{u}) = M_f(\mathbf{u} - \mathbf{r}_K\mathbf{u}) = M_K(\mathbf{u} - \mathbf{r}_K\mathbf{u}) = \{0\}.$$

Thus, the global interpolant $\mathbf{r}_h\mathbf{u} \in V_h$ can be defined using $\mathbf{r}_h\mathbf{u}\,|_K = \mathbf{r}_K\mathbf{u}$ for all $K \in \mathcal{T}_h$.

3.2. Nédélec basis functions

As described before, the DG FEM is advantageous for problems in electromagnetism (see [3]). It provides a good performance combined with an easy implementation. However, the quality of a FEM does also depend on the selected basis functions. Finite element methods in general and thus also DG FEM can suffer from spurious modes. These are numerical but nonphysical solutions of a problem. Yet, when choosing appropriate basis functions, these modes can be prevented. Buffa and Perugia proved that the DG FEM solution is spurious-free when using elementwise Nédélec elements of the first family (conforming in $\mathrm{H}(\mathrm{curl};\Omega)$) for the DG approximation [3].

Nédélec's idea is based on the fact that in electromagnetics the curl of the field and the field itself are often of similar importance. The convergence of the method is then dominated by the order of the approximation of the curl. Thus, to obtain a better balance

in accuracy of the representation of the field and its curl, the degrees of freedom that do not affect the curl are removed.

For the order $p = 1$ basis functions of this kind were already known and discussed in the 1970s. However, the most important publication was, and still is [15], in which Nédélec introduces a whole family of new basis functions in $\mathbb{R}^3$.

Only in 2005 a general way of finding Nédélec's basis functions in affine coordinates of any order and in any dimension was established [5]. This construction process in general and for the example of $p = 1$ will be described in the next section.

3.2.1. Construction of Nédélec's basis functions

The main property that general basis functions have to fulfill is to be non-zero in a very limited number of elements. As further requirements, the basis functions have to be linearly independent and span the complete target space Σ. The test functions that are used to obtain the weak formulation of the problem should also be a member of this space. Additionally, the basis functions should be nearly orthogonal such that any function in Σ can be approximated accurately by the superposition of a limited number of basis functions [11].

In [5], a way is shown to construct such basis functions for the Nédélec space of dimension N and order p. In this process, we will use notations for multi-indexing: The considered set of multi-indices is given by

$$I(N,p) = \left\{ \boldsymbol{\alpha} = (\alpha_1, \ldots, \alpha_N) \mid \alpha_i \geq 0, \sum_{i=1}^{N} \alpha_i = p \right\},$$

where $\mathbf{x}^{\boldsymbol{\alpha}} = x_1^{\alpha_1} \cdot \ldots \cdot x_N^{\alpha_N}$ for $\mathbf{x} \in \mathbb{R}^N$ and $\alpha_i \in \mathbb{N}$, $i = 1, \ldots, N$. There is a partition of this set into p disjoint subsets

$$I_j(N,p) = \{\boldsymbol{\beta} \in I(N,p) \mid \text{exactly } j \text{ components of the vector } \boldsymbol{\beta} \text{ are non-zero}\},$$

where $I_j(N,p) = \emptyset$ if $j > p$.

We know that the set $\mathcal{S}_p$ contains all homogeneous polynomials $\mathbf{q}$ of R_p. Let $\mathbf{q}$ be of the form

$$\mathbf{q} = \sum_{l=1}^{N} \left(\sum_{\boldsymbol{\alpha} \in I(N,p)} \right) c_{\alpha,l} \mathbf{x}^{\boldsymbol{\alpha}} \mathbf{e}_l, \tag{3.1}$$

where $\mathbf{e}_l$ denotes the l-th unit vector.

Then the space $\mathcal{S}_p$ can be characterised with the help of the following theorem:

Theorem 3.23. *A homogeneous polynomial with the representation* (3.1) *is in R_p if and only if*

$$\sum_{l=1}^{N} c_{\boldsymbol{\beta}-\mathbf{e}_l,l} = 0 \qquad \forall \boldsymbol{\beta} \in I(N, p+1). \tag{3.2}$$

Equation (3.2) characterises the space $\mathcal{S}_p$ as defined in Definition 3.14. Thus, solving the null space for this equation yields a basis of the space of homogeneous polynomials.

Consider a vector $\boldsymbol{\beta} \in I_j(N, p+1)$ and choose integers $l(1), \ldots, l(j)$ such that

$$\boldsymbol{\beta}_{l(m)} \begin{cases} > 0 & \text{for all } m \in \{1, \ldots, j\}, \\ = 0 & \text{otherwise.} \end{cases}$$

We can then find a collection of $j-1$ functions for each of these vectors $\boldsymbol{\beta}$ by

$$B_p^{\boldsymbol{\beta}} = \{\mathbf{x}^{\boldsymbol{\beta}-e_{l(m)}} e_{l(m)} - \mathbf{x}^{\boldsymbol{\beta}-e_{l(m+1)}} e_{l(m+1)}, \quad m = 1, \ldots, j-1\}.$$

For each j we have

$$B_p^j = \bigcup_{\boldsymbol{\beta} \in I_j(N,p+1)} B_p^{\boldsymbol{\beta}}$$

and the set

$$B_p = B_p^2 \cup \ldots \cup B_p^N,$$

which is a basis of $\mathcal{S}_p$. The proof can be done by showing the linear independence of the vectors in this set and by comparing the dimension of the set with the one of $\mathcal{S}_p$. Details can be found in [5].

Now, we can concentrate on N-simplicial elements. They have $N+1$ vertices v_j, where $j = 1, \ldots, N+1$, with Lagrangian basis functions λ_i, where $i = 1, \ldots, N+1$, such that $\lambda_i(v_j) = \delta_{ij}$. Let us write $\boldsymbol{\lambda} = (\lambda_1, \ldots, \lambda_{N+1})^t$.

When determining the basis of $\mathcal{S}_p$ in the dimension $N+1$, we can perform a substitution. For that purpose, select any basis function

$$b_{\boldsymbol{\beta}}(x, e_{l(m)}, e_{l(m+1)}) = \mathbf{x}^{\boldsymbol{\beta}-e_{l(m)}} - \mathbf{x}^{\boldsymbol{\beta}-e_{l(m+1)}}, \boldsymbol{\beta} \in I(N+1, p+1).$$

Then replace $\mathbf{x}$ by $\boldsymbol{\lambda}$, $e_{l(m)}$ by $\nabla\lambda_{l(m)}$ and $e_{l(m+1)}$ by $\nabla\lambda_{l(m+1)}$. A new set of functions

$$\Lambda_p^j = \{b_{\boldsymbol{\beta}}(\lambda, \nabla\lambda_{l(m)}, \nabla\lambda_{l(m+1)}) \mid b_{\boldsymbol{\beta}}(\mathbf{x}, e_{l(m)}, e_{l(m+1)})\}$$

is obtained, which now consists of functions in $\mathbb{R}^N$.

The set $\Lambda_p = \bigcup_{j=2,\ldots,N+1} \Lambda_p^j$ is then a basis of the Nédélec space.

Note that there is a natural correspondence between $I_j(N, p+1)$ and Nédélec's edge, face and interior degrees of freedom for $j = 1, 2, 3$, respectively, when choosing $N = 3$.

3.2.2. Basis functions of order $p = 1$

The established process for the determination of Nédélec's basis functions will be shown by the example of $N = 3$ and $p = 1$. That means that we compute first-order functions on tetrahedral elements. The results for higher orders can be found in the Appendix A.3.

As a first step we have to determine the set of multi-indices $I(N+1, p+1) = I(4,2)$ by the union of its partition into

$$I_1(4,2) = \left\{ \begin{pmatrix} 2 \\ 0 \\ 0 \\ 0 \end{pmatrix}, \begin{pmatrix} 0 \\ 2 \\ 0 \\ 0 \end{pmatrix}, \begin{pmatrix} 0 \\ 0 \\ 2 \\ 0 \end{pmatrix}, \begin{pmatrix} 0 \\ 0 \\ 0 \\ 2 \end{pmatrix} \right\}$$

and

$$I_2(4,2) = \left\{ \begin{pmatrix} 1 \\ 1 \\ 0 \\ 0 \end{pmatrix}, \begin{pmatrix} 1 \\ 0 \\ 1 \\ 0 \end{pmatrix}, \begin{pmatrix} 1 \\ 0 \\ 0 \\ 1 \end{pmatrix}, \begin{pmatrix} 0 \\ 1 \\ 1 \\ 0 \end{pmatrix}, \begin{pmatrix} 0 \\ 1 \\ 0 \\ 1 \end{pmatrix}, \begin{pmatrix} 0 \\ 0 \\ 1 \\ 1 \end{pmatrix} \right\}.$$

Next, consider the vectors in $I_2(4,2)$ step by step. As an example let us look at $\boldsymbol{\beta} = \begin{pmatrix} 1 \\ 1 \\ 0 \\ 0 \end{pmatrix} \in I_2(4,2)$. Choose integers $l(1) = 1$ and $l(2) = 2$. Then a basis function of $\mathcal{S}_p$ in dimension $N+1 = 4$ is given by

$$b_{\boldsymbol{\beta}} = \mathbf{x}^{\boldsymbol{\beta}-\mathbf{e}_1}\mathbf{e}_1 - \mathbf{x}^{\boldsymbol{\beta}-\mathbf{e}_2}\mathbf{e}_2 = x_2\mathbf{e}_1 - x_1\mathbf{e}_2.$$

Rewrite this function by substituting the variables as described above to obtain

$$b_{\boldsymbol{\beta}}(\boldsymbol{\lambda}, \nabla\lambda_1, \nabla\lambda_2) = \lambda_2\nabla\lambda_1 - \lambda_1\nabla\lambda_2.$$

Repeating this procedure for all $\boldsymbol{\beta} \in I(4,2) = I_2(4,2)$, we find the set of basis functions

$$\Lambda_1 = \{\lambda_j\nabla\lambda_i - \lambda_i\nabla\lambda_j, \quad i,j = 1,2,3,4, i < j\}.$$

We will need the curl of the basis functions when discretising the problem using the DG FEM. For the computation of the curl we use the identities

$$\nabla \times (fA) = f \cdot (\nabla \times A) - A \times (\nabla f)$$

and

$$\nabla (f \cdot g) = f\nabla g + g\nabla f.$$

For the general basis function of order $p = 1$, we get

$$\begin{aligned} \psi_{ij} =& \lambda_j\nabla\lambda_i - \lambda_i\nabla\lambda_j \\ \nabla \times \psi_{ij} =& \nabla \times \lambda_j\nabla\lambda_i - \nabla \times \lambda_i\nabla\lambda_j \\ =& \lambda_j \underbrace{(\nabla \times \nabla\lambda_i)}_{=0} - \nabla\lambda_i \times \nabla\lambda_j - \lambda_i \underbrace{(\nabla \times \nabla\lambda_j)}_{=0} + \nabla\lambda_j \times \nabla\lambda_i \\ =& \nabla\lambda_j \times \nabla\lambda_i + \nabla\lambda_j \times \nabla\lambda_i \\ =& 2(\nabla\lambda_j \times \nabla\lambda_i). \end{aligned}$$

The curl for the higher-order functions can be found in Appendix A.3.

4. Discretisation of the time-harmonic Maxwell equations

The DG FEM with Nédélec basis functions on tetrahedra, which were described in the previous chapter, will now be applied to the time-harmonic Maxwell equation (2.8). After the determination of the weak formulation, we can find elementwise solutions that can be assembled to an overall solution.

4.1. Notation

Let us start with the presentation of some sets and notations that will be used. For the FEM we divide the domain $\Omega \subset \mathbb{R}^3$ into a set of tetrahedra $\mathcal{T}_h = \{K\}$. Remember, that h stands for the maximal diameter of the elements in the set. Denote the set of all faces of the elements by $\mathcal{F}_h = \{F\}$ with the partition $\mathcal{F}_h = \mathcal{F}_h^i \cup \mathcal{F}_h^b$, where the first subset consists of the interior and the second of the boundary faces.

When considering one element K, we use v_i for the vertices, s_i as a notation for the faces, $i = 1, \ldots, 4$, and e_j, $j = 1, \ldots, 6$, for the edges. $\boldsymbol{\tau}_j$ is the unit tangential vector on the edge e_j.

Define the considered FEM space by

$$\Sigma_h^p := \{\mathbf{u} \in [L^2(\Omega)]^3 \mid \mathbf{u} \text{ is Nédélec function of order } p \text{ in each element} K \in \mathcal{T}_h\}.$$

The test functions that we use for the determination of the weak formulation are also members of this space.

For the DG FEM we need the following definitions:

Definition 4.1. Let $F \in \mathcal{F}_h$ be the face between two elements K^L and K^R in $\mathcal{T}_h$, where $\mathbf{n}^L$ and $\mathbf{n}^R$ are the respective outward pointing normal unit vectors at that face. We define the *tangential jump* by

$$[\![\mathbf{u}]\!] = \mathbf{n}^L \times \mathbf{u}^L + \mathbf{n}^R \times \mathbf{u}^R$$

and the *average*

$$\{\{\mathbf{u}\}\} = \frac{\mathbf{u}^L + \mathbf{u}^R}{2},$$

where $\mathbf{u}^L$ and $\mathbf{u}^R$ are the values of the trace of $\mathbf{u}$ at ∂K^L and ∂K^R, respectively.

At the boundary Γ of Ω, we set

$$[\![\mathbf{u}]\!] = \mathbf{u} \qquad \text{and} \qquad \{\{\mathbf{u}\}\} = \mathbf{n} \times \mathbf{u}.$$

Definition 4.2. For $\mathbf{u} \in \Sigma_h^p$, we define two lifting operators. The global lifting operator $\mathcal{L} : [L^2(\mathcal{F}_h^i)]^3 \mapsto \Sigma_h^p$ is given by

$$(\mathcal{L}(\mathbf{u}), \mathbf{v}) = \int_{\mathcal{F}_h^i} \mathbf{u} \cdot [\![\mathbf{v}]\!] \, \mathrm{d}\, A, \qquad \forall \mathbf{v} \in \Sigma_h^p$$

and the local lifting operator $\mathcal{R}_{\mathcal{F}} : [L^2(F)]^3 \mapsto \Sigma_h^p$ by

$$(\mathcal{R}_F(\mathbf{u}), \mathbf{v}) = \int_F \mathbf{u} \cdot \{\{\mathbf{v}\}\} \, \mathrm{d}\, A, \qquad \forall \mathbf{v} \in \Sigma_h^p.$$

$\mathcal{R}_F$ vanishes outside the elements connected to the face F such that we can write

$$\mathcal{R}(\mathbf{u}) = \sum_{F \in \mathcal{F}_h} \mathcal{R}_F(\mathbf{u}), \qquad \forall \mathbf{u} \in [L^2(\mathcal{F}_h)]^3$$

for the global lifting operator $\mathcal{R} : [\mathrm{L}^2(\mathcal{F}_h)]^3 \mapsto \Sigma_h^p$, which is defined by

$$(\mathcal{R}(\mathbf{u}), \mathbf{v}) = \int_{\mathcal{F}_h} \mathbf{u} \cdot \{\{\mathbf{v}\}\} \, \mathrm{d}\, A, \qquad \forall \mathbf{v} \in \Sigma_h^p.$$

With these definitions we can proceed with applying the DG FEM.

4.2. Weak formulation

We want to find the weak formulation for the curl-curl operator as described in (2.8).

To simplify the problem, we transform the second-order PDE into a system of first-order equations. For that purpose, we introduce the vector $\mathbf{q} = \nabla \times \mathbf{E}$ and rewrite (2.8) as

$$\begin{cases} \nabla \times \mu_r^{-1} \mathbf{q} - k^2 \varepsilon_r \mathbf{E} = \mathbf{F} \\ \qquad\qquad\qquad\quad \mathbf{q} = \nabla \times \mathbf{E}. \end{cases} \tag{4.1}$$

We now can determine the weak formulation of the system (4.1) by following the standard procedure for a Galerkin approach. First, we multiply the equations by arbitrary test functions $\boldsymbol{\varphi}, \boldsymbol{\pi} \in \Sigma_h^p$:

$$\begin{cases} \left(\nabla_h \times \mu_r^{-1} \mathbf{q}_h, \boldsymbol{\varphi}\right) - k^2 \varepsilon_r \left(\mathbf{E}_h, \boldsymbol{\varphi}\right) = \left(\mathbf{F}, \boldsymbol{\varphi}\right) \\ \qquad\qquad\qquad\qquad\qquad\quad \left(\mathbf{q}_h, \boldsymbol{\pi}\right) = \left(\nabla_h \times \mathbf{E}_h, \boldsymbol{\pi}\right). \end{cases} \tag{4.2}$$

Here, the index h indicates that we consider the finite element approximation and ∇_h is the elementwise application of the gradient operator.

Using Green's theorem as stated in Lemma 3.8, we can modify the following two expressions by partial integration:

$$\begin{aligned}\left(\nabla_h \times \mu_r^{-1}\mathbf{q}_h, \boldsymbol{\varphi}\right) &= \left(\mu_r^{-1}\mathbf{q}_h, \nabla_h \times \boldsymbol{\varphi}\right) + \langle \gamma_t(\mu_r^{-1}\mathbf{q}_h), \boldsymbol{\varphi}\rangle_{\partial\Omega} \\ &= \left(\mu_r^{-1}\mathbf{q}_h, \nabla_h \times \boldsymbol{\varphi}\right) + \sum_{K\in\mathcal{T}_h} \int_{\partial K} \left(\mathbf{n} \times \left(\mu_r^{-1}\mathbf{q}_h^*\right)\right) \cdot \boldsymbol{\varphi} \,\mathrm{d}\, A \end{aligned} \tag{4.3}$$

and similarly

$$\begin{aligned}(\nabla_h \times \mathbf{E}_h, \boldsymbol{\pi}) &= (\mathbf{E}_h, \nabla_h \times \boldsymbol{\pi}) + \langle \gamma_t(\mathbf{E}_h), \boldsymbol{\pi}\rangle_{\partial\Omega} \\ &= (\mathbf{E}_h, \nabla_h \times \boldsymbol{\pi}) + \sum_{K\in\mathcal{T}_h} \int_{\partial K} (\mathbf{n} \times \mathbf{E}_h^*) \cdot \boldsymbol{\pi} \,\mathrm{d}\, A.\end{aligned}$$

Applying the identity $(\nabla \times \mathbf{A}) \cdot \mathbf{B} = \nabla \cdot (\mathbf{A} \times \mathbf{B}) + (\nabla \times \mathbf{B} \cdot \mathbf{A})$ and after another integration by parts, we find

$$(\nabla_h \times \mathbf{E}_h, \boldsymbol{\pi}) = \int_\Omega (\nabla_h \times \mathbf{E}_h) \cdot \boldsymbol{\pi} \,\mathrm{d}\, V + \sum_{K\in\mathcal{T}_h} \int_{\partial K} (\mathbf{n} \times (\mathbf{E}_h^* - \mathbf{E}_h)) \cdot \boldsymbol{\pi} \,\mathrm{d}\, A. \tag{4.4}$$

Due to discontinuities at the faces, the trace $\gamma_t(\cdot)$ of $\mathbf{q}_h$ and $\mathbf{E}_h$ is not well-defined at the element boundaries ∂K. Thus, the flux notation ($\mathbf{E}_h^*$ and $\mathbf{q}_h^*$) is used there.

By directly evaluating the sum over all faces of the elements, we find the identity

$$\sum_{K\in\mathcal{T}_h} \int_{\partial K} (\mathbf{n} \times \mathbf{u}) \cdot \mathbf{v} \,\mathrm{d}\, A = -\int_{\mathcal{F}_h^i} \{\{\mathbf{u}\}\} \cdot [\![\mathbf{v}]\!] \,\mathrm{d}\, A + \int_{\mathcal{F}_h^i} \{\{\mathbf{v}\}\} \cdot [\![\mathbf{u}]\!] \,\mathrm{d}\, A + \int_{\mathcal{F}_h^b} (\mathbf{n} \times \mathbf{u}) \cdot \mathbf{v} \,\mathrm{d}\, A.$$

Using this relation and the former two considerations (4.3) and (4.4), we obtain the system

$$\begin{cases} \left(\mu_r^{-1}\mathbf{q}_h, \nabla_h \times \boldsymbol{\varphi}\right) - k^2\varepsilon_r \left(\mathbf{E}_h, \boldsymbol{\varphi}\right) + \displaystyle\int_{\mathcal{F}_h^b} \left(\mathbf{n} \times \left(\mu_r^{-1}\mathbf{q}_h^*\right)\right) \cdot \boldsymbol{\varphi} \,\mathrm{d}\, A \\ \qquad + \displaystyle\int_{\mathcal{F}_h^i} \{\{\mu_r^{-1}\mathbf{q}_h^*\}\} \cdot [\![\boldsymbol{\varphi}]\!] \,\mathrm{d}\, A + \int_{\mathcal{F}_h^i} \{\{\boldsymbol{\varphi}\}\} \cdot [\![\mu_r^{-1}\mathbf{q}_h^*]\!] \,\mathrm{d}\, A = (\mathbf{F}, \boldsymbol{\varphi}) \\ \qquad\qquad (\nabla_h \times \mathbf{E}_h, \boldsymbol{\pi}) + \displaystyle\int_{\mathcal{F}_h^b} (\mathbf{n} \times (\mathbf{E}_h^* - \mathbf{E}_h)) \cdot \boldsymbol{\pi} \,\mathrm{d}\, A \\ \quad - \displaystyle\int_{\mathcal{F}_h^i} \{\{\mathbf{E}_h^* - \mathbf{E}_h\}\} \cdot [\![\boldsymbol{\pi}]\!] \,\mathrm{d}\, A + \int_{\mathcal{F}_h^i} \{\{\boldsymbol{\pi}\}\} \cdot [\![\mathbf{E}_h^* - \mathbf{E}_h]\!] \,\mathrm{d}\, A = (\mathbf{q}_h, \boldsymbol{\pi}) \,. \end{cases} \tag{4.5}$$

With the help of the definition of the global lifting operators and the jump and average at the boundary we can express $\mathbf{q}_h$ in terms of $\mathbf{E}_h$

$$\mathbf{q}_h = \nabla_h \times \mathbf{E}_h - \mathcal{L}\left(\{\{\mathbf{E}_h^* - \mathbf{E}_h\}\}\right) + \mathcal{R}\left([\![\mathbf{E}_h^* - \mathbf{E}_h]\!]\right)$$

and insert this result into the first equation of (4.5). This gives us the following weak formulation:
Find $\mathbf{E}_h \in \Sigma_h^p$ such that for all $\boldsymbol{\varphi} \in \Sigma_h^p$

$$\begin{aligned}\mathcal{B}\left(\mathbf{E}_h, \boldsymbol{\varphi}\right) := &\left(\mu_r^{-1}\left(\nabla_h \times \mathbf{E}_h\right), \nabla_h \times \boldsymbol{\varphi}\right) - k^2 \varepsilon_r \left(\mathbf{E}_h, \boldsymbol{\varphi}\right) \\ &- \int_{\mathcal{F}_h^i} \{\{\mathbf{E}_h^* - \mathbf{E}_h\}\} \cdot [\![\mu_r^{-1}\left(\nabla_h \times \boldsymbol{\varphi}\right)]\!] \,\mathrm{d}\, A - \int_{\mathcal{F}_h^i} \{\{\mu_r^{-1}\mathbf{q}_h^*\}\} \cdot [\![\boldsymbol{\varphi}]\!] \,\mathrm{d}\, A \\ &+ \int_{\mathcal{F}_h^i} [\![\mathbf{E}_h^* - \mathbf{E}_h]\!] \cdot \{\{\mu_r^{-1}\left(\nabla_h \times \boldsymbol{\varphi}\right)\}\} \,\mathrm{d}\, A + \int_{\mathcal{F}_h^i} [\![\mu_r^{-1}\mathbf{q}_h^*]\!] \cdot \{\{\boldsymbol{\varphi}\}\} \,\mathrm{d}\, A \\ &+ \int_{\mathcal{F}_h^b} \left(\mathbf{n} \times \left(\mathbf{E}_h^* - \mathbf{E}_h\right)\right) \cdot \left(\nabla_h \times \boldsymbol{\varphi}\right) \mathrm{d}\, A - \int_{\mathcal{F}_h^b} \mu_r^{-1}\mathbf{q}_h^* \cdot \left(\mathbf{n} \times \boldsymbol{\varphi}\right) \mathrm{d}\, A \qquad = \left(\mathbf{F}, \boldsymbol{\varphi}\right),\end{aligned} \tag{4.6}$$

with the bilinear form $\mathcal{B}\left(\mathbf{E}_h, \boldsymbol{\varphi}\right)$.

4.3. Numerical Fluxes

The weak formulation does not yet specify the numerical flux. Following [20], two different versions are presented within this framework. For reasons of simplicity we will only consider the case of vacuum or dry air, which corresponds to $\mu_r = \varepsilon_r = 1$.

4.3.1. The interior penalty flux

The interior penalty flux penalises jumps at interior faces with a penalty term containing the parameter α_F and is defined by:

$$\begin{aligned} \mathbf{E}_h^* &= \{\{\mathbf{E}_h\}\}, & \mathbf{q}_h^* &= \{\{\nabla_h \times \mathbf{E}_h\}\} - \alpha_F [\![\mathbf{E}_h]\!] \text{ if } F \in \mathcal{F}_h^i \\ \mathbf{n} \times \mathbf{E}_h^* &= \mathbf{g}, & \mathbf{q}_h^* &= \nabla_h \times \mathbf{E}_h - \alpha_F \left(\mathbf{n} \times \mathbf{E}_h\right) + \alpha_F \mathbf{g} \text{ if } F \in \mathcal{F}_h^b \end{aligned}$$

Using this flux, the face integrals in the bilinear form can be transformed, where some of the terms drop out. The weak formulation (4.6) can be rewritten as

$$\begin{aligned}\mathcal{B}_{IP}(\mathbf{E}_h, \boldsymbol{\varphi}) &:= (\nabla_h \times \mathbf{E}_h, \nabla_h \times \boldsymbol{\varphi}) - k^2 (\mathbf{E}_h, \boldsymbol{\varphi}) \\ &\quad - \int_{\mathcal{F}_h} [\![\mathbf{E}_h]\!] \cdot \{\{\nabla_h \times \boldsymbol{\varphi}\}\} \,\mathrm{d}\, A - \int_{\mathcal{F}_h} \{\{\nabla_h \times \mathbf{E}_h\}\} \cdot [\![\boldsymbol{\varphi}]\!] \,\mathrm{d}\, A \\ &\quad + \int_{\mathcal{F}_h} \alpha_F [\![\mathbf{E}_h]\!] \cdot [\![\boldsymbol{\varphi}]\!] \,\mathrm{d}\, A \\ &= (\mathbf{F}, \boldsymbol{\varphi}) - \int_{\mathcal{F}_h^b} \mathbf{g} \cdot (\nabla_h \times \boldsymbol{\varphi}) \,\mathrm{d}\, A + \int_{\mathcal{F}_h^b} \alpha_F \mathbf{g} \cdot (\mathbf{n} \times \boldsymbol{\varphi}) \,\mathrm{d}\, A \qquad =: \mathcal{I}_{IP}.\end{aligned} \tag{4.7}$$

Here, $\mathcal{B}_{IP}$ is a bilinear and $\mathcal{I}_{IP}$ a linear form. Note that, due to the definition of the average and jump at the boundaries, we do not have to distinguish between interior and boundary faces any more. Instead we can generalise the equations to all faces $\mathcal{F}_h$.

We obtain the weak formulation with the IP flux for the time-harmonic Maxwell equations which can be formulated as follows:
Find $\mathbf{E}_h \in \Sigma_h^p$ such that for all $\boldsymbol{\varphi} \in \Sigma_h^p$ equation (4.7) is satisfied.

4.3.2. The Brezzi formulation for the flux

Alternatively, we can use the numerical flux presented by Brezzi et al. [2]:

$$\begin{aligned} \mathbf{E}_h^* &= \{\{\mathbf{E}_h\}\}, & \mathbf{q}_h^* &= \{\{\mathbf{q}_h\}\} - \beta([\![\mathbf{E}_h]\!]) \text{ if } F \in \mathcal{F}_h^i \\ \mathbf{n} \times \mathbf{E}_h^* &= \mathbf{g}, & \mathbf{q}_h^* &= \mathbf{q}_h - \beta(\mathbf{n} \times \mathbf{E}_h) + \beta(\mathbf{g}) \text{ if } F \in \mathcal{F}_h^b, \end{aligned}$$

where $\beta(\mathbf{u}_h) = \eta_F \{\{\mathcal{R}_F(\mathbf{u}_h)\}\}$ for $F \in \mathcal{F}_h$ and parameter $\eta_F \in \mathbb{R}$.

As done for the IP flux, the bilinear form can be transformed to

$$\begin{aligned}\mathcal{B}(\mathbf{E}_h, \boldsymbol{\varphi}) &= (\nabla_h \times \mathbf{E}_h, \nabla_h \times \boldsymbol{\varphi}) - k^2 (\mathbf{E}_h, \boldsymbol{\varphi}) \\ &\quad - \int_{\mathcal{F}_h} [\![\mathbf{E}_h]\!] \cdot \{\{\nabla_h \times \boldsymbol{\varphi}\}\} \,\mathrm{d}\, A - \int_{\mathcal{F}_h} \{\{\nabla_h \times \mathbf{E}_h\}\} \cdot [\![\boldsymbol{\varphi}]\!] \,\mathrm{d}\, A \\ &\quad - \int_{\mathcal{F}_h} \{\{\mathcal{R}([\![\mathbf{E}_h^* - \mathbf{E}_h]\!])\}\} \cdot [\![\boldsymbol{\varphi}]\!] \,\mathrm{d}\, A + \sum_{F \in \mathcal{F}_h} \int_F \eta_F \{\{\mathcal{R}([\![\mathbf{E}_h]\!])\}\} \cdot [\![\boldsymbol{\varphi}]\!] \,\mathrm{d}\, A \\ &\quad + \int_{\mathcal{F}_h^b} \mathbf{g} \cdot (\nabla_h \times \boldsymbol{\varphi}) \,\mathrm{d}\, A - \sum_{F \in \mathcal{F}_h^b} \int_F \eta_F \mathcal{R}_F(\mathbf{g}) \cdot (\mathbf{n} \times \boldsymbol{\varphi}) \,\mathrm{d}\, A\end{aligned}$$

Using n_f, the number of faces of an element, we can approximate the following integral

$$\begin{aligned}
&\int_{\mathcal{F}_h} \{\{\mathcal{R}\left([\![\mathbf{E}_h^* - \mathbf{E}_h]\!]\right)\}\} \cdot [\![\boldsymbol{\varphi}]\!] \,\mathrm{d}\, A = \left(\mathcal{R}\left([\![\mathbf{E}_h^* - \mathbf{E}_h]\!]\right), \mathcal{R}\left([\![\boldsymbol{\varphi}]\!]\right)\right) \\
&\approx n_f \sum_{F \in \mathcal{F}_h} \left(\mathcal{R}_F\left([\![\mathbf{E}_h^* - \mathbf{E}_h]\!]\right), \mathcal{R}_F\left([\![\boldsymbol{\varphi}]\!]\right)\right) \\
&= -n_f \sum_{F \in \mathcal{F}_h} \left(\mathcal{R}_F\left([\![\mathbf{E}_h]\!]\right), \mathcal{R}_F\left([\![\boldsymbol{\varphi}]\!]\right)\right) + n_f \sum_{F \in \mathcal{F}_h} \left(\mathcal{R}_F\left(\mathbf{g}\right), \mathcal{R}_F\left([\![\boldsymbol{\varphi}]\!]\right)\right)
\end{aligned}$$

We can then rewrite the weak formulation: Find $\mathbf{E}_h \in \Sigma_h^p$ such that for all $\boldsymbol{\varphi} \in \Sigma_h^p$

$$\begin{aligned}
\mathcal{B}_{BR}\left(\mathbf{E}_h, \boldsymbol{\varphi}\right) &:= \left(\nabla_h \times \mathbf{E}_h, \nabla_h \times \boldsymbol{\varphi}\right) - k^2 \left(\mathbf{E}_h, \boldsymbol{\varphi}\right) \\
&\quad - \int_{\mathcal{F}_h} [\![\mathbf{E}_h]\!] \cdot \{\{\nabla_h \times \boldsymbol{\varphi}\}\} \,\mathrm{d}\, A - \int_{\mathcal{F}_h} \{\{\nabla_h \times \mathbf{E}_h\}\} \cdot [\![\boldsymbol{\varphi}]\!] \,\mathrm{d}\, A \\
&\quad + \sum_{F \in \mathcal{F}_h} \left(\eta_F + n_f\right) \left(\mathcal{R}_F\left([\![\mathbf{E}_h]\!]\right), \mathcal{R}_F\left([\![\boldsymbol{\varphi}]\!]\right)\right) \qquad (4.8) \\
&= \left(F, \boldsymbol{\varphi}\right) - \int_{\mathcal{F}_h^b} \mathbf{g} \left(\nabla_h \times \boldsymbol{\varphi}\right) \mathrm{d}\, A \\
&\quad + \sum_{F \in \mathcal{F}_h^b} \left(\eta_F + n_f\right) \left(\mathcal{R}_F\left(\mathbf{g}\right), \mathcal{R}_F\left(\mathbf{n} \times \boldsymbol{\varphi}\right)\right) \qquad =: \mathcal{I}_{BR}.
\end{aligned}$$

4.4. Discontinuous Galerkin

The discontinuous Galerkin method uses an expansion in spatial basis functions to approximate the unknown electric field:

$$\mathbf{E}(\mathbf{r}) \approx \mathbf{E}_h(\mathbf{r}) = \sum_{j=1}^{N} \mathbf{E}_j(\mathbf{r}) \boldsymbol{\varphi}_j(\mathbf{r}) \qquad (4.9)$$

with $\boldsymbol{\varphi}_j \in \Sigma_h^p$ being the Nédélec basis functions as defined in Section 3.2.

This expansion (4.9) is, together with the test functions $\boldsymbol{\varphi}_i \in \Sigma_h^p$ from the basis function set, inserted into the weak formulations for the two numerical fluxes (4.7) and (4.8). Subsequently, we have to solve the following linear system

$$\sum_{j=1}^{N} \mathbf{E}_j S_{ij} = f_i. \qquad (4.10)$$

To solve eigenvalue problems, we have to consider the 0-source wave equation (see (2.9)). Then f_i in the system (4.10) has to be modified such that the term containing the source F has to be set to zero.

4.4.1. Interior penalty flux

We first apply the Galerkin discretisation to the weak formulation of the Maxwell problem using the interior penalty flux. This results in the equations

$$\begin{aligned}
&\sum_{j=1}^{N} \mathbf{E}_j \left(\left(\nabla_h \times \boldsymbol{\varphi}_j, \nabla_h \times \boldsymbol{\varphi}_i \right) - k^2 \left(\boldsymbol{\varphi}_j, \boldsymbol{\varphi}_i \right) \right. \\
&\qquad \left. - \int_{\mathcal{F}_h} [\![\boldsymbol{\varphi}_j]\!] \cdot \{\{ \nabla_h \times \boldsymbol{\varphi}_i \}\} \,\mathrm{d}\, A - \int_{\mathcal{F}_h} \{\{ \nabla_h \times \boldsymbol{\varphi}_k \}\} \cdot [\![\boldsymbol{\varphi}_i]\!] \,\mathrm{d}\, A + \int_{\mathcal{F}_h} \alpha_F [\![\boldsymbol{\varphi}_j]\!] \cdot [\![\boldsymbol{\varphi}_i]\!] \,\mathrm{d}\, A \right) \\
&= (\mathbf{F}, \boldsymbol{\varphi}_i) - \int_{\mathcal{F}_h^b} \mathbf{g} \cdot (\nabla_h \times \boldsymbol{\varphi}_i) \,\mathrm{d}\, A + \int_{\mathcal{F}_h^b} \alpha_F \mathbf{g} \cdot (\mathbf{n} \times \boldsymbol{\varphi}_i) \,\mathrm{d}\, A
\end{aligned}$$

for $i = 1, \ldots, N$.

As stated before, we can rewrite this to obtain a linear system of the form (4.10). For the IP DG method we find that

$$\begin{aligned}
S_{ij} &= \int_{\Omega} \left(\nabla_h \times \boldsymbol{\varphi}_j \right) \cdot (\nabla_h \times \boldsymbol{\varphi}_i) \,\mathrm{d}\, V - k^2 \int_{\Omega} \boldsymbol{\varphi}_j \cdot \boldsymbol{\varphi}_i \,\mathrm{d}\, V \\
&\quad - \int_{\mathcal{F}_h} [\![\boldsymbol{\varphi}_j]\!] \cdot \{\{ \nabla_h \times \boldsymbol{\varphi}_i \}\} \,\mathrm{d}\, A - \int_{\mathcal{F}_h} \{\{ \nabla_h \times \boldsymbol{\varphi}_k \}\} \cdot [\![\boldsymbol{\varphi}_i]\!] \,\mathrm{d}\, A + \int_{\mathcal{F}_h} \alpha_F [\![\boldsymbol{\varphi}_j]\!] \cdot [\![\boldsymbol{\varphi}_i]\!] \,\mathrm{d}\, A \\
&= \sum_{K \in \mathcal{T}_h} \left(\int_K \left(\nabla_h \times \boldsymbol{\varphi}_j \right) \cdot (\nabla_h \times \boldsymbol{\varphi}_i) \,\mathrm{d}\, V - k^2 \int_K \boldsymbol{\varphi}_j \cdot \boldsymbol{\varphi}_i \,\mathrm{d}\, V \right) \\
&\quad + \sum_{F \in \mathcal{F}_h} \left(- \int_F [\![\boldsymbol{\varphi}_j]\!] \cdot \{\{ \nabla_h \times \boldsymbol{\varphi}_i \}\} \,\mathrm{d}\, A - \int_F \{\{ \nabla_h \times \boldsymbol{\varphi}_k \}\} \cdot [\![\boldsymbol{\varphi}_i]\!] \,\mathrm{d}\, A + \int_F \alpha_F [\![\boldsymbol{\varphi}_j]\!] \cdot [\![\boldsymbol{\varphi}_i]\!] \,\mathrm{d}\, A \right)
\end{aligned}$$

and

$$\begin{aligned}
f_i &= \int_{\Omega} \mathbf{F} \cdot \boldsymbol{\varphi}_i \,\mathrm{d}\, V - \int_{\mathcal{F}_h^b} \mathbf{g} \cdot (\nabla_h \times \boldsymbol{\varphi}_i) \,\mathrm{d}\, A + \int_{\mathcal{F}_h^b} \alpha_F \mathrm{g} \cdot (n \times \boldsymbol{\varphi}_i) \,\mathrm{d}\, A \\
&= \sum_{K \in \mathcal{T}_h} \int_K \mathbf{F} \cdot \boldsymbol{\varphi}_i \,\mathrm{d}\, V + \sum_{F \in \mathcal{F}_h^b} \left(- \int_F \mathbf{g} \cdot (\nabla_h \times \boldsymbol{\varphi}_i) \,\mathrm{d}\, A + \int_F \alpha_F \mathbf{g} \cdot (\mathbf{n} \times \boldsymbol{\varphi}_i) \,\mathrm{d}\, A \right).
\end{aligned}$$

4.4.2. Brezzi flux formulation

Similarly, we can find a system of type (4.10) for the Brezzi formulation of the flux, where

$$\begin{aligned} S_{ij} = &\sum_{K\in\mathcal{T}_h} \left(\int_K \left(\nabla_h \times \boldsymbol{\varphi}_j\right) \cdot \left(\nabla_h \times \boldsymbol{\varphi}_i\right) \mathrm{d}\, V - k^2 \int_K \boldsymbol{\varphi}_j \cdot \boldsymbol{\varphi}_i \,\mathrm{d}\, V \right) \\ &- \sum_{F\in\mathcal{F}_h} \left(\int_F [\![\boldsymbol{\varphi}_j]\!] \cdot \{\{\nabla_h \times \boldsymbol{\varphi}_i\}\} \,\mathrm{d}\, A - \int_{\mathcal{F}_h} \{\{\nabla_h \times \boldsymbol{\varphi}_j\}\} \cdot [\![\boldsymbol{\varphi}_i]\!] \,\mathrm{d}\, A \right. \\ &\left. + \left(\eta_F + n_f\right) \left(\mathcal{R}_F \left([\![\boldsymbol{\varphi}_j]\!] \right), \mathcal{R}_F \left(\{\{\boldsymbol{\varphi}_i\}\} \right) \right) \right) \end{aligned}$$

and

$$\begin{aligned} f_i = &\sum_{K\in\mathcal{T}_h} \int_K \mathbf{F} \cdot \boldsymbol{\varphi}_i \,\mathrm{d}\, V - \sum_{F\in\mathcal{F}_h} \int_F \mathbf{g} \cdot \left(\nabla_h \times \boldsymbol{\varphi}_i\right) \mathrm{d}\, A \\ &+ \sum_{F\in\mathcal{F}_h^b} \left(\eta_F + n_f\right) \left(\mathcal{R}_F \left(\mathbf{g}\right), \mathcal{R}_F \left(\mathbf{n} \times \boldsymbol{\varphi}_i\right) \right). \end{aligned}$$

4.5. Computation of the numerical solution

Finally, the linear system (4.10) allows us to compute a solution per element. These results are in the end assembled to find a general solution of the problem. As we work on the reference element, the integrals that were described in the previous section have to be transformed to that element and its faces. Furthermore, we have to apply Gauß quadrature for the numerical evaluation of the integrals. More information on these topics can be found in the Appendices A.1 and A.2, respectively.

5. Application of Nédélec's basis functions to hpGEM

As an extension of the C++ software package hpGEM, the Nédélec basis functions are implemented. Thus, they can be used to solve Maxwell's equations numerically. Also, the functionality of the new code is tested.

5.1. The software package hpGEM

The C++ software package hpGEM (see [18]) was developed by the chair of Mathematics in Computational Science (MaCS) at the University of Twente, Netherlands, to apply discontinuous Galerkin methods to a variety of physical problems. It helps particularly to numerically solve partial differential equations from the fields of fluid mechanics and electromagnetism, among which we also find the Maxwell equations. The toolkits PETSc and SLEPc are used to solve linear systems and eigenvalue problems, respectively. The hpGEM package provides a wide range of features. Some of them are:

- It handles various mesh geometries in one, two and three dimensions. Even hybrid grids that involve different shapes of elements are supported. Furthermore, periodic and moving meshes are possible. For complicated domains and meshes the commercial packages Rhinoceros and Centaur are needed.
- Sample applications are available that provide examples of space and space-time discontinuous Galerkin routines for nonlinear hyperbolic equations.
- Gauß integration rules up to at least order seven for all supported polytopes are included to build higher-order finite element discretisations.
- It includes a global algebraic system assembly.
- Both p- and h-refinement are possible.
- Predefined sets of basis functions are used.

One of the applications of the package is DG-Max. It implements the Maxwell discretisation according to the numerical technique described in this work. This includes the mesh generation, and the finite element method. It enables one to deal with different kinds of problems, such as the computation of the smallest eigenvalues and the solutions of the time-dependent or -harmonic Maxwell system. Further, the setup can be changed regarding features like the boundary conditions, the type of the used numerical flux and the values of the piecewise constant dielectric function ε_r.

`DG-Max` currently uses the basis functions of Ainsworth and Coyle [1]. These can, however, produce spurious modes in our setting. Thus, it is of great interest to include the Nédélec basis functions, presented in Section 3.2, into the code. The files `BasisFunctionCollection_Curl.cpp` and `BasisFunctionCollection_Curl.hpp` have to adapted corresponding to Nédélec's approach. Buffa and Perugia showed that these functions do not lead to spurious modes [3]. However, we still have to test if the order of accuracy of the new basis functions is satisfactory and comparable to the ones of Ainsworth and Coyle.

We will now present some examples to show the correct functionality of the application `DG-Max` with Nédélec basis functions. The settings that we use within this framework are default features of the application. They are typically used for numerical experiments as done for example in [20]. We test basis functions up to polynomial order $p = 4$.

5.2. The accuracy of the numerical solution to the time-harmonic Maxwell problem

In a first step, the error of the numerical solution to the problem (2.8) is determined. It can then be used to find the order of accuracy, while decreasing h.

To be able to compute the error of the numerical solution, the exact solution is defined to be a combination of sine and cosine waves. The initial conditions and source term in the code are then adjusted to fit this result. The error is given by

$$\max_t \|\mathbf{E}(\mathbf{r}, t) - \mathbf{E}_h(\mathbf{r}, t)\|,$$

where $\mathbf{E}$ is the analytical and $\mathbf{E}_h$ the numerical solution for the mesh parameter h as specified in Definition 3.1.

Let us now consider a refinement of the mesh resulting in a sequence $h_1 > h_2 > h_3 > \ldots$ of maximal diameters of the tetrahedra. The FEM is said to converge with order s to the exact solution if we can find a constant C, which is independent of the mesh parameter and the solution, such that

$$\|\mathbf{E} - \mathbf{E}_{h_n}\| \leq C \cdot {h_n}^s \quad \forall h_n, \quad n = 1, 2, 3, \ldots.$$

In the Landau notation, this can be written as

$$\|\mathbf{E} - \mathbf{E}_{h_n}\| \in \mathcal{O}\left({h_n}^s\right).$$

When taking the logarithm on both sides of this inequality, we can determine s by computing the slope of

$$\log\left(\|\mathbf{E} - \mathbf{E}_{h_n}\|\right) \leq \log\left(C\right) + s \log\left(h_n\right).$$

Using two different points $(h_i, \mathbf{E}_{h_i})$ and $(h_j, \mathbf{E}_{h_j})$, we obtain

$$q = \frac{\log\left(\|\mathbf{E} - \mathbf{E}_{h_j}\|\right) - \log\left(\|\mathbf{E} - \mathbf{E}_{h_i}\|\right)}{\log\left(h_j\right) - \log\left(h_i\right)}, \quad i < j.$$

For the realisation of these computations, some of the variables have to be discussed.

Running the code we can specify two natural numbers: the order of the basis functions p, and n. To understand the meaning of the latter, we have to give a short overview of how the structured tetrahedral mesh is constructed for our tests. We consider a unit cube as the domain of computation. It is divided into several congruent subcubes, which are then split into five tetrahedra each. This is done by forming an inner tetrahedron of which the edges are the diagonals of the faces of the brick. Four smaller tetrahedra emerge as a consequence at the corners of the cubes. In this setup, n defines in how many pieces of the same length each of the edges of the unit cube has to be split to obtain n^3 smaller bricks. This results in a total number of $N = n^3 \cdot 5$ elements. Their maximal diameter h equals two times the radius of the circumcircle of the equilateral tetrahedra at the interior of each brick. It is given by $h = 2\frac{\sqrt{6}}{4} \cdot a$, where a is the length of the edges. Using Pythagoras' identity, a can be computed based on the size of the smaller cubes, leading to $a = \sqrt{2} \cdot \frac{1}{n}$. Finally, we find that

$$h = \frac{\sqrt{3}}{n}.$$

When solving the time-harmonic problem, the output of `DG-Max` provides us with the L^2-, the H (curl)-, and the DG-norm for the chosen values of n and p. Thus, we have all information needed to compute the order of accuracy of the method. In each refinement step we will double the number n.

In [9] the DG-norm is defined. For h being the diameter of the face that is considered, we obtain the this norm by

$$\|\mathbf{u}\|_{DG}^2 := \|\mathbf{u}\|_0^2 + |\mathbf{u}|_{DG}^2, \quad \text{where } |\mathbf{u}|_{DG}^2 := \|\nabla_h \times \mathbf{u}\|_0^2 + \|\mathrm{h}^{1/2}\{\{\mathbf{u}\}\}\|_{0,\mathcal{F}_h}^2.$$

Furthermore, Houston et al. established the orders of convergence for the DG-norm and the L^2-norm and proved them. Following their considerations, we can expect the order s of the error to be equal to p in the case of the DG-norm and $p+1$ for the L^2-norm when considering smooth solutions on convex domains [9].

In [20] the optimal parameters for both kinds of fluxes are determined. However, in order to simplify this relations, these values are slightly modified. This hardly has any influence on the convergence rate of the DG methods. For our examples we choose a parameter of $\alpha_F = 140$ for the IP flux and $\eta_F = 1.4$ for the formulation of Brezzi.

We will apply `DG-Max` to the domain $\Omega = [0,1]^3$. The values ε_r and μ_r are set to 1, corresponding to vacuum or dry air. Also, we will fix the wave vector to be $\mathbf{k}^2 = 1$. In the following, further settings for our tests are described.

5.2.1. Homogeneous boundaries

We first want to examine the setting with homogeneous boundary conditions $\mathbf{n} \times \mathbf{E} = 0$. This represents a solid walls of the domain made of perfectly conducting material.

In this case, the exact solution for the general time-dependent system (2.8) at a position $\mathbf{r} = (x, y, z)^t$ is given by

$$\mathbf{E}(\mathbf{r}, t) = \begin{pmatrix} \sin(\pi y)\sin(\pi z) \\ \sin(\pi z)\sin(\pi x) \\ \sin(\pi x)\sin(\pi y) \end{pmatrix} \cos\left(\sqrt{2}\pi t\right).$$

The cosine term, however, is not needed for the time-harmonic problem.

By plugging this solution into the partial differential equations, we find a source term

$$\mathbf{F} = \begin{pmatrix} \sin(\pi y)\sin(\pi z) \\ \sin(\pi z)\sin(\pi x) \\ \sin(\pi x)\sin(\pi y) \end{pmatrix} \left(2\pi^2 - 1\right).$$

The initial condition is only of interest when considering the behaviour of the field depending on the time t and would be given by $\mathbf{E}(\mathbf{r}, t = 0)$.

Observations and results

The output of the code for Ainsworth-Coyle and Nédélec basis functions and for both fluxes are given in the Tables B.1 and B.3. Unfortunately, long computational times limit us to only few possibilities for the parameter n and thus to a small number of values for our evaluations. This problem appears throughout the whole testing process.

We know that the `DG-Max` application performs well with the basis functions by Ainsworth and Coyle. Thus, in a first step, let us compare the values of the errors of the numerical solution with Nédélec's basis function set to the results with the well-tested ones. For both kinds of numerical fluxes and all choices of p and n one can see that the values of the DG-norm (and also of the H(curl)-norm, which is not listed) are quite similar. Different results are found for the L^2-norm, where the error values are of same magnitude, but still differ between the basis functions of Ainsworth-Coyle and Nédélec.

Based on the measured values, we can determine the order of accuracy of the methods. This is done as described at the beginning of this chapter. The refinement of the mesh is performed by increasing m so that $n = 2^m$. The number of tetrahedra is thus multiplied with 8 in each refinement step. We compute the order based on the L^2-norm and the DG-norm.

The order of accuracy is computed for both the Brezzi flux formulation (see Table B.2) and the IP flux (see Table B.4). Again, we compare the Ainsworth-Coyle basis functions with those proposed by Nédélec. We considered a convex domain and found smooth numerical solutions in all cases so that we can expect the accuracy of the methods to be as proven in [9]. Our tests confirm the correct order for the already tested functions of Ainsworth and Coyle. The set of Nédélec converges with $\mathcal{O}(h^p)$ in the DG-norm for the maximal diameter h of the mesh and the order of the basis functions p. For the error in the L^2-norm we can observe convergence, whose order is, however, not optimal. Consistently, it performs with one order less than expected. Hence, $s = p$ instead of

$s = p + 1$. As the H (curl)- and DG-norms are more accurate and cover more details of the function space of consideration, for the moment, we can still assume that the new basis functions show the correct functionality. Nonetheless, the reduction of the convergence rate needs to be analysed.

These observations do not depend on the choice of the numerical flux. Yet, it is found that the IP flux suffers more from varying values of the penalty parameter, while the Brezzi formulation leads to a more robust performance.

5.2.2. Periodic boundary conditions

Let us now consider periodic boundary conditions. In this case, the exact solution is defined to be

$$\mathbf{E}(\mathbf{r}) = \begin{pmatrix} \sin(\pi y)\sin(\pi z) \\ \sin(\pi z)\sin(\pi x) \\ \sin(\pi x)\sin(\pi y) \end{pmatrix}$$

resulting in a source term of

$$\mathbf{F} = \begin{pmatrix} \sin(\pi y)\sin(\pi z) \\ \sin(\pi z)\sin(\pi x) \\ \sin(\pi x)\sin(\pi y) \end{pmatrix} \left(8\pi^2 - 1\right).$$

Note that only even numbers for n are possible for periodic boundary conditions.

Observations and results

The computed errors for this setting are shown in Tables B.5 and B.7. A direct comparison shows the same results as in the case of homogeneous boundary conditions.

The order of accuracy for the DG FEM on the domain of a unit cell with periodic boundary conditions is calculated for the Brezzi and the IP flux. For the Brezzi flux, only a few data points were attained so that no representative convergence rate could be obtained (see Table B.6). For the IP flux (Table B.8) we get the same result as for the homogeneous boundary conditions. While the Ainsworth-Coyle basis functions perform as expected, those of Nédélec reach the predicted order of accuracy only for the DG-norm. In the L^2-norm, the convergence rate is by one order less than expected.

5.3. The accuracy of the eigenvalue computations for the time-harmonic Maxwell equations

Next, we examine the computation of eigenvalues. Our main goal is to determine the accuracy when refining the mesh, but it is also of interest to confirm our expectations that no spurious modes are obtained.

Similar to the accuracy computations for the time-harmonic solution (see Section 5.2), we take the unit cube $\Omega = [0,1]^3$ as domain, choose $\mu_r = \varepsilon_r = 1$ and compare the Ainsworth-Coyle and Nédélec basis functions for both homogeneous and periodic boundary conditions. We want to concentrate on the default eigenvalues for the wave vector $\mathbf{k} = \mathbf{0}$. The eigenvalue solver is set to find the 24 positive eigenvalues that are the closest to a chosen target value. This value can be determined by prior knowledge of the expected eigenvalues. In our case, we chose it to be 60 ($\approx 5\pi^2$). In all cases we were able to find the 17 smallest positive eigenvalues for the problem with homogeneous boundary conditions and twelve for periodic boundaries. Eigenvalues equal to zero have to be filtered out manually.

Eigenvalues, as given in [20], can be written as

$$\omega^2 = \pi^2(l^2 + m^2 + n^2),$$

where l, m and n are non-negative integers satisfying $lm + ln + mn > 0$. For all three variables being positive, two identical eigenvalues can be associated with linearly independent eigenfunctions. To simplify the comparison, we will list the eigenvalues after dividing them by π^2.

The errors in the eigenvalues are computed as $\frac{\|\omega^2 - \omega_h^2\|_{\mathrm{L}^2}}{\omega^2}$, where ω_h^2 are the results of the numerical calculations. Again, we refine the mesh and can, similar to the considerations in Section 5.2, compute the accuracy.

The order of accuracy for the eigenvalue computations is proven to be $\mathcal{O}(h^{2p})$. This is shown in [3] and [9].

Observations and results

As mentioned before, the eigenvalues are divided by π^2 for simplicity. The values for both sets of basis functions, both types of boundary conditions and the two different kinds of numerical fluxes are listed in the appendix. In particular, check Tables B.9 to B.12 (homogeneous boundaries, Brezzi flux), B.17 to B.20 (homogeneous boundaries, IP flux), B.25 to B.27 (periodic boundaries, Brezzi flux) and B.31 to B.33 (periodic boundaries, IP flux).

We can observe that the values get closer to the exact values when increasing the polynomial order of the basis functions and the number of elements for both basis function sets. Thus, we can conclude that the eigenvalues converge to the correct values. Often, the results for $n = 1$, which means $N = 5$, are not listed. This is due to the fact that the very coarse grid does not allow for accurate eigenvalue computations. The results can therefore hardly be matched to the expected eigenvalues. While for a small numbers of elements, some spurious modes were detected for the Ainsworth-Coyle basis functions, we could not make the same observations for the set of Nédélec. These modes were filtered out manually before creating the tables. Furthermore, not always the correct multiplicity of the eigenvalues is found. This happens for both kinds of basis functions, however, more often for Nédélec's functions. Reasons for this are possibly the non-optimal penalty parameter of the fluxes and the relatively coarse meshes. It shows that these

missing values occur more often when using the IP flux, which is more susceptible to changes in the parameter.

Tables B.13 to B.16 (homogeneous boundaries, Brezzi flux), B.21 to B.24 (homogeneous boundaries, IP flux), B.28 to B.30 (periodic boundaries, Brezzi flux) and B.34 to B.36 (periodic boundaries, IP flux) show the error and resulting order of accuracy for Nédélec's basis functions. During the tests, it was not possible to obtain the results for large values of n within reasonable computational times. This also makes it hardly possible to find reliable values for the order of accuracy. Therefore, we abstain from comparing them to the expected values.

6. Accurate computations of the local density of states

Light sources contain particles in excited states. These can spontaneously drop to a lower level of energy. The difference in energy is released in the form of photons. The number of these decays in a unit time step is called the light emission rate. The occurrence of the various phenomena inside a photonic crystal depends on whether this rate changes and, if it does, on the speed of these changes. Thus, to control the behaviour of light in a structure, it is of interest to consider the local density of states (LDOS). This value, a count of the electromagnetic states present at a certain frequency and for a given orientation of the dipolar emitters, is proportional to the emission rate.

As the LDOS directly depends on a Green's function, for which analytical calculations are not possible due to the complex structure of photonic crystals, accurate numerical approximations are necessary. In this chapter, the formula for the LDOS is given and a version which is related to the eigenfunctions is derived. Finally, we present the method that was introduced in [26]. It applies a delta-convergent sequence and linear interpolation and provides an alternative formulation for the computation of the LDOS.

6.1. The local density of states

Within a given frequency interval a wave can only occupy certain energy states. The corresponding wave vectors and propagation directions depend on the medium in which the wave propagates. The *density of states* (DOS) is the number of available states of a quantum system for a given frequency range:

$$N(\omega) = \frac{1}{(2\pi)^3} \sum_n \int_{BZ1} \delta\left(\omega - \omega_{n,\mathbf{K}}\right) \mathrm{d}\,\mathbf{K},$$

where n enumerates the states, $\mathbf{K}$ is the wave vector, $\omega_{n,\mathbf{K}}$ the eigenmode that is specified by n and $\mathbf{K}$, and ω is a given frequency. The integration is performed over the first Brillouin zone. A high DOS value means that the wave can occupy many states, while with a DOS of zero no states are available. In that case, we have a band gap [19]. In this context, δ stands for the Dirac delta distribution, which will be discussed shortly.

Definition 6.1. A continuous linear functional on the space of test functions D is called a *distribution*.

The space of distributions is the dual space D' of the space of smooth test functions D. It forms a generalisation of the class of locally integrable functions.

As distributions, in a way, extend the notion of functions, they are also called *generalised functions*. Thus, they characterise a kind of solution for differential equations that is no solution in the classical sense.

Interpretations of Dirac's delta distribution are that it describes either an instantaneous action or a charge, which is concentrated at one point ξ. The following properties characterise the behaviour of $\delta(x-\xi)$:

1. $\delta(x-\xi) = 0 \qquad x \neq \xi$
2. $\int_a^b \delta(x-\xi)\,\mathrm{d}\,x = \begin{cases} 0 & a,b < \xi \text{ or } \xi < a,b \\ 1 & a \leq \xi \leq b \end{cases}$
3. $\int_{-\infty}^{\infty} \delta(x-\xi)\,\mathrm{d}\,x = 1$
4. $$\int_{-\infty}^{\infty} \delta(x-\xi)\cdot f(x)\,\mathrm{d}\,x = f(\xi) \tag{6.1}$$

   (sifting/reproducing property)

The *local density of states* (LDOS) is the local variation of the DOS and is given by

$$N(\omega, \mathbf{r}, \mathbf{e}_d) = \frac{3}{(2\pi)^3} \sum_n \left(\mathbf{e}_d^t \cdot |\mathbf{E}_{n,\mathbf{K}}|^2 \cdot \mathbf{e}_d\right) \delta\left(\omega_{n,\mathbf{K}} - \omega\right), \tag{6.2}$$

where $\mathbf{r}$ is the position of the emitter, $\mathbf{e}_d$ is the orientation of the dipole moment and $\mathbf{E}_{n,\mathbf{K}}(\mathbf{r})$ denote the eigenfunctions of the quantised electric field at a position $\mathbf{r}$ for the n-th eigenstate and the wave vector $\mathbf{K}$ [16]. n is the band index. For suboptimal cases with finite crystals, the LDOS does not go down to zero at band gaps. However, light inside these gaps is attenuated.

In quantum physics, Fermi's Golden Rule provides the possibility to calculate the transition rate. In other words, the probability for transitions from an initial state to another state is determined for a given time interval. It can be written as

$$\Gamma(\omega) = \frac{\pi d^2 \omega}{\hbar \varepsilon_0} N(\omega, \mathbf{r}, \mathbf{e}_d),$$

where Γ is the spontaneous emission rate, $\mathbf{e}_d$ is the orientation and d the amplitude of the dipole moment, ε_0 is the permittivity or dielectric constant and $\hbar$ the reduced Planck constant [21]. The LDOS N is the density of the final states of such transitions that happen due to perturbations. A proportionality between the spontaneous emission rate Γ and the LDOS is now clearly visible.

In [21], the position-dependent spontaneous emission rate is defined by

$$\Gamma(\omega, \mathbf{r}, \mathbf{e}_d) = \frac{6 d^2 \omega^2}{\hbar \varepsilon_0 c^2} \left(\mathbf{e}_d^t \cdot \mathrm{Im}\left(\mathbf{G}(\mathbf{r}, \mathbf{r}; \omega)\right) \cdot \mathbf{e}_d\right),$$

with $\mathrm{Im}\left(()\cdot\right)$ denoting the imaginary part and $\mathbf{G}\left(\cdot,\cdot;\omega\right)$ the Greens function for the time-harmonic Maxwell equations. By applying Fermi's Golden Rule, we can find another version of the LDOS which directly depends on Green's function:

$$N\left(\omega,\mathbf{r},\mathbf{e}_d\right)=\frac{6\omega}{\pi c^2}\left(\mathbf{e}_d^t\cdot\mathrm{Im}\left(\mathbf{G}\left(\mathbf{r},\mathbf{r};\omega\right)\right)\cdot\mathbf{e}_d\right)=\frac{2\omega}{\pi c^2}\mathrm{Im}\left(\mathrm{Tr}\left(\mathbf{G}\left(\mathbf{r},\mathbf{r};\omega\right)\right)\right). \tag{6.3}$$

To evaluate this term, numerical calculations are necessary [19].

Similar to the presentation in [17], it will now be shown how Equation (6.2) can be derived from the term for the LDOS (6.2), which is based on the emission rate. One method to numerically approximate Green's function is the expansion in eigenfunctions.

Since the crystals underlie a discrete translation symmetry, we can apply the Bloch-Floquet theorem. It states that normal modes can be written as

$$\mathbf{E}=\mathbf{E}_{\mathbf{K}}(\mathbf{r})\cdot e^{-i\mathbf{K}\cdot\mathbf{r}},$$

where $\mathbf{K}\cdot\mathbf{r}$ implies the inner product of the two vectors. $\mathbf{E}_{\mathbf{K}}$ is periodic with the structures periodicity and $\mathbf{K}$ the so-called Bloch wave vector. The frequency ω and $\mathbf{K}$ are connected by a dispersion relation $\omega=\omega(\mathbf{K})$ [25]. We say that $\mathbf{E}_{\mathbf{K}}$ are modes of the quantised or $\mathbf{K}$-shifted electric field. The latter name refers to the fact that the term $e^{-i\mathbf{K}\cdot\mathbf{r}}$ describes a shift of the periodic function.

The wave operator of the final form of the problem (2.8) is self-adjoint (or Hermitian). Thus, the eigenfunctions of the Maxwell system are orthogonal to each other and, by the above mentioned theorem of Bloch and Floquet, we can represent them by

$$\mathbf{E}_n=\mathbf{E}_{n,\mathbf{K}}(\mathbf{r})\cdot e^{-i\mathbf{K}\cdot\mathbf{r}}$$

for each band index n. In the case of a finite crystal, the eigenfunctions become normal quasi-modes with a finite width such that this representation is still valid.

The functions $\mathbf{E}_{n,\mathbf{K}}$ satisfy the wave equation with a zero source (see (2.9)) and fulfill the orthogonality relation

$$\int_{\Omega}\mathbf{E}_{n,\mathbf{K}}(\mathbf{r})\cdot\mathbf{E}_{n,\mathbf{K}'}^t(\mathbf{r})\,\mathrm{d}\,\mathbf{r}=\delta_{\mathbf{K},\mathbf{K}'}, \tag{6.4}$$

where ^{t} stands for the complex transposed and $\delta_{\mathbf{K},\mathbf{K}'}$ is the Kronecker delta symbol.

We now denote by $(\omega_{n,\mathbf{K}},\mathbf{E}_{n,\mathbf{K}})$ the n-th eigenvalue and -function of an eigenproblem for a shift by $\mathbf{K}$. Considering a fixed frequency ω, which is no eigenvalue, the Green's function can be expanded into

$$\mathbf{G}\left(\mathbf{r},\mathbf{r}';\omega\right)=\int_{BZ1}\sum_n\mathbf{A}_{n,\mathbf{K}}\left(\mathbf{r}',\omega\right)\mathbf{E}_{n,\mathbf{K}}\left(\mathbf{r}\right)\mathrm{d}\,\mathbf{K}, \tag{6.5}$$

with expansion coefficients $A_{n,\mathbf{K}}$ depending on the position $\mathbf{r}'$ and the frequency ω.

Recall that the Green's function is the solution of the wave equation (2.8) with δ-function source

$$\nabla^2 \mathbf{G}\left(\mathbf{r}, \mathbf{r}'; \omega\right) - k^2 \mathbf{G}\left(\mathbf{r}, \mathbf{r}'; \omega\right) = \nabla^2 \mathbf{G}\left(\mathbf{r}, \mathbf{r}'; \omega\right) - \frac{\omega^2}{c^2} \mathbf{G}\left(\mathbf{r}, \mathbf{r}'; \omega\right) = \delta\left(\mathbf{r} - \mathbf{r}'\right). \quad (6.6)$$

To determine the expansion coefficients, we plug the approximation of the Green's function (6.5) into (6.6) and obtain

$$\int_{BZ1} \sum_n \mathbf{A}_{n,\mathbf{K}}\left(\mathbf{r}', \omega\right) \left(\nabla \times \nabla \times \mathbf{E}_{n,\mathbf{K}}\left(\mathbf{r}\right) - \frac{\omega^2}{c^2} \mathbf{E}_{n,\mathbf{K}}\left(\mathbf{r}\right) \right) \mathrm{d}\,\mathbf{K} = \delta\left(\mathbf{r} - \mathbf{r}'\right).$$

As the eigenfunctions satisfy the wave equation (2.9), we can rewrite this term as

$$\int_{BZ1} \sum_n \mathbf{A}_{n,\mathbf{K}}\left(\mathbf{r}', \omega\right) \left(\frac{\omega_{n,\mathbf{K}}^2}{c^2} - \frac{\omega^2}{c^2} \right) \mathbf{E}_{n,\mathbf{K}}\left(\mathbf{r}\right) \mathrm{d}\,\mathbf{K} = \delta\left(\mathbf{r} - \mathbf{r}'\right).$$

Then we take the L^2 inner product with $\mathbf{E}^t_{n,\mathbf{K}'}(\mathbf{r})$ on both sides. Using the orthogonality condition (6.4) and applying an inverse Fourier transform on the left hand side as well as employing the sifting property of the delta distribution, see equation (6.1), on the right hand side, the coefficients can be specified to be

$$\mathbf{A}_{n,\mathbf{K}'}\left(\mathbf{r}', \omega\right) = \frac{c^2}{\omega_{n,\mathbf{K}'}^2 - \omega^2} \mathbf{E}^t_{n,\mathbf{K}'}\left(\mathbf{r}'\right). \quad (6.7)$$

The result (6.7) can be plugged into the expansion (6.5):

$$\mathbf{G}\left(\mathbf{r}, \mathbf{r}'; \omega\right) = \frac{1}{(2\pi)^3} \sum_n c^2 \int_{BZ1} \frac{\mathbf{E}_{n,\mathbf{K}}(\mathbf{r}) \mathbf{E}^t_{n,\mathbf{K}}(\mathbf{r}')}{\omega_{n,\mathbf{K}}^2 - \omega^2} \mathrm{d}\,\mathbf{K}. \quad (6.8)$$

For the LDOS, we need to determine the imaginary part of the Green's function. It is obvious that $\mathbf{E}_{n,\mathbf{K}}(\mathbf{r}) \mathbf{E}^t_{n,\mathbf{K}}(\mathbf{r}')$ is real and $\frac{1}{\omega_{n,\mathbf{K}}^2 - \omega^2}$ is real for all $\omega_{n,\mathbf{K}}^2 \neq \omega^2$. Thus, we can only have imaginary parts for $-\omega_{n,\mathbf{K}} = \omega$ or $\omega_{n,\mathbf{K}} = \omega$, which are poles of the function (6.8). For the evaluation of the integral $\int_{BZ1} \frac{1}{\omega_{n,\mathbf{K}}^2 - \omega^2} \mathrm{d}\,\mathbf{K}$ we have to use complex analysis. All different modes and thus all possible values of $\mathbf{K}$ are covered while restricting the examinations to the first Brillouin zone, as we did. By a dispersion relation, ω directly depends on $\mathbf{K}$ such that all frequencies can be reached. We can therefore similarly observe the integral

$$\int_{-\infty}^{\infty} \frac{1}{\omega_{n,\mathbf{K}}^2 - \omega^2} \mathrm{d}\,\omega = \int_{-\infty}^{\infty} f(\omega) \mathrm{d}\,\omega. \quad (6.9)$$

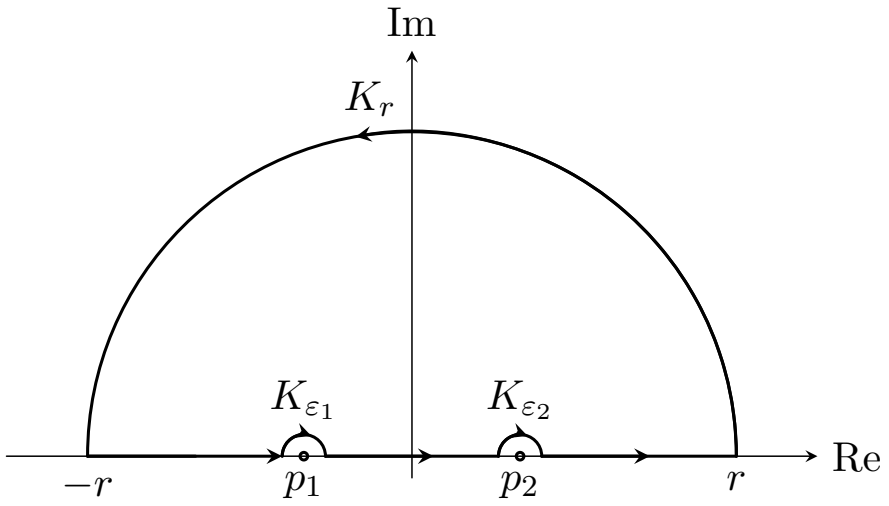

Figure 6.1.: The positively oriented simple closed integration path for solving (6.9) with complex analysis.

For solving (6.9), we can apply the residue theorem from complex analysis. For that purpose, we consider the positively oriented simple closed integration path that is shown in Figure 6.1. Then, the integral along that curve is given by

$$\begin{aligned}\oint_\gamma f(\omega)\,\mathrm{d}\,\omega &= \left(\oint_{-r}^{p_1-\varepsilon_1} - \oint_{K_{\varepsilon_1}} + \oint_{p_1+\varepsilon_1}^{p_2-\varepsilon_2} - \oint_{K_{\varepsilon_2}} + \oint_{p_2+\varepsilon_2}^{r} + \oint_{K_r}\right) f(\omega)\,\mathrm{d}\,\omega \\ &= 2\pi i \sum_m \mathrm{res}_{\omega_m}(f),\end{aligned}$$

where m counts the singularities inside the contour and $\mathrm{res}_s(f)$ stands for the residue of the function f at a given singularity s. In this case, the only singularities are given by the two poles, which were already mentioned. However, the integration path was constructed such that these singularities are not enclosed. The integral over K_r converges to 0 for $r \to \infty$. Hence, for this limit consideration, we obtain

$$\left(\oint_{-\infty}^{p_1-\varepsilon_1} + \oint_{p_1+\varepsilon_1}^{p_2-\varepsilon_2} + \oint_{p_2+\varepsilon_2}^{\infty}\right) f(\omega)\,\mathrm{d}\,\omega = \left(\oint_{K_{\varepsilon_1}} + \oint_{K_{\varepsilon_2}}\right) f(\omega)\,\mathrm{d}\,\omega.$$

For $p_{1,2}$ being poles of the function and $K_{\varepsilon_{1,2}}(t) = p_{1,2} + \varepsilon_{1,2} \cdot e^{i\pi t}, \quad 0 \le t \le 1$, the limit is given by

$$\lim_{\varepsilon_{1,2}\to 0} \oint_{K_{\varepsilon_{1,2}}} f(\omega)\,\mathrm{d}\,\omega = \pi i \mathrm{res}_{p_{1,2}}(f).$$

The residue at a pole p of order l can be computed by

$$\mathrm{res}_p(f) = \frac{1}{(l-1)!}\frac{\mathrm{d}^{l-1}}{\mathrm{d}\,\omega^{l-1}}\left((p-\omega)^l f(\omega)\right)|_{\omega=p},$$

such that for $p_1 = -\omega_{n,\mathbf{K}}$ and $p_2 = \omega_{n,\mathbf{K}}$, both of order $l_{1,2} = 1$, the residues can be computed to be

$$\mathrm{res}_{p_1=-\omega_{n,\mathbf{K}}} = \frac{\omega_{n,\mathbf{K}} - \omega}{(\omega_{n,\mathbf{K}} - \omega)(\omega_{n,\mathbf{K}} + \omega)}\Big|_{\omega=-\omega_{n,\mathbf{K}}} = \frac{-1}{2\omega_{n,\mathbf{K}}} \qquad \text{and} \qquad \mathrm{res}_{p_2=\omega_{n,\mathbf{K}}} = \frac{1}{2\omega_{n,\mathbf{K}}}.$$

As these imaginary parts can only be obtained for $\omega^2 \neq \omega_{n,\mathbf{K}}^2$, we can use the Dirac distribution to express this instantaneous event. After applying the limits of $\mathbf{r} \to \infty$ and $\varepsilon_{1,2} \to 0$, the integral (6.9) can be represented in the following way:

$$\begin{aligned}\int_{-\infty}^{\infty} f(\omega)\,\mathrm{d}\,\omega &= \lim_{r\to\infty}\left(\lim_{\varepsilon_1,\varepsilon_2\to 0}\left(\oint_\gamma f(\omega)\,\mathrm{d}\,\omega\right)\right) \\ &= \frac{i\pi}{2\omega_{n,\mathbf{K}}}\left(\delta\left(\omega_{n,\mathbf{K}} - \omega\right) - \delta\left(\omega_{n,\mathbf{K}} + \omega\right)\right).\end{aligned}$$

We can drop the term that corresponds to the negative pole $\omega = -\omega_{n,\mathbf{K}}$, as it is reasonable to consider only positive frequencies in this context. Finally, the imaginary part of the Green's function can be written as

$$\mathrm{Im}\left(\mathbf{G}\left(\mathbf{r},\mathbf{r};\omega\right)\right) = \frac{1}{(2\pi)^3}\frac{\pi c^2}{2\omega}\sum_n |\mathbf{E}_{n,\mathbf{K}}|^2 \delta\left(\omega_{n,\mathbf{K}} - \omega\right).$$

Then, this result can be used in the expression (6.2) to find the formulation of the LDOS given in Equation (6.2). When the orientation of the emitter is not fixed, we can average over all orientations to obtain

$$N(\omega,\mathbf{r}) = \frac{1}{(2\pi)^3}\sum_n \int_{BZ1} |\mathbf{E}_{n,\mathbf{K}}(\mathbf{r})|^2 \delta\left(\omega - \omega_{n,\mathbf{K}}\right)\mathrm{d}\,\mathbf{K}.$$

6.2. Computations

Next, we have to find a way to compute the LDOS given in Equation (6.2) as accurately as possible. For the case of an infinite crystal, the Green's function can be computed analytically. However, for real photonic crystals with a limited size, we have to approximate the formula. To that end, we have to find an expression for the Brillouin zone integral

$$\int_{BZ1} f(\mathbf{K})\delta\left(\omega - \omega(\mathbf{K})\right)\mathrm{d}\,\mathbf{K}. \tag{6.10}$$

One option to evaluate the integral is the linear tetrahedron method. A detailed description can be found in [4]. For this technique, we split the integral over the first Brillouin zone into integrals over non-overlapping tetrahedra to substitute (6.10). Inside each of the solids, $f(\mathbf{K})$ and $\omega(\mathbf{K})$ are then interpolated linearly. The corners of the tetrahedra are expressed in terms of $\mathbf{K}$ and named $\mathbf{K}_0$, $\mathbf{K}_1$, $\mathbf{K}_2$ and $\mathbf{K}_3$. Approximate

$\omega(\mathbf{K})$ by $\omega_0 + a\,(\mathbf{K} - \mathbf{K}_0)$. The evaluation of the integrals over the disjoint tetrahedra is then straightforward. The drawback of this method is the restriction of the accuracy of the computations by the linear interpolation. This problem is of particular importance, when the solution of the Maxwell equations is obtained using higher-order accurate finite element methods.

Alternatively, consider the identity

$$\delta(g(x)) = \sum_{m=1}^{n} \frac{\delta(x - x_m)}{|g'(x_m)|}$$

for the delta distribution, where x_m runs through the simple zeros of $g(x)$ [12]. In our case, $g(x)$ is given by the function $(\omega - \omega(\mathbf{K}))$. If we could find an expression for the dispersion relation, it would be possible to find its zeros. Then, we could evaluate the integral (6.10) analytically. However, the relation $\omega(\mathbf{K})$ is complicated for three-dimensional photonic crystals where any direction of propagation is possible, as it depends on the polarization state. Furthermore, the dielectric function ε_r has to be known for the calculations. In [25], the dispersion relation for light travelling in only one direction is given by

$$\left(\mathbf{K}^2 - \omega^2\mu_r\varepsilon_{r,0})\right)\left((\mathbf{K} - \mathbf{G})^2 - \omega^2\mu_r\varepsilon_{r,0}\right) - \left(\omega^2\mu_r|\varepsilon_{r,1}|\right)^2 = 0.$$

Here, $\varepsilon_{r,0}, \varepsilon_{r,1}$ denote the zeroth and first Fourier component of the periodic dielectric tensor ε_r, $\mathbf{G}$ corresponds to the reciprocal lattice vector in the direction of propagation. Although the formula is not even accurate, it is already complex. A more general setup would thus make it necessary to impose even larger assumptions. Still, the term for $\omega(\mathbf{K})$ would get even more involved.

Additionally, the computation of the LDOS is used as an alternative to an explicit representation of the dispersion relation. The complexity of this ansatz as well as the paradoxical usage of an expression for $\omega(\mathbf{K})$ make this method impractical for our purposes.

Hence, we are going to use another possibility to describe the Dirac delta distribution by expressing it in terms of a converging sequence. All elements of the sequence should have their maximum at a fixed point and this value should increase while the graph gets narrower when moving along the sequence [12]. These properties are ensured by the following definition:

Definition 6.2. A sequence $s_j(x)$ is called a *delta-convergent sequence* if

$$\lim_{j\to\infty} \int_{-\infty}^{\infty} s_j(x) f(x)\,\mathrm{d}\,x = f(0)$$

for all functions $f(x)$ that are sufficiently smooth for $-\infty < x < \infty$. Thus, delta-convergent sequences satisfy

$$\lim_{j\to\infty} s_j = \delta(x).$$

If the charge is located at a point $x = \xi$ instead of $x = 0$, these equations have to be modified to

$$\lim_{j\to\infty} \int_{-\infty}^{\infty} s_j(x-\xi) f(x)\,\mathrm{d}\,x = f(\xi) \quad \text{and} \qquad \lim_{j\to\infty} s_j(x-\xi) = \delta(x-\xi).$$

Such sequences are for example the Gaussian sequence

$$s_j(x) = \sqrt{\frac{j}{\pi}} e^{-jx^2}$$

or Lorentzian functions

$$s_j(x) = \frac{1}{\pi} \frac{j}{1 + j^2 x^2}.$$

A modified version of the latter one is

$$s_j(x) = \frac{1}{2\pi} \frac{j}{\frac{1}{4} + j^2 x^2}.$$

The Complex Photonic Systems group (CoPS) in the Department of Science and Technology at the University of Twente focuses its research on controlling light and optical processes in nanophotonic structures. Regarding the solution of Maxwell's equations in photonic crystals, they cooperate with the MaCS group. In 2014, members of CoPS introduced a new approach for the computation of the LDOS. We will now present the idea that is explained in [26].

In [26] the ansatz of delta-convergent sequences is applied, which supports our own conclusions. They decide on using modified Loretzians, because these functions describe well how the frequency width of the modes increases based on the finite size of the photonic crystal. Further, the value m is chosen to be $\frac{L}{a}$, where L is the size of the crystal and a the lattice constant in the corresponding direction. Then, m is equal to the number of wave vectors in the Brillouin zone. The LDOS can thus be written as

$$\begin{aligned} N(\omega, \mathbf{r}) &= \frac{1}{(2\pi)^3} \sum_n \left(\lim_{j\to\infty} \frac{1}{2\pi} \int_{BZ1} \frac{j}{\frac{1}{4} + j^2 \left(\omega - \omega_{n,\mathbf{K}}\right)^2} |\mathbf{E}_{n,\mathbf{K}}|^2 \,\mathrm{d}\,\mathbf{K} \right) \\ &\approx \frac{1}{(2\pi)^3} \sum_n \left(\lim_{j\to m} \frac{1}{2\pi} \int_{BZ1} \frac{j}{\frac{1}{4} + j^2 \left(\omega - \omega_{n,\mathbf{K}}\right)^2} |\mathbf{E}_{n,\mathbf{K}}|^2 \,\mathrm{d}\,\mathbf{K} \right) \\ &\approx \frac{1}{(2\pi)^3} \frac{1}{m} \sum_n \sum_{j=1}^{m} \frac{1}{2\pi} \frac{j}{\frac{1}{4} + j^2 \left(\omega - \omega_{n,\mathbf{K}}\right)^2} |\mathbf{E}_{n,\mathbf{K}}|^2. \end{aligned}$$

In the first step, the finite size of the crystal is taken into account by limiting j as mentioned above. The second approximation shows the quadrature of the integral. This is possible as we integrate over all wave vectors in the first Brillouin zone, which are

enumerated by the values of $j = 1, \ldots, m$. From a computational view, that leaves us with an easy sum instead of the integral over the whole Brillouin zone.

In a next step, the eigenfunctions are approximated. To that end, we represent the Bloch wave vector by its real and imaginary parts $\mathrm{Re}\,(\mathbf{K})$ and $\mathrm{Im}\,(\mathbf{K})$, respectively. Within bands, we have propagating Bloch modes and thus $\mathrm{Im}\,(\mathbf{K}) = 0$ and $\mathbf{K}$ is real. But in a band gap, light is damped and $\mathbf{K}$ becomes complex. While the real part of the vector is fixed at the value it has at the Brillouin zone edge, namely $\mathrm{Re}\,(\mathbf{K}) = \frac{\pi}{a}$, the imaginary part depends on the frequency. Starting at zero at both edges of the gap it increases to a maximum value at its center.

Let us consider the wave vector $\mathbf{K} = \mathrm{Re}\,(\mathbf{K}) + i\mathrm{Im}\,(\mathbf{K})$ inside a band gap. There, the waves are damped exponentially as a result of Bragg diffraction:

$$\begin{aligned}\mathbf{E}_n &= \mathbf{E}_{n,\mathbf{K}}(\mathbf{r}) \cdot e^{-i\mathbf{K}\cdot\mathbf{r}} = \mathbf{E}_{n,\mathbf{K}}(\mathbf{r}) \cdot e^{i(\mathrm{Re}(\mathbf{K})+i\mathrm{Im}(\mathbf{K}))\cdot\mathbf{r}} = \mathbf{E}_{n,\mathbf{K}}(\mathbf{r}) \cdot e^{i\mathrm{Re}(\mathbf{K})\cdot\mathbf{r}} \cdot e^{-\mathrm{Im}(\mathbf{K})\cdot\mathbf{r}} \\ &= \hat{\mathbf{E}}_{n,\mathbf{K}}(\mathbf{r}) \cdot e^{-\mathrm{Im}(\mathbf{K})\cdot\mathbf{r}},\end{aligned}$$

where $\hat{\mathbf{E}}_{n,\mathbf{K}}$ is periodic and interpolates the field $\mathbf{E}_{n,\mathbf{K}}$ between the edges of Bloch modes. The imaginary part of the Bloch wave vector is obtained from band structure calculations.

To obtain $\hat{\mathbf{E}}_{n,\mathbf{K}}$, the field values and amplitudes are approximated inside the gap. For that purpose, we use the fact that waves propagate at the edges of the gap. Therefore, the absolute value of the field has the same period as the crystal in these places. The position of the maximum of the field is interpolated linearly into the gap by taking the values at both edges into account. The amplitude is obtained by linear interpolation between the values at the two edges of the gap. This provides a technique to approximate $\mathbf{E}_{n,\mathbf{K}}$.

The attenuation of the resulting field $\hat{\mathbf{E}}_{n,\mathbf{K}}$ is then expressed by multiplying the value by the corresponding decaying factor. Finally, the local density of states can be approximated by

$$N(\omega, \mathbf{r}) \approx \frac{1}{(2\pi)^4} \frac{1}{m} \sum_{i=1}^{n} \sum_{j=1}^{m} \frac{j}{\frac{1}{4} + j^2 \left(\omega - \omega_{n,\mathbf{K}}\right)^2} |\hat{\mathbf{E}}_{n,\mathbf{K}}|^2 e^{-2\mathrm{Im}(\mathbf{K})\mathbf{r}}.$$

This model is a promising approach for finding a highly accurate numerical method to compute the LDOS.

7. Conclusion and outlook

In this work, a method for computing the light propagation in photonic crystals was presented. First, a mathematical model for the time-harmonic Maxwell equations, which describe light propagation, was developed. The usage of the discontinuous Galerkin finite element method was motivated and applied to the problem. As a main achievement, Nédélec basis functions are employed to the DG discretization of the problem. Since they are free of spurious modes, they are an improvement compared to the basis functions of Ainsworth and Coyle. This is interesting for the software package `hpGEM`, which provides the tools to solve PDEs from the fields of fluid mechanics and electromagnetism with the DG FEM. Its application `DG-Max` implements the discretisation and solution of the considered problem. Up to now, the basis functions only the basis functions of Ainsworth and Coyle were available in `hpGEM`. Here, Nédélec's functions were included to and tested in the software environment. This includes the evaluation of the errors and the accuracy of the solution and the eigenvalue computations for the time-harmonic Maxwell equations.

Furthermore, the local density of states is discussed, which is closely linked to the behaviour of light in a photonic crystal. An approach for the computation of these values are described.

7.1. Nédélec's basis functions

Due to its mathematical properties, the basis function set introduced by Nédélec in 1980 is beneficial for solving the time-harmonic Maxwell equations with the DG FEM. As far as tests were possible during this study taking the memory and computing time limitations into account, we can assume that Nédélec's basis functions perform as expected. This holds only for the special problems considered in our case. Before adding the basis functions of Nédélec to the general package `hpGEM`, advantages of these basis functions as well as those of Ainsworth and Coyle have to be analysed in more detail. The choice of basis functions should be left open for the general case, because the benefits, which Nédélec's set of functions provides for the Maxwell problem, do not necessarily hold for other applications.

The approval of the functionality of the described basis functions must be seen as preliminary decision, rather than a final one. The tests were carried out with a computer with a quite low performance. This led to strong restrictions regarding the tests. Due to long computational times, only a small amount of data could be collected. This made the evaluation difficult. The determination of the order of accuracy was hardly possible for the time-harmonic solution and not at all for the eigenvalue calculations.

At any rate, all tests that were performed should be rerun and expanded to finer meshes. This will hopefully confirm the obtained results. The sub-optimal accuracy of the time-harmonic solution in the L^2-norm, which we observed, has to be checked. If these results prove to be true also for more detailed tests, further analysis on that topic is necessary, including also theoretical investigations.

Moreover, more complicated test cases should be considered. As an example, it should be tested if the code for the eigenvalue computations performs correctly for all choices of the wave vector k. This would enable us to plot the band structure of the considered structure. The `DG-Max`-code provides a possibility to compute the eigenvalues for 61 different values of the wave vector inside the first Brillouin zone. The value of k is changed in the three directions separately. Taking steps of $\frac{\pi}{20}$ k moves from $(0,0,0)^t$ to $(\pi,0,0)^t$, from $(\pi,0,0)^t$ to $(\pi,\pi,0)^t$ and from $(\pi,\pi,0)^t$ to $(\pi,\pi,\pi)^t$. Due to the limited possibilities during this study, these expensive computations could be carried out for n being maximal two. n is connected to the mesh size, in particular being the parameter for the code which influences the number of elements N of the mesh by $N = n^3 \cdot 5$. The coarse mesh prohibited a meaningful evaluation. Future work, however, could include these tests for larger values of n. In this setting, not only single-material structures should be observed. Additionally, the examination of simple layered structures, like the Bragg stack, would be possible. The Bragg stack describes a structure containing of two layers, e. g. both half as wide as the unit cube and with $\varepsilon_r = 1$ in the first layer and $\varepsilon_r = 13$ in the second.

Even though a lot of work still remains, first results showed that Nédélec's basis functions are a convincing choice for the DG FEM for time-harmonic Maxwell equations.

7.2. The local density of states

The approach, which was presented for the computations of the local density of states, needs further analysis. The CoPS group tested it for the one-dimensional case, resulting in a first verification of the model. However, own examinations would be necessary. It would be of importance to check the compatibility with the `DG-Max` application. The accuracy in that framework should not be below the accuracy of the eigenvalue computations. It might be a good idea to include only the usage of the Lorentzians, first. This would take the finite crystal size into account, but leaves the approximation of the eigenfunctions for later considerations. With a more reliable eigenvalue solver the first step could already yield good results. It should be checked if the model is able to handle band crossings, which can appear for higher frequencies or when considering large parts of the Brillouin zone.

Of course, future work should also include a broadly based research for alternative techniques.

7.3. Improvement of the algorithm in general

In general, the whole algorithm could be improved in several directions. For instance, the code could be sped up by removing the null space of the curl-curl operator or by preconditioning. As another possibility the flexibility of the mesh could be increased or the refinement of the mesh could be automated. Furthermore, the algorithm could be extended to being able to handle defects in the crystal instead of only perfect unit cells. This would give a large improvement for designing photonic crystals for applications like waveguides. These are just some examples on the large amount of future work that still needs to be done in this field.

A. Further information

A.1. Coordinate transformations of integrals

In Chapter 3, the idea of using a reference element was introduced. Computations are performed on this simple domain and the results are then transformed to the physical element of consideration by an affine mapping. Later in that chapter, the special curl-conforming transformation is explained.

However, not only the basis functions have to be transformed. When developing the DG FEM, the weak formulation of the partial differential equation has to be considered considered as well. This results in integrals over the elements. Thus, a transformation from an integral over a reference element to one which considers the domain of the physical element has to be applied. Therefore, we use the standard identity

$$\int_K \mathbf{u} \,\mathrm{d}\, K = \int_{\hat{K}} (\mathbf{u} \circ F_K) \, |B_K| \,\mathrm{d}\, \hat{K}.$$

A.2. Quadrature of the integrals

While solving the PDE with a finite element method, we have to evaluate integrals numerically. A general form for the quadrature of integrals using order N is

$$\int_A f(\mathbf{x}) \,\mathrm{d}\, \mathbf{x} = \sum_{i=1}^{N} w_i f(\xi_i),$$

where w_i are the so-called weights, ξ_i denote distinct nodes and A is the domain of integration. Different rules vary in the choice of the nodes and weights and are available for various types of reference elements.

It is necessary to find suitable integration points and weights. We can use any system of linearly independent functions satisfying two conditions. First, we should be able to determine their integrals analytically and, secondly, the order of accuracy should be reasonably good. For Gauß-type quadrature rules we take the sum over weighted function values of non-equidistantly distributed integration points. Nodes and weights can be determined by solving the system of non-linear algebraic equations that is obtained after inserting a sufficient number of linearly dependent functions of known integral [22].

For the DG FEM with a tetrahedral mesh, we want to apply quadrature rules for triangles (for the boundaries of the elements) and on tetrahedra (for the interior). They

are obtained by transforming the integrated function to the reference quadrilateral or brick, respectively. Consequently, composite Gauß quadrature rules are applied [22].

To find rules that are exact up to the order p of our basis functions, we have to choose N to be large enough. The most restrictive term regarding the order N in the weak formulation (4.6) of the Maxwell problem is the multiplication of two basis functions. Therefore, taking $N \leq 2p$ for the quadrature rule provides us with sufficient accuracy.

For tables of weights and nodes for the Gauß quadrature on triangles and tetrahedra, please check [22, chapter4].

A.3. Basis functions of higher order

With the same method as described in Section 3.2, the basis functions for orders $p = 2$ to $p = 5$ are determined. In addition, the curl of the basis functions is computed. The results of order $p = 2$ are shown in the following section. After calculating the edge, face and element basis functions of several different orders, we can find a pattern and thus find general expressions for any p.

Order $p = 2$

We find basis functions on directed edges e_{ij} between vertices v_i and v_j, $i < j$,

$$\Lambda_2 = \left\{ \lambda_j^2 \nabla\lambda_i - \lambda_i\lambda_j\nabla\lambda_j, \lambda_i\lambda_j\nabla\lambda_j - \lambda_i^2\nabla\lambda_i \right\}$$

and on faces f_{ijk} with vertices v_i, v_j and v_k, $i < j < k$,

$$\Lambda_3 = \{\lambda_j\lambda_k\nabla\lambda_i - \lambda_i\lambda_k\nabla\lambda_j, \lambda_i\lambda_k\nabla\lambda_j - \lambda_i\lambda_j\nabla\lambda_k\}$$

The total set of basis functions is then given by $\Lambda = \Lambda_2 \bigcup \Lambda_3$.

The gradients can be computed to be (in order of appearance of the basis functions Ψ_{ij} and Ψ_{ijk}):

$$\nabla\Psi_{ij} = 3\lambda_j \left(\nabla\lambda_j \times \nabla\lambda_i\right)$$

$$\nabla\Psi_{ij} = 3\lambda_i \left(\nabla\lambda_j \times \nabla\lambda_i\right)$$

$$\nabla\Psi_{ijk} = 2\lambda_k \left(\nabla\lambda_j \times \nabla\lambda_i\right) + \left(\lambda_i\nabla\lambda_j - \lambda_j\nabla\lambda_i\right) \times \nabla\lambda_k$$

$$\nabla\Psi_{ijk} = 2\lambda_i \left(\nabla\lambda_k \times \nabla\lambda_j\right) + \left(\lambda_j\nabla\lambda_k - \lambda_k\nabla\lambda_j\right) \times \nabla\lambda_i$$

General order p

For each the edges, faces and elements, we can find a general form of writing the basis functions for all p.

On the directed edge between vertices v_i and v_j, $i < j$ (as can already be assumed based on $p = 1$ and $p = 2$) the basis functions are given by

$$\Psi_{ij} = \lambda_i^l \lambda_j^m \left(\lambda_j \nabla\lambda_i - \lambda_i \nabla\lambda_j\right),$$

where $0 \leq l, m \leq p-1$, $l+m = p-1$. They appear for all orders $p \geq 1$. The corresponding curl can be determined to be

$$\nabla\Psi_{ij} = (l + m + 2)\, \lambda_i^l \lambda_j^m \left(\nabla\lambda_j \times \nabla\lambda_i\right).$$

For the faces between the vertices v_i, v_j and v_k, $i < j < k$, we can find the basis functions

$$\begin{aligned}
\Psi_{1,ijk} =& \lambda_i^l \lambda_j^m \lambda_k^{n+1} \left(\lambda_j \nabla\lambda_i - \lambda_i \nabla\lambda_j\right) \\
\Psi_{2,ijk} =& \lambda_i^{l+1} \lambda_j^m \lambda_k^n \left(\lambda_k \nabla\lambda_j - \lambda_j \nabla\lambda_i\right),
\end{aligned}$$

where $0 \leq l, m, n \leq p-2$, $l + m + n = p - 2$. The curl is given by

$$\begin{aligned}
\nabla\Psi_{1,ijk} =& (l + m + 2)\, \lambda_i^l \lambda_j^m \lambda_k^{n+1} \left(\nabla\lambda_j \times \nabla\lambda_i\right) \\
&+ (n + 1)\, \lambda_i^l \lambda_j^m \lambda_k^n \left(\nabla\lambda_k \times \left(\lambda_j \nabla\lambda_i - \lambda_i \nabla\lambda_j\right)\right) \\
\nabla\Psi_{2,ijk} =& (m + n + 2)\, \lambda_i^{l+1} \lambda_j^m \lambda_k^n \left(\nabla\lambda_k \times \nabla\lambda_j\right) \\
&+ (l + 1)\, \lambda_i^l \lambda_j^m \lambda_k^n \left(\nabla\lambda_k \times \left(\lambda_j \nabla\lambda_i - \lambda_i \nabla\lambda_j\right)\right).
\end{aligned}$$

The basis functions for the entire element exist for order $p \geq 3$. They are expressed with the help of the Lagrange basis functions for all four vertices:

$$\begin{aligned}
\Psi_{1,1234} =& \lambda_1^l \lambda_2^m \lambda_3^{n+1} \lambda_4^{r+1} \left(\lambda_2 \nabla\lambda_1 - \lambda_1 \nabla\lambda_2\right) \\
\Psi_{2,1234} =& \lambda_1^{l+1} \lambda_2^m \lambda_3^n \lambda_4^{r+1} \left(\lambda_3 \nabla\lambda_2 - \lambda_2 \nabla\lambda_3\right) \\
\Psi_{3,1234} =& \lambda_1^{l+1} \lambda_2^{m+1} \lambda_3^n \lambda_4^r \left(\lambda_4 \nabla\lambda_3 - \lambda_3 \nabla\lambda_4\right),
\end{aligned}$$

where $0 \leq l, m, n, r \leq p-3$, $l + m + n + r = p - 3$. We can find the curls to be

$$\begin{aligned}
\nabla\Psi_{1,1234} =& (l + m + 2)\, \lambda_1^l \lambda_2^m \lambda_3^{n+1} \lambda_4^{r+1} \left(\nabla\lambda_2 \times \nabla\lambda_1\right) \\
&+ (n + 1)\, \lambda_1^l \lambda_2^m \lambda_3^n \lambda_4^{r+1} \left(\nabla\lambda_3 \times \left(\lambda_2 \nabla\lambda_1 - \lambda_1 \nabla\lambda_2\right)\right) \\
&+ (r + 1)\, \lambda_1^l \lambda_2^m \lambda_3^{n+1} \lambda_4^r \left(\nabla\lambda_4 \times \left(\lambda_2 \nabla\lambda_1 - \lambda 1 \nabla\lambda_2\right)\right) \\
\nabla\Psi_{2,1234} =& (m + n + 2)\, \lambda_1^{l+1} \lambda_2^m \lambda_3^n \lambda_4^{r+1} \left(\nabla\lambda_3 \times \nabla\lambda_2\right) \\
&+ (l + 1)\, \lambda_1^l \lambda_2^m \lambda_3^n \lambda_4^{r+1} \left(\nabla\lambda_1 \times \left(\lambda_3 \nabla\lambda_2 - \lambda_2 \nabla\lambda_3\right)\right) \\
&+ (r + 1)\, \lambda_1^{l+1} \lambda_2^m \lambda_3^n \lambda_4^r \left(\nabla\lambda_4 \times \left(\lambda_3 \nabla\lambda_2 - \lambda 2 \nabla\lambda_3\right)\right) \\
\nabla\Psi_{1,1234} =& (n + r + 2)\, \lambda_1^{l+1} \lambda_2^{m+1} \lambda_3^n \lambda_4^r \left(\nabla\lambda_4 \times \nabla\lambda_3\right) \\
&+ (l + 1)\, \lambda_1^l \lambda_2^{m+1} \lambda_3^n \lambda_4^r \left(\nabla\lambda_1 \times \left(\lambda_4 \nabla\lambda_3 - \lambda_3 \nabla\lambda_4\right)\right) \\
&+ (m + 1)\, \lambda_1^{l+1} \lambda_2^m \lambda_3^n \lambda_4^r \left(\nabla\lambda_2 \times \left(\lambda_4 \nabla\lambda_3 - \lambda 3 \nabla\lambda_4\right)\right).
\end{aligned}$$

These results are used for the changes of the `hpGEM`-code discussed in Chapter 5.

B. Tables

Here, all tables containing the values and results discussed throughout the testing of the `hpGEM` package can be found.

B.1. The accuracy of the numerical solution to the time-harmonic Maxwell problem

In this section the errors of the numerical solutions and the corresponding computed orders of accuracy as described in Section 5.2 are listed. This includes homogeneous and periodic boundary conditions, the Brezzi and IP flux formulations and the basis function sets of Ainsworth-Coyle as well as those of Nédélec.

B.1.1. Homogeneous boundary conditions

First, homogeneous boundary conditions are considered.

	Ainsworth-Coyle		Nédélec		
	$\|\mathbf{E}-\mathbf{E}_h\|_{\mathrm{L}^2}$	$\|\mathbf{E}-\mathbf{E}_h\|_{DG}$	$\|\mathbf{E}-\mathbf{E}_h\|_{\mathrm{L}^2}$	$\|\mathbf{E}-\mathbf{E}_h\|_{\mathrm{H(curl)}}$	$\|\mathbf{E}-\mathbf{E}_h\|_{DG}$
$p=1$					
$N=5$	2.9160E-01	4.0233E-00	3.2771E-01	4.0487E-00	4.0627E-00
$N=40$	2.5192E-01	1.8536E-00	4.3000E-01	1.9286E-00	1.9345E-00
$N=320$	5.2906E-02	9.5273E-01	2.3367E-01	1.0066E-00	1.0079E-00
$N=2560$	–	–	1.1937E-01	5.0824E-01	5.0852E-01
$p=2$					
$N=5$	2.6768E-01	1.2834E-00	3.5889E-01	1.2443E-00	1.2715E-00
$N=40$	2.9329E-02	4.8757E-01	1.0782E-01	4.9609E-01	4.9767E-01
$p=3$					
$N=5$	5.4841E-02	8.6251E-01	1.1784E-01	8.7221E-01	8.7358E-01
$N=40$	4.3092E-03	9.6475E-02	1.7124E-02	9.8274E-02	9.8398E-02
$p=4$					
$N=5$	2.2580E-02	1.0833E-01	3.4513E-02	1.0719E-01	1.0813E-01
$N=40$	5.2082E-04	1.5244E-02	2.1707E-03	1.5645E-02	1.5655E-02

Table B.1.: Error in the numerical solution for different norms computed on the unit cell with homogeneous boundary conditions and using the Brezzi flux formulation in the DG FEM. Calculations are carried out for Ainsworth-Coyle and Nédélec basis functions.

			Ainsworth-Coyle		Nédélec	
			order (L^2)	order (DG)	order (L^2)	order (DG)
$p=1$						
$N=5$	$\rightarrow$	$N=40$	0.221	1.118	-0.392	1.070
$N=40$	$\rightarrow$	$N=320$	2.462	0.960	0.880	0.941
$N=320$	$\rightarrow$	$N=2560$	–	–	0.969	0.987
$p=2$						
$N=5$	$\rightarrow$	$N=40$	3.190	1.396	1.735	1.353
$p=3$						
$N=5$	$\rightarrow$	$N=40$	3.670	3.160	3.381	3.150
$p=4$						
$N=5$	$\rightarrow$	$N=40$	5.438	2.829	3.991	2.788

Table B.2.: The order of accuracy of the DG FEM calculated as described at the beginning of Section 5.2. The computations are conducted for the domain of a unit cell with homogeneous boundary conditions and using the Brezzi flux formulation. Ainsworth-Coyle and Nédélec basis functions are compared.

	Ainsworth-Coyle		Nédélec		
	$\|\mathbf{E}-\mathbf{E}_h\|_{\mathrm{L}^2}$	$\|\mathbf{E}-\mathbf{E}_h\|_{DG}$	$\|\mathbf{E}-\mathbf{E}_h\|_{\mathrm{L}^2}$	$\|\mathbf{E}-\mathbf{E}_h\|_{\mathrm{H(curl)}}$	$\|\mathbf{E}-\mathbf{E}_h\|_{DG}$
$p=1$					
$N=5$	5.2299E-01	4.2613E-00	5.5907E-01	4.3084E-00	4.3089E-00
$N=40$	2.9434E-01	1.9557E-00	4.4632E-01	2.0383E-00	2.0385E-00
$N=320$	6.2216E-02	9.9251E-01	2.3532E-01	1.0600E-00	1.0602E-00
$N=2560$	1.2202E-02	4.8571E-01	1.1942E-01	5.2871E-01	5.2882E-01
$p=2$					
$N=5$	3.0592E-01	1.4829E-00	4.2563E-01	1.5581E-00	1.5587E-00
$N=40$	3.1428E-02	5.0528E-01	1.0890E-01	5.2703E-01	5.2721E-01
$N=320$	3.2844E-03	1.3116E-01	2.8747E-02	1.3844E-01	1.3853E-01
$p=3$					
$N=5$	5.9269E-02	8.8299E-01	1.2072E-01	8.9685E-01	8.9709E-01
$N=40$	4.2700E-03	9.8680E-02	1.7258E-02	1.0198E-01	1.0203E-01
$N=320$	1.8923E-04	1.3096E-02	2.2374E-03	1.3510E-02	1.3552E-02
$p=4$					
$N=5$	2.2916E-02	1.1691E-01	3.5682E-02	1.2199E-01	1.2209E-01
$N=40$	4.8469E-04	1.5657E-02	2.1674E-03	1.5997E-02	1.6007E-02

Table B.3.: Error in the numerical solution of different norms computed on the unit cell with homogeneous boundary conditions and using the IP flux in the DG FEM. Calculations are carried out for Ainsworth-Coyle and Nédélec basis functions.

			Ainsworth-Coyle		Nédélec	
			order (L^2)	order (DG)	order (L^2)	order (DG)
$p=1$						
$N=5$	$\rightarrow$	$N=40$	0.829	1.124	3.593	1.080
$N=40$	$\rightarrow$	$N=320$	2.242	0.979	0.923	0.943
$N=320$	$\rightarrow$	$N=2560$	2.350	1.031	0.979	1.003
$p=2$						
$N=5$	$\rightarrow$	$N=40$	3.283	1.553	1.967	1.564
$N=40$	$\rightarrow$	$N=320$	3.258	1.946	1.921	1.928
$p=3$						
$N=5$	$\rightarrow$	$N=40$	3.795	3.161	2.806	3.136
$N=40$	$\rightarrow$	$N=320$	4.496	2.914	2.947	2.912
$p=4$						
$N=5$	$\rightarrow$	$N=40$	5.563	2.901	4.041	2.931

Table B.4.: The order of accuracy of the DG FEM calculated as described at the beginning of Section 5.2. The computations are conducted for the domain of a unit cell with homogeneous boundary conditions and using the IP flux. Ainsworth-Coyle and Nédélec basis functions are compared.

B.1.2. Periodic boundary conditions

Then, the functionality of the periodic boundary conditions is tested.

	Ainsworth-Coyle		Nédélec		
	$\|\mathbf{E}-\mathbf{E}_h\|_{\mathrm{L}^2}$	$\|\mathbf{E}-\mathbf{E}_h\|_{DG}$	$\|\mathbf{E}-\mathbf{E}_h\|_{\mathrm{L}^2}$	$\|\mathbf{E}-\mathbf{E}_h\|_{\mathrm{H(curl)}}$	$\|\mathbf{E}-\mathbf{E}_h\|_{DG}$
$p=1$					
$N=40$	2.8315E-01	8.0153E-00	3.1674E-01	8.0157E-00	8.0410E-00
$N=320$	7.8529E-01	3.7502E-00	4.2904E-01	3.7820E-00	3.7907E-00
$N=2560$	–	–	2.3354E-01	1.9718E-00	1.9733E-00
$p=2$					
$N=40$	8.7998E-01	2.6575E-00	3.5652E-01	2.4062E-00	2.4614E-00
$p=3$					
$N=40$	9.3049E-02	1.7210E-00	1.3268E-01	1.7345E-01	1.7367E-01
$p=4$					
$N=40$	8.4310E-02	2.2801E-01	–	–	–

Table B.5.: Error in the numerical solution of different norms computed on the unit cell with periodic boundary conditions and using the Brezzi flux formulation in the DG FEM. Calculations are carried out for Ainsworth-Coyle and Nédélec basis functions.

			Ainsworth-Coyle		Nédélec	
			order (L^2)	order (DG)	order (L^2)	order (DG)
$p=1$						
$N=40$	$\rightarrow$	$N=320$	-1.472	1.096	-0.438	1.085
$N=320$	$\rightarrow$	$N=2560$	–	–	0.877	0.942

Table B.6.: The order of accuracy of the DG FEM calculated as described at the beginning of Section 5.2. The computations are conducted for the domain of a unit cell with periodic boundary conditions and using the Brezzi flux formulation. Ainsworth-Coyle and Nédélec basis functions are compared.

	Ainsworth-Coyle		Nédélec		
	$\|\mathbf{E}-\mathbf{E}_h\|_{\mathrm{L}^2}$	$\|\mathbf{E}-\mathbf{E}_h\|_{DG}$	$\|\mathbf{E}-\mathbf{E}_h\|_{\mathrm{L}^2}$	$\|\mathbf{E}-\mathbf{E}_h\|_{\mathrm{H(curl)}}$	$\|\mathbf{E}-\mathbf{E}_h\|_{DG}$
$p=1$					
$N=40$	5.1160E-01	8.4678E-00	5.4757E-01	8.5588E-00	8.5600E-00
$N=320$	7.9627E-01	3.9248E-00	4.4358E-01	3.9909E-00	3.9914E-00
$N=2560$	1.1043E-01	1.9392E-00	2.3431E-01	2.0574E-00	2.0578E-00
$N=20480$	1.5009E-02	9.4445E-01	1.1911E-01	1.0111E-00	1.0115E-00
$p=2$					
$N=40$	8.9083E-01	3.0170E-00	4.2431E-01	3.0121E-00	3.0135E-00
$N=320$	7.5562E-02	1.0087E-00	1.0901E-01	1.0383E-00	1.0388E-00
$N=2560$	5.4339E-03	3.6719E-01	2.8663E-02	2.7845E-01	2.7877E-01
$p=3$					
$N=40$	9.4595E-02	1.7625E-00	1.3475E-01	1.7814E-00	1.7820E-00
$N=320$	1.2577E-02	1.9873E-01	1.7198E-02	2.0308E-01	2.0344E-01
$p=4$					
$N=40$	8.4366E-02	2.4471E-01	3.5718E-02	2.3634E-01	2.3662E-01

Table B.7.: Error in the numerical solution of different norms computed on the unit cell with periodic boundary conditions and using the IP flux in the DG FEM. Calculations are carried out for Ainsworth-Coyle and Nédélec basis functions.

			Ainsworth-Coyle		Nédélec	
			order (L^2)	order (DG)	order (L^2)	order (DG)
$p = 1$						
$N = 40$	$\rightarrow$	$N = 320$	-0.638	1.109	-0.392	1.101
$N = 320$	$\rightarrow$	$N = 2560$	2.850	1.017	0.880	0.956
$N = 2560$	$\rightarrow$	$N = 20480$	2.879	1.458	1.038	1.025
$p = 2$						
$N = 40$	$\rightarrow$	$N = 320$	2.911	1.581	1.968	1.537
$N = 320$	$\rightarrow$	$N = 2560$	3.798	1.458	1.927	1.898
$p = 3$						
$N = 40$	$\rightarrow$	$N = 320$		3.149	2.970	3.131

Table B.8.: The order of accuracy of the DG FEM calculated as described at the beginning of Section 5.2. The computations are conducted for the domain of a unit cell with periodic boundary conditions and using the IP flux. Ainsworth-Coyle and Nédélec basis functions are compared.

B.2. The accuracy of the eigenvalue computations for the Maxwell problem

The eigenvalues for both types of numerical fluxes are listed. Furthermore, the errors of the eigenvalue computations and the corresponding order of accuracy for Nédélec's basis functions are presented.

	Ainsworth-Coyle			Nédélec	
expected	$N = 5$	$N = 40$	$N = 320$	$N = 40$	$N = 320$
2	3.989517	2.325243	2.092188	1.921157	1.986089
2	3.989517	2.325243	2.092188	1.921157	1.986089
2	3.989517	2.325243	2.092188	1.921157	1.986089
3	7.347626	4.066462	3.203803	4.333374	3.012086
3	7.347626	4.066462	3.203803	4.333374	3.012086
5	11.481380	5.744246	5.544179	5.707445	4.827141
5	11.481380	5.744246	5.544179	5.707445	4.827141
5	11.481380	5.744246	5.544179	5.707445	4.827141
5	12.193098	8.390553	5.544179	7.632618	4.827141
5	12.193098	8.390553		7.632618	4.827141
5	12.193098	8.390553		7.632618	4.827141
6	15.727188	10.510892	6.762504	8.127985	5.841230
6	15.727188	10.510892	6.762504	8.127985	5.841230
6	15.727188	10.510892	6.762504	8.127985	5.841230
6	23.609118	10.648430	6.790371	8.872788	5.917906
6	23.609118	10.648430	6.790371	8.872788	5.917906
6	23.609118	10.648430	6.790371	9.510186	5.917906

Table B.9.: The eigenvalues of the time-harmonic Maxwell equations divided by π^2 for homogeneous boundary conditions and the Brezzi flux formulation. We consider the Ainsworth-Coyle basis functions as well as those of Nédélec, both of order $p = 1$.

	Ainsworth-Coyle			Nédélec	
expected	$N = 5$	$N = 40$	$N = 320$	$N = 5$	$N = 40$
2	2.173152	2.023379	2.001676	1.832689	1.995802
2	2.173152	2.023379	2.001676	1.832689	1.995802
2	2.173152	2.023379	2.001676	1.832689	1.995802
3	4.003570	4.066462	3.005611	3.720219	2.936346
3	4.003570	4.066462	3.005611	3.720219	2.936346
5	6.406003	5.164960	5.023303	4.418297	4.560061
5	6.406003	5.164960	5.023303		4.560061
5	6.406003	5.164960	5.023303		4.560061
5	8.921440	5.303728	5.023303	4.440845	5.087234
5	8.921440	5.303728		4.440845	5.087234
5	8.921440	5.303728		4.440845	5.087234
6	11.657019	6.376197	6.039846	6.135862	6.068820
6	11.657019	6.376197	6.039846	6.135862	6.068820
6	11.657019	6.376197	6.039846	6.135862	6.068820
6	11.676408	6.488295	6.041019	8.300746	6.112407
6	11.676408	6.488295	6.041019	8.300746	6.112407
6	11.676408	6.488295	6.041019	8.300746	6.112407

Table B.10.: The eigenvalues of the time-harmonic Maxwell equations divided by π^2 for homogeneous boundary conditions and the Brezzi flux formulation. We consider the Ainsworth-Coyle basis functions as well as those of Nédélec, both of order $p = 2$.

	Ainsworth-Coyle		Nédélec	
expected	$N = 5$	$N = 40$	$N = 5$	$N = 40$
2	2.056822	2.000934	2.031045	2.000324
2	2.056822	2.000934	2.031045	2.000324
2	2.056822	2.000934	2.031045	2.000324
3	3.229837	3.007847	3.217972	3.007244
3	3.229837	3.007847	3.217972	3.007244
5	5.265708	5.030104	4.229326	5.016980
5	5.265708	5.030104	4.229326	5.016980
5	5.265708	5.030104	4.229326	5.016980
5	5.532334	5.030104	5.029418	5.001425
5	5.532334	5.030104	5.029418	5.001425
5	5.532334	5.030104	5.029418	5.001425
6	6.764523	6.053528	6.376072	5.999523
6	6.764523	6.053528	6.376072	5.999523
6	6.764523	6.053528	6.376072	5.999523
6	7.366976	6.053528		6.031114
6	7.366976	6.053528		6.031114
6	7.366976	6.053528		6.031114

Table B.11.: The eigenvalues of the time-harmonic Maxwell equations divided by π^2 for homogeneous boundary conditions and the Brezzi flux formulation. We consider the Ainsworth-Coyle basis functions as well as those of Nédélec, both of order $p = 3$.

	Ainsworth-Coyle		Nédélec	
expected	$N = 5$	$N = 40$	$N = 5$	$N = 40$
2	2.001482	2.000024	1.998178	2.000016
2	2.001482	2.000024	1.998178	2.000016
2	2.001482	2.000024	1.998178	2.000016
3	3.012553	3.000023	2.997333	2.999904
3	3.012553	3.000023	2.997333	2.999904
5	5.224655	5.001617	5.085339	5.000597
5	5.224655	5.001617	5.085339	5.000597
5	5.224655	5.001617	5.085339	5.000597
5	5.224655	5.001617	5.165563	5.000773
5	5.224655	5.001617	5.165563	5.000773
5	5.224655	5.001617	5.165563	5.000773
6	6.436586	6.004116	6.081371	6.001560
6	6.436586	6.004116	6.081371	6.001560
6	6.436586	6.004116	6.081371	6.001560
6	6.563491	6.004116	6.410231	6.002695
6	6.563491	6.004116	6.410231	6.002695
6	6.563491	6.004116	6.410231	6.002695

Table B.12.: The eigenvalues of the time-harmonic Maxwell equations divided by π^2 for homogeneous boundary conditions and the Brezzi flux formulation. We consider the Ainsworth-Coyle basis functions as well as those of Nédélec, both of order $p = 4$.

	$N = 40$		$N = 320$	
eigenvalue	$\frac{\|\omega^2-\omega_h^2\|_{\mathrm{L}^2}}{\omega^2}$	order	$\frac{\|\omega^2-\omega_h^2\|_{\mathrm{L}^2}}{\omega^2}$	order
$2\pi^2$	3.94215E-02	–	6.95554E-03	2.503
$2\pi^2$	3.94215E-02	–	6.95554E-03	2.503
$2\pi^2$	3.94215E-02	–	6.95554E-03	2.503
$3\pi^2$	4.44458E-01	–	4.02869E-03	6.786
$3\pi^2$	4.44458E-01	–	4.02869E-03	6.786
$5\pi^2$	1.41489E-01	–	3.45718E-02	2.033
$5\pi^2$	1.41489E-01	–	3.45718E-02	2.033
$5\pi^2$	1.41489E-01	–	3.45718E-02	2.033
$5\pi^2$	5.26524E-01	–	3.45718E-02	3.929
$5\pi^2$	5.26524E-01	–	3.45718E-02	3.929
$5\pi^2$	5.26524E-01	–	3.45718E-02	3.929
$6\pi^2$	3.54664E-01	–	2.64618E-02	3.744
$6\pi^2$	3.54664E-01	–	2.64618E-02	3.744
$6\pi^2$	3.54664E-01	–	2.64618E-02	3.744
$6\pi^2$	4.78798E-01	–	1.36824E-02	5.129
$6\pi^2$	4.78798E-01	–	1.36824E-02	5.129
$6\pi^2$	5.85031E-01	–	1.36824E-02	5.418

Table B.13.: The error in the eigenvalues of the Maxwell problem and the corresponding order of accuracy for homogeneous boundary conditions and the Brezzi flux formulation. We consider Nédélec basis functions of order $p = 1$.

	$N = 5$		$N = 40$	
eigenvalue	$\frac{\|\omega^2-\omega_h^2\|_{\mathrm{L}^2}}{\omega^2}$	order	$\frac{\|\omega^2-\omega_h^2\|_{\mathrm{L}^2}}{\omega^2}$	order
$2\pi^2$	8.36556E-02	–	2.09921E-03	5.317
$2\pi^2$	8.36556E-02	–	2.09921E-03	5.317
$3\pi^2$	2.40073E-01	–	2.12179E-02	3.500
$3\pi^2$	2.40073E-01	–	2.12179E-02	3.500
$5\pi^2$	1.16341E-01	–	8.79878E-02	0.403
$5\pi^2$	1.16341E-01	–	8.79878E-02	0.403
$5\pi^2$	1.16341E-01	–	8.79878E-02	0.403
$5\pi^2$	1.11831E-01	–	1.74467E-02	2.680
$5\pi^2$	1.11831E-01	–	1.74467E-02	2.680
$5\pi^2$	1.11831E-01	–	1.74467E-02	2.680
$6\pi^2$	2.26437E-02	–	1.14694E-02	0.981
$6\pi^2$	2.26437E-02	–	1.14694E-02	0.981
$6\pi^2$	2.26437E-02	–	1.14694E-02	0.981
$6\pi^2$	3.83458E-01	–	1.87344E-02	4.355
$6\pi^2$	3.83458E-01	–	1.87344E-02	4.355
$6\pi^2$	3.83458E-01	–	1.87344E-02	4.355

Table B.14.: The error in the eigenvalues of the Maxwell problem and the corresponding order of accuracy for homogeneous boundary conditions and the Brezzi flux formulation. We consider Nédélec basis functions of order $p = 2$.

	$N = 5$		$N = 40$	
eigenvalue	$\frac{\|\omega^2-\omega_h^2\|_{\mathrm{L}^2}}{\omega^2}$	order	$\frac{\|\omega^2-\omega_h^2\|_{\mathrm{L}^2}}{\omega^2}$	order
$2\pi^2$	1.55227E-02	–	1.62073E-04	6.582
$2\pi^2$	1.55227E-02	–	1.62073E-04	6.582
$2\pi^2$	1.55227E-02	–	1.62073E-04	6.582
$3\pi^2$	7.26563E-02	–	2.41478E-03	4.911
$3\pi^2$	7.26563E-02	–	2.41478E-03	4.911
$5\pi^2$	1.54135E-01	–	2.85057E-04	9.079
$5\pi^2$	1.54135E-01	–	2.85057E-04	9.079
$5\pi^2$	1.54135E-01	–	2.85057E-04	9.079
$5\pi^2$	5.88356E-03	–	3.39600E-03	0.793
$5\pi^2$	5.88356E-03	–	3.39600E-03	0.793
$5\pi^2$	5.88356E-03	–	3.39600E-03	0.793
$6\pi^2$	6.26786E-02	–	7.95609E-05	9.622
$6\pi^2$	6.26786E-02	–	7.95609E-05	9.622
$6\pi^2$	6.26786E-02	–	7.95609E-05	9.622
$6\pi^2$	–	–	5.18570E-03	–
$6\pi^2$	–	–	5.18570E-03	–
$6\pi^2$	–	–	5.18570E-03	–

Table B.15.: The error in the eigenvalues of the Maxwell problem and the corresponding order of accuracy for homogeneous boundary conditions and the Brezzi flux formulation. We consider Nédélec basis functions of order $p = 3$.

	$N = 5$		$N = 40$	
eigenvalue	$\frac{\|\omega^2-\omega_h^2\|_{\mathrm{L}^2}}{\omega^2}$	order	$\frac{\|\omega^2-\omega_h^2\|_{\mathrm{L}^2}}{\omega^2}$	order
$2\pi^2$	9.11273E-04	–	8.06506E-06	6.820
$2\pi^2$	9.11273E-04	–	8.06506E-06	6.820
$2\pi^2$	9.11273E-04	–	8.06506E-06	6.820
$3\pi^2$	8.88134E-04	–	3.19568E-05	4.798
$3\pi^2$	8.88134E-04	–	3.19568E-05	4.798
$5\pi^2$	1.70678E-02	–	1.19295E-04	7.161
$5\pi^2$	1.70678E-02	–	1.19295E-04	7.161
$5\pi^2$	1.70678E-02	–	1.19295E-04	7.161
$5\pi^2$	3.31126E-02	–	1.54657E-04	7.742
$5\pi^2$	3.31126E-02	–	1.54657E-04	7.742
$5\pi^2$	3.31126E-02	–	1.54657E-04	7.742
$6\pi^2$	1.35618E-02	–	2.59590E-04	5.707
$6\pi^2$	1.35618E-02	–	2.59590E-04	5.707
$6\pi^2$	1.35618E-02	–	2.59590E-04	5.707
$6\pi^2$	6.83718E-02	–	4.49167E-04	7.250
$6\pi^2$	6.83718E-02	–	4.49167E-04	7.250
$6\pi^2$	6.83718E-02	–	4.49167E-04	7.250

Table B.16.: The error in the eigenvalues of the Maxwell problem and the corresponding order of accuracy for homogeneous boundary conditions and the Brezzi flux formulation. We consider Nédélec basis functions of order $p = 4$.

	Ainsworth-Coyle		Nédélec	
expected	$N = 40$	$N = 320$	$N = 40$	$N = 320$
2	2.462907	2.115748	1.960473	1.993534
2	2.462907	2.115748	1.960473	1.993534
2	2.462907	2.115748	1.960473	1.993534
3	4.642731	3.248040	4.547980	3.032881
3	4.642731	3.248040	4.547980	3.032881
5	6.243371	5.680280	6.388551	4.880312
5	6.243371	5.680280	6.388551	4.880312
5	6.243371	5.680280	6.388551	4.880312
5		5.680098		4.880337
5		5.680098		4.880337
5		5.680098		4.880337
6	9.376376	6.970310	8.862083	5.923920
6	9.376376	6.970310	8.862083	5.923920
6	9.376376	6.970310	8.862083	5.923920
6		6.918196	9.047705	6.010060
6		6.918196	9.047705	6.010060
6		6.918196	9.047705	6.010060

Table B.17.: The eigenvalues of the time-harmonic Maxwell equations divided by π^2 for homogeneous boundary conditions and the IP flux. We consider the Ainsworth-Coyle basis functions as well as those of Nédélec, both of order $p = 1$.

	Ainsworth-Coyle			Nédélec		
expected	$N = 5$	$N = 40$	$N = 320$	$N = 5$	$N = 40$	$N = 320$
2	2.299003	2.029092	2.001730	1.895775	2.001562	2.000001
2	2.299003	2.029092	2.001730	1.895775	2.001562	2.000001
2	2.299003	2.029092	2.001730	1.895775	2.001562	2.000001
3	4.368109	3.026672	3.005740	4.448459	2.944495	3.003401
3	4.368109	3.026672	3.005740	4.448459	2.944495	3.003401
5	7.622032	5.202780	5.023878	7.986376	4.627896	5.001013
5	7.622032	5.202780	5.023878	7.986376	4.627896	5.001013
5	7.622032	5.202780	5.023878	7.986376	4.627896	5.001013
5		5.392528	5.023880		5.124574	5.001014
5		5.392528	5.023880		5.124574	5.001014
5		5.392528	5.023880		5.124574	5.001014
6		6.472326	6.040603		6.223178	6.011078
6		6.472326	6.040603		6.223178	6.011078
6		6.472326	6.040603		6.223178	6.011078
6		6.600697	6.041408		6.259462	6.021748
6		6.600697	6.041408		6.259462	6.021748
6		6.600697	6.041408		6.259462	6.021748

Table B.18.: The eigenvalues of the time-harmonic Maxwell equations divided by π^2 for homogeneous boundary conditions and the IP flux. We consider the Ainsworth-Coyle basis functions as well as those of Nédélec, both of order $p = 2$.

	Ainsworth-Coyle		Nédélec	
expected	$N = 5$	$N = 40$	$N = 5$	$N = 40$
2	2.069669	2.000992	2.041764	2.000390
2	2.069669	2.000992	2.041764	2.000390
2	2.069669	2.000992	2.041764	2.000390
3	3.320226	3.008612	3.337336	3.009536
3	3.320226	3.008612	3.337336	3.009536
5	5.335751	5.028795	4.407611	5.006151
5	5.335751	5.028795	4.407611	5.006151
5	5.335751	5.028795	4.407611	5.006151
5	5.627701	5.033064	5.104582	5.023819
5	5.627701	5.033064	5.104582	5.023819
5	5.627701	5.033064	5.104582	5.023819
6	6.901687	6.055216	6.642249	6.018554
6	6.901687	6.055216	6.642249	6.018554
6	6.901687	6.055216	6.642249	6.018554
6	7.607924	6.057801	7.225726	6.035535
6	7.607924	6.057801		6.035535
6	7.607924	6.057801		6.035535

Table B.19.: The eigenvalues of the time-harmonic Maxwell equations divided by π^2 for homogeneous boundary conditions and the IP flux. We consider the Ainsworth-Coyle basis functions as well as those of Nédélec, both of order $p = 3$.

	Ainsworth-Coyle		Nédélec	
expected	$N = 5$	$N = 40$	$N = 5$	$N = 40$
2	2.001799	2.000024	1.998822	2.000015
2	2.001799	2.000024	1.998822	2.000015
2	2.001799	2.000024	1.998822	2.000015
3	3.013596	3.000022	2.799304	2.999907
3	3.013596	3.000022	2.799304	2.999907
5	5.231505	5.001408	5.171833	5.000812
5	5.231505	5.001408	5.171833	5.000812
5	5.231505	5.001408	5.171833	5.000812
5	5.261293	5.001614	5.232830	5.000807
5	5.261293	5.001614	5.232830	5.000807
5	5.261293	5.001614	5.232830	5.000807
6	6.555025	6.003727	6.432361	6.002661
6	6.555025	6.003727	6.432361	6.002661
6	6.555025	6.003727	6.432361	6.002661
6	6.629222	6.004006	6.490984	6.002966
6	6.629222	6.004006	6.490984	6.002966
6	6.629222	6.004006	6.490984	6.002966

Table B.20.: The eigenvalues of the time-harmonic Maxwell equations divided by π^2 for homogeneous boundary conditions and the IP flux. We consider the Ainsworth-Coyle basis functions as well as those of Nédélec, both of order $p = 4$.

	$N = 40$		$N = 320$	
eigenvalue	$\frac{\|\omega^2-\omega_h^2\|_{\mathrm{L}^2}}{\omega^2}$	order	$\frac{\|\omega^2-\omega_h^2\|_{\mathrm{L}^2}}{\omega^2}$	order
$2\pi^2$	1.97637E-02	–	3.23279E-03	2.612
$2\pi^2$	1.97637E-02	–	3.23279E-03	2.612
$2\pi^2$	1.97637E-02	–	3.23279E-03	2.612
$3\pi^2$	5.15993E-01	–	1.09604E-02	5.557
$3\pi^2$	5.15993E-01	–	1.09604E-02	5.557
$5\pi^2$	2.77710E-01	–	2.39376E-02	3.536
$5\pi^2$	2.77710E-01	–	2.39376E-02	3.536
$5\pi^2$	2.77710E-01	–	2.39376E-02	3.536
$5\pi^2$	–	–	2.39325E-02	–
$5\pi^2$	–	–	2.39325E-02	–
$5\pi^2$	–	–	2.39325E-02	–
$6\pi^2$	4.77014E-01	–	1.26801E-02	5.233
$6\pi^2$	4.77014E-01	–	1.26801E-02	5.233
$6\pi^2$	4.77014E-01	–	1.26801E-02	5.233
$6\pi^2$	5.07951E-01	–	1.67661E-03	8.243
$6\pi^2$	5.07951E-01	–	1.67661E-03	8.243
$6\pi^2$	5.07951E-01	–	1.67661E-03	8.243

Table B.21.: The error in the eigenvalues of the Maxwell problem and the corresponding order of accuracy for homogeneous boundary conditions and the IP flux. We consider Nédélec basis functions of order $p = 1$.

	$N = 5$		$N = 40$		$N = 320$	
eigenvalue	$\frac{\|\omega^2-\omega_h^2\|_{L^2}}{\omega^2}$	order	$\frac{\|\omega^2-\omega_h^2\|_{L^2}}{\omega^2}$	order	$\frac{\|\omega^2-\omega_h^2\|_{L^2}}{\omega^2}$	order
$2\pi^2$	5.21125E-02	–	7.80910E-04	6.060	5.67288E-07	10.427
$2\pi^2$	5.21125E-02	–	7.80910E-04	6.060	5.67288E-07	10.427
$2\pi^2$	5.21125E-02	–	7.80910E-04	6.060	5.67288E-07	10.427
$3\pi^2$	4.82820E-01	–	1.85016E-02	4.706	1.13364E-03	4.029
$3\pi^2$	4.82820E-01	–	1.85016E-02	4.706	1.13364E-03	4.029
$5\pi^2$	5.97275E-01	–	7.44208E-02	3.005	2.02764E-04	8.520
$5\pi^2$	5.97275E-01	–	7.44208E-02	3.005	2.02764E-04	8.520
$5\pi^2$	5.97275E-01	–	7.44208E-02	3.005	2.02764E-04	8.520
$5\pi^2$	–	–	2.49148E-02	–	2.02825E-04	6.941
$5\pi^2$	–	–	2.49148E-02	–	2.02825E-04	6.941
$5\pi^2$	–	–	2.49148E-02	–	2.02825E-04	6.941
$6\pi^2$	–	–	3.71963E-02	–	1.84639E-03	4.332
$6\pi^2$	–	–	3.71963E-02	–	1.84639E-03	4.332
$6\pi^2$	–	–	3.71963E-02	–	1.84639E-03	4.332
$6\pi^2$	–	–	4.32437E-02	–	3.62466E-03	3.577
$6\pi^2$	–	–	4.32437E-02	–	3.62466E-03	3.577
$6\pi^2$	–	–	4.32437E-02	–	3.62466E-03	3.577

Table B.22.: The error in the eigenvalues of the Maxwell problem and the corresponding order of accuracy for homogeneous boundary conditions and the IP flux. We consider Nédélec basis functions of order $p = 2$.

	$N = 5$		$N = 40$	
eigenvalue	$\frac{\|\omega^2-\omega_h^2\|_{\mathrm{L}^2}}{\omega^2}$	order	$\frac{\|\omega^2-\omega_h^2\|_{\mathrm{L}^2}}{\omega^2}$	order
$2\pi^2$	2.08821E-02	–	1.94952E-04	6.743
$2\pi^2$	2.08821E-02	–	1.94952E-04	6.743
$2\pi^2$	2.08821E-02	–	1.94952E-04	6.743
$3\pi^2$	1.12445E-01	–	3.17861E-03	5.145
$3\pi^2$	1.12445E-01	–	3.17861E-03	5.145
$5\pi^2$	1.18478E-01	–	1.23012E-03	6.590
$5\pi^2$	1.18478E-01	–	1.23012E-03	6.590
$5\pi^2$	1.18478E-01	–	1.23012E-03	6.590
$5\pi^2$	2.09163E-02	–	4.76370E-03	2.134
$5\pi^2$	2.09163E-02	–	4.76370E-03	2.134
$5\pi^2$	2.09163E-02	–	4.76370E-03	2.134
$6\pi^2$	1.07042E-01	–	3.09238E-03	5.113
$6\pi^2$	1.07042E-01	–	3.09238E-03	5.113
$6\pi^2$	1.07042E-01	–	3.09238E-03	5.113
$6\pi^2$	2.04288E-01	–	5.92252E-03	5.108
$6\pi^2$	2.04288E-01	–	5.92252E-03	5.108
$6\pi^2$	2.04288E-01	–	5.92252E-03	5.108

Table B.23.: The error in the eigenvalues of the Maxwell problem and the corresponding order of accuracy for homogeneous boundary conditions and the IP flux. We consider Nédélec basis functions of order $p = 3$.

	$N = 5$		$N = 40$	
eigenvalue	$\frac{\|\omega^2-\omega_h^2\|_{L^2}}{\omega^2}$	order	$\frac{\|\omega^2-\omega_h^2\|_{L^2}}{\omega^2}$	order
$2\pi^2$	5.88970E-04	–	7.71043E-06	6.255
$2\pi^2$	5.88970E-04	–	7.71043E-06	6.255
$2\pi^2$	5.88970E-04	–	7.71043E-06	6.255
$3\pi^2$	6.68987E-02	–	3.09774E-05	11.077
$3\pi^2$	6.68987E-02	–	3.09774E-05	11.077
$5\pi^2$	3.43666E-02	–	1.61465E-04	7.734
$5\pi^2$	3.43666E-02	–	1.61465E-04	7.734
$5\pi^2$	3.43666E-02	–	1.61465E-04	7.734
$5\pi^2$	4.65655E-02	–	1.62418E-04	8.163
$5\pi^2$	4.65655E-02	–	1.62418E-04	8.163
$5\pi^2$	4.65655E-02	–	1.62418E-04	8.163
$6\pi^2$	7.20601E-01	–	4.43459E-04	10.666
$6\pi^2$	7.20601E-01	–	4.43459E-04	10.666
$6\pi^2$	7.20601E-01	–	4.43459E-04	10.666
$6\pi^2$	8.18307E-02	–	4.94289E-04	7.371
$6\pi^2$	8.18307E-02	–	4.94289E-04	7.371
$6\pi^2$	8.18307E-02	–	4.94289E-04	7.371

Table B.24.: The error in the eigenvalues of the Maxwell problem and the corresponding order of accuracy for homogeneous boundary conditions and the IP flux. We consider Nédélec basis functions of order $p = 4$.

	Ainsworth-Coyle		Nédélec	
expected	$N = 40$	$N = 320$	$N = 40$	$N = 320$
4	4.737702	4.347081	2.629281	3.814782
4	4.737702	4.347081	2.629281	3.814782
4	4.737702	4.347081	2.629281	3.814782
4	4.737702	4.347081	2.629281	3.814782
4	4.737702	4.347081	2.629281	3.814782
4	4.737702	4.347081	2.629281	3.814782
4	5.454062	4.347081	5.690690	3.814782
4	5.454062	4.347081	5.690690	3.814782
4	5.454062	4.347081	5.690690	3.814782
4	5.454062	4.347081	5.690690	3.814782
4	5.454062	4.347081	5.690690	
4	5.454062	4.347081	5.690690	

Table B.25.: The eigenvalues of the time-harmonic Maxwell equations divided by π^2 for periodic boundary conditions and the Brezzi flux formulation. We consider the Ainsworth-Coyle basis functions as well as those of Nédélec, both of order $p = 1$.

	Ainsworth-Coyle	Nédélec	
expected	$N = 40$	$N = 40$	$N = 320$
4	4.038316	3.761830	3.999209
4	4.038316	3.761830	3.999209
4	4.038316	3.761830	3.999209
4	4.038316	3.761830	3.999209
4	4.038316	3.761830	3.999209
4	4.038316	3.761830	3.999209
4	4.268175	4.233741	3.999209
4	4.268175	4.233741	3.999209
4	4.268175	4.233741	3.999209
4	4.268175	4.233741	3.999209
4	4.268175	4.233741	3.999209
4	4.268175	4.233741	3.999209

Table B.26.: The eigenvalues of the time-harmonic Maxwell equations divided by π^2 for periodic boundary conditions and the Brezzi flux formulation. We consider the Ainsworth-Coyle basis functions as well as those of Nédélec, both of order $p = 2$.

expected	Ainsworth-Coyle $p = 3, \quad N = 40$	Nédélec $p = 3, \quad N = 40$	Ainsworth-Coyle $p = 4, \quad N = 40$	Nédélec $p = 4, \quad N = 40$
4	4.001863	3.988441	4.000043	3.999587
4	4.001863	3.988441	4.000043	3.999587
4	4.001863	3.988441	4.000043	3.999587
4	4.001863	3.988441	4.000043	3.999587
4	4.001863	3.988441	4.000043	3.999587
4	4.001863	3.988441	4.000043	3.999587
4	4.017457	4.014236	4.000725	4.000545
4	4.017457	4.014236	4.000725	4.000545
4	4.017457	4.014236	4.000725	4.000545
4	4.017457	4.014236	4.000725	4.000545
4	4.017457	4.014236	4.000725	4.000545
4	4.017457	4.014236	4.000725	4.000545

Table B.27.: The eigenvalues of the time-harmonic Maxwell equations divided by π^2 for periodic boundary conditions and the Brezzi flux formulation. We consider the Ainsworth-Coyle basis functions as well as those of Nédélec, both of order $p = 3$ and $p = 4$.

eigenvalue	$N = 40$ $\frac{\|\omega^2-\omega_h^2\|_{\mathrm{L}^2}}{\omega^2}$	order	$N = 320$ $\frac{\|\omega^2-\omega_h^2\|_{\mathrm{L}^2}}{\omega^2}$	order
$4\pi^2$	3.42680E-01	–	4.63044E-02	2.888
$4\pi^2$	3.42680E-01	–	4.63044E-02	2.888
$4\pi^2$	3.42680E-01	–	4.63044E-02	2.888
$4\pi^2$	3.42680E-01	–	4.63044E-02	2.888
$4\pi^2$	3.42680E-01	–	4.63044E-02	2.888
$4\pi^2$	3.42680E-01	–	4.63044E-02	2.888
$4\pi^2$	4.22672E-01	–	4.63044E-02	3.190
$4\pi^2$	4.22672E-01	–	4.63044E-02	3.190
$4\pi^2$	4.22672E-01	–	4.63044E-02	3.190
$4\pi^2$	4.22672E-01	–	4.63044E-02	3.190
$4\pi^2$	4.22672E-01	–	–	–
$4\pi^2$	4.22672E-01	–	–	–

Table B.28.: The error in the eigenvalues of the Maxwell problem and the corresponding order of accuracy for periodic boundary conditions and the Brezzi flux formulation. We consider Nédélec basis functions of order $p = 1$.

	$N = 40$		$N = 320$	
eigenvalue	$\frac{\|\omega^2-\omega_h^2\|_{\mathrm{L}^2}}{\omega^2}$	order	$\frac{\|\omega^2-\omega_h^2\|_{\mathrm{L}^2}}{\omega^2}$	order
$4\pi^2$	5.95425E-02	–	1.97820E-04	8.234
$4\pi^2$	5.95425E-02	–	1.97820E-04	8.234
$4\pi^2$	5.95425E-02	–	1.97820E-04	8.234
$4\pi^2$	5.95425E-02	–	1.97820E-04	8.234
$4\pi^2$	5.95425E-02	–	1.97820E-04	8.234
$4\pi^2$	5.95425E-02	–	1.97820E-04	8.234
$4\pi^2$	5.84352E-02	–	1.97820E-04	8.207
$4\pi^2$	5.84352E-02	–	1.97820E-04	8.207
$4\pi^2$	5.84352E-02	–	1.97820E-04	8.207
$4\pi^2$	5.84352E-02	–	1.97820E-04	8.207
$4\pi^2$	5.84352E-02	–	1.97820E-04	8.207
$4\pi^2$	5.84352E-02	–	1.97820E-04	8.207

Table B.29.: The error in the eigenvalues of the Maxwell problem and the corresponding order of accuracy for periodic boundary conditions and the Brezzi flux formulation. We consider Nédélec basis functions of order $p = 2$.

	$p = 3$, $N = 40$	$p = 4$ $N = 320$
eigenvalue	$\frac{\|\omega^2-\omega_h^2\|_{\mathrm{L}^2}}{\omega^2}$	$\frac{\|\omega^2-\omega_h^2\|_{\mathrm{L}^2}}{\omega^2}$
$4\pi^2$	3.55897E-03	1.03388E-04
$4\pi^2$	3.55897E-03	1.03388E-04
$4\pi^2$	3.55897E-03	1.03388E-04
$4\pi^2$	3.55897E-03	1.03388E-04
$4\pi^2$	3.55897E-03	1.03388E-04
$4\pi^2$	3.55897E-03	1.03388E-04
$4\pi^2$	2.88970E-03	1.36135E-04
$4\pi^2$	2.88970E-03	1.36135E-04
$4\pi^2$	2.88970E-03	1.36135E-04
$4\pi^2$	2.88970E-03	1.36135E-04
$4\pi^2$	2.88970E-03	1.36135E-04
$4\pi^2$	2.88970E-03	1.36135E-04

Table B.30.: The error in the eigenvalues of the Maxwell problem for periodic boundary conditions and the Brezzi flux formulation. We consider Nédélec basis functions of order $p = 3$ and $p = 4$.

	Ainsworth-Coyle		Nédélec	
expected	$N = 40$	$N = 320$	$N = 40$	$N = 320$
4	4.805947	4.428548	2.723988	3.859787
4	4.805947	4.428548	2.723988	3.859787
4	4.805947	4.428548	2.723988	3.859787
4	4.805947	4.428548	2.723988	3.859787
4	4.805947	4.428548	2.723988	3.859787
4	4.805947	4.428548	2.723988	3.859787
4	6.240312		6.408342	3.859787
4	6.240312		6.408342	3.859787
4	6.240312		6.408342	
4	6.240312		6.408342	
4	6.240312		6.408342	
4	6.240312			

Table B.31.: The eigenvalues of the time-harmonic Maxwell equations divided by π^2 for periodic boundary conditions and the IP flux. We consider the Ainsworth-Coyle basis functions as well as those of Nédélec, both of order $p = 1$.

	Ainsworth-Coyle		Nédélec	
expected	$N = 40$	$N = 320$	$N = 40$	$N = 320$
4	4.044400	4.011886	3.791082	4.002704
4	4.044400	4.011886	3.791082	4.002704
4	4.044400	4.011886	3.791082	4.002704
4	4.044400	4.011886	3.791082	4.002704
4	4.044400	4.011886	3.791082	4.002704
4	4.044400	4.011886		4.002704
4	4.342215	4.011886	4.345547	4.002704
4	4.342215	4.011886	4.345547	4.002704
4	4.342215	4.011886	4.345547	4.002704
4	4.342215	4.011886	4.345547	4.002704
4	4.342215	4.011886	4.345547	4.002704
4	4.342215	4.011886		

Table B.32.: The eigenvalues of the time-harmonic Maxwell equations divided by π^2 for periodic boundary conditions and the IP flux. We consider the Ainsworth-Coyle basis functions as well as those of Nédélec, both of order $p = 2$.

expected	Ainsworth-Coyle $p = 3, \quad N = 40$	Nédélec $p = 3, \quad N = 40$	Ainsworth-Coyle $p = 4, \quad N = 40$	Nédélec $p = 4, \quad N = 40$
4	4.001953	3.989216	4.000800	3.999597
4	4.001953	3.989216	4.000800	3.999597
4	4.001953	3.989216	4.000800	3.999597
4	4.001953	3.989216	4.000800	3.999597
4	4.001953	3.989216	4.000800	3.999597
4	4.001953	3.989216	4.000800	3.999597
4	4.020750	4.022007	4.000801	4.000842
4	4.020750	4.022007	4.000801	4.000842
4	4.020750	4.022007	4.000801	4.000842
4	4.020750	4.022007	4.000801	4.000842
4	4.020750	4.022007	4.000801	4.000842
4	4.020750	4.022007	4.000801	4.000842

Table B.33.: The eigenvalues of the time-harmonic Maxwell equations divided by π^2 for periodic boundary conditions and the IP flux. We consider the Ainsworth-Coyle basis functions as well as those of Nédélec, both of order $p = 3$ and $p = 4$.

	$N = 40$		$N = 320$	
eigenvalue	$\frac{\|\omega^2-\omega_h^2\|_{\mathrm{L}^2}}{\omega^2}$	order	$\frac{\|\omega^2-\omega_h^2\|_{\mathrm{L}^2}}{\omega^2}$	order
$4\pi^2$	3.19003E-01	–	3.50532E-02	3.186
$4\pi^2$	3.19003E-01	–	3.50532E-02	3.186
$4\pi^2$	3.19003E-01	–	3.50532E-02	3.186
$4\pi^2$	3.19003E-01	–	3.50532E-02	3.186
$4\pi^2$	3.19003E-01	–	3.50532E-02	3.186
$4\pi^2$	3.19003E-01	–	3.50532E-02	3.186
$4\pi^2$	6.02085E-01	–	3.50532E-02	4.102
$4\pi^2$	6.02085E-01	–	3.50532E-02	4.102
$4\pi^2$	6.02085E-01	–	–	–
$4\pi^2$	6.02085E-01	–	–	–
$4\pi^2$	6.02085E-01	–	–	–
$4\pi^2$	6.02085E-01	–	–	–

Table B.34.: The error in the eigenvalues of the Maxwell problem and the corresponding order of accuracy for periodic boundary conditions and the IP flux. We consider Nédélec basis functions of order $p = 1$.

	$N = 40$		$N = 320$	
eigenvalue	$\frac{\|\omega^2-\omega_h^2\|_{L^2}}{\omega^2}$	order	$\frac{\|\omega^2-\omega_h^2\|_{L^2}}{\omega^2}$	order
$4\pi^2$	5.22296E-02	–	6.76000E-04	6.285
$4\pi^2$	5.22296E-02	–	6.76000E-04	6.285
$4\pi^2$	5.22296E-02	–	6.76000E-04	6.285
$4\pi^2$	5.22296E-02	–	6.76000E-04	6.285
$4\pi^2$	5.22296E-02	–	6.76000E-04	6.285
$4\pi^2$	–	–	6.76000E-04	–
$4\pi^2$	8.63868E-02	–	6.76000E-04	7.011
$4\pi^2$	8.63868E-02	–	6.76000E-04	7.011
$4\pi^2$	8.63868E-02	–	6.76000E-04	7.011
$4\pi^2$	8.63868E-02	–	6.76000E-04	7.011
$4\pi^2$	8.63868E-02	–	6.76000E-04	7.011
$4\pi^2$	–	–	–	–

Table B.35.: The error in the eigenvalues of the Maxwell problem and the corresponding order of accuracy for periodic boundary conditions and the IP flux. We consider Nédélec basis functions of order $p = 2$.

	$p = 3$, $N = 40$	$p = 4$ $N = 320$
eigenvalue	$\frac{\|\omega^2-\omega_h^2\|_{L^2}}{\omega^2}$	$\frac{\|\omega^2-\omega_h^2\|_{L^2}}{\omega^2}$
$4\pi^2$	2.69607E-03	1.00703E-04
$4\pi^2$	2.69607E-03	1.00703E-04
$4\pi^2$	2.69607E-03	1.00703E-04
$4\pi^2$	2.69607E-03	1.00703E-04
$4\pi^2$	2.69607E-03	1.00703E-04
$4\pi^2$	2.69607E-03	1.00703E-04
$4\pi^2$	5.50185E-03	2.10475E-04
$4\pi^2$	5.50185E-03	2.10475E-04
$4\pi^2$	5.50185E-03	2.10475E-04
$4\pi^2$	5.50185E-03	2.10475E-04
$4\pi^2$	5.50185E-03	2.10475E-04
$4\pi^2$	5.50185E-03	2.10475E-04

Table B.36.: The error in the eigenvalues of the Maxwell problem for periodic boundary conditions and the IP flux. We consider Nédélec basis functions of order $p = 3$ and $p = 4$.

C. Bibliography

[1] M. Ainsworth and J. Coyle. “Hierarchic finite element bases on unstructured tetrahedral meshes”. In: *International Journal for Numerical Methods in Engineering* 58.14 (2003), pp. 2103–2130.

[2] F. Brezzi, G. Manzini, D. Marini, P. Pietra, and A. Russo. “Discontinuous finite elements for diffusion problems”. In: *Atti Convegno in onore di F. Brioschi (Milano 1997), Istituto Lombardo, Accademia di Scienze e Lettere* (1999), pp. 197–217.

[3] A. Buffa and I. Perugia. “Discontinuous Galerkin approximation of the Maxwell eigenproblem”. In: *SIAM Journal on Numerical Analysis* 44.5 (2006), pp. 2198–2226.

[4] K. Busch and S. John. “Photonic band gap formation in certain self-organizing systems”. In: *Physical Review E* 58.3 (1998), p. 3896.

[5] J. Gopalakrishnan, L. García-Castillo, and L. Demkowicz. “Nédélec spaces in affine coordinates”. In: *Computers & Mathematics with Applications* 49.7-8 (2005), pp. 1285–1294.

[6] D. Griffiths. *Introduction to electrodynamics*. 3rd ed. Upper Saddle River, New Jersey: Prentice Hall, 1999.

[7] M. Grote, A. Schneebeli, and D. Schätzau. “Interior penalty discontinuous Galerkin method for Maxwell’s equations: Energy norm error estimates”. In: *Journal of Computational and Applied Mathematics* 204.2 (2007), pp. 375 –386.

[8] J. Hesthaven and T. Warburton. “High–order nodal discontinuous Galerkin methods for the Maxwell eigenvalue problem”. In: *Philosophical Transactions of the Royal Society of London. Series A: Mathematical, Physical and Engineering Sciences* 362.1816 (2004), pp. 493–524.

[9] P. Houston, I. Perugia, A. Schneebeli, and D. Schätzau. “Interior penalty method for the indefinite time-harmonic Maxwell equations”. In: *Numerische Mathematik* 100.3 (2005), pp. 485–518.

[10] J. Joannopoulos, S. Johnson, J. Winn, and R. Meade. *Photonic crystals: molding the flow of light*. Princeton university press, 2011.

[11] J. van Kan, F. Vermolen, and A. Segal. *Numerical Methods in Scientific Computing*. VSSD, 2006.

[12] R. Kanwal. *Generalized Functions: Theory and Applications*. Birkhäuser, 2004.

[13] O. Kiriyenko, W. Hergert, S. Wackerow, M. Beleites, and H. Graener. “Photonic/Plasmonic Structures from Metallic Nanoparticles in a Glass Matrix”. In: *Proceedings of the Comsol conference Hannover*. 2008.

[14] P. Monk. *Finite element methods for Maxwell's equations*. Oxford University Press, 2003.

[15] J. Nédélec. "Mixed finite elements in $\mathbb{R}^3$". In: *Numerische Mathematik* 35.3 (1980), pp. 315–341.

[16] I. S. Nikolaev, W. L. Vos, and A. F. Koenderink. "Accurate calculation of the local density of optical states in inverse-opal photonic crystals". In: *Journal of the Optical Society of America B* 26.5 (2009), pp. 987–997.

[17] L. Novotny and B. Hecht. *Principles of nano-optics*. Cambridge university press, 2012.

[18] L. Pesch, A. Bell, W. Solie, V. Ambati, B. O., and J. van der Vegt. "hpGEM — A sofware framework for discontinuous Galerkin finite element Methods". In: *ACM Transactions on Mathematical Software* 33.4 (2007).

[19] V. Prosentsov and A. Lagendijk. "The local density of states in finite size photonic structures, small particles approach". In: *Photonics and Nanostructures-Fundamentals and Applications* 5.4 (2007), pp. 189–199.

[20] D. Sármány, F. Izsák, and J. van der Vegt. "Optimal Penalty Parameters for Symmetric Discontinuous Galerkin Discretisations of the Time-Harmonic Maxwell Equations". In: *Journal of Scientific Computing* 44.3 (2010), pp. 219–254.

[21] H. Thyrrestrup, A. Hartsuiker, J.-M. Gérard, and W. Vos. "Non-exponential spontaneous emission dynamics for emitters in a time-dependent optical cavity". In: *Optics Express* 21 (2013), pp. 23130–23144.

[22] P. Šolin, K. Segeth, and I. Doležel. *Higher-order finite element methods*. Studies in advanced mathematics. Chapman & Hall/CRC, 2004.

[23] L. Woldering, R. Tjerkstra, and W. Vos. "Photonic Crystal Fabrication". In: *The Encyclopedia of Materials: science and technology* 7 (2011). Ed. by J. Buschow, R. Cahn, M. Flemings, B. Ilschner, E. Kramer, S. Mahajan, and P. Veyssiere.

[24] M. Wubs and A. Lagendijk. "Local optical density of states in finite crystals of plane scatterers". In: *Physical Review E* 65 (2002), p. 046612.

[25] A. Yariv and P. Yeh. *Optical Waves in Crystals*. Wiley, 1984.

[26] E. Yeganegi, A. Lagendijk, A. P. Mosk, and W. L. Vos. "Local density of optical states in the band gap of a finite one-dimensional photonic crystal". In: *Physical Review B* 89.4 (2014), p. 045123.